UNIVERSITY OF NAPLES
FEDERICO II

CHEMICAL ENGINEERING DEPARTMENT

Study of Direct Methanol Fuel Cell for Small and Medium Scale Applications

Ph.D. student:
Luca Micoli

Supervisor:
Prof. Maria Turco

Scientific Committee:
Prof. V. Caprio
Prof. M. Casciola

ABSTRACT

Fuel cells, in general, are attractive because they provide an innovative alternative to current power sources due to higher efficiencies, use of renewable fuels, and a lower environmental impact. The direct methanol fuel cell (DMFC), in particular, has generated interest towards portable electronic devices, with a potential to offer 10 times higher power densities than current lithium-ion rechargeable batteries. Among the several different types of fuel cells, the DMFC offers the most promising alternative for portable power applications, because it is a low temperature, environmentally benign device, and its fuel is portable and inexpensive. Therefore, considerable research effort is focused on improving the efficiency of the DMFC.

The development of the DMFCs technology requires increasing the catalytic activity of the electrode components and the performance of the polymer electrolyte membrane. Methanol crossover, that is diffusion of some fuel from the anode to the cathode through the membrane, is the major problem of DMFCs because it causes a direct reaction of methanol with oxygen, so leading to a reduction of the cell efficiency. In this work, in order to increase the performance of the electrolyte membrane, new nano-composite materials have been proposed based on a Nafion matrix modified with the addition of a layered inorganic proton conductor such as α-$Zr(HPO_4)_2$ H_2O (ZrP). Two different preparation methods have been proposed to fill the Nafion membrane with the α-zirconium phosphate, obtaining Nafion composite membrane containing high aspect ratio particles of exfoliated α-zirconium phosphate ($NZrP_{exf}$) and Nafion composite membranes with loadings of in situ grown α-zirconium phosphate ($NZrP_{isg}$). The ZrP content has been varied in the range 1-7 wt. % and the dry thickness of the membranes between 70 and 120 µm.

Nafion/ZrP composite membranes have been studied for methanol permeability, proton conductivity and swelling measurement. The membranes were characterized and the permeability was studied under different conditions: temperature from 20 to 80 °C; mixing rate at 0 and 450 rpm. The performances were compared to that of commercial Nafion membrane.

A new laboratory apparatus and a suitable experimental procedure have been developed for the measurement of methanol permeability. This procedure allows an easy calculation of the permeability and an accurate control of methanol concentration and temperature, due to efficient stirring.

$NZrP_{isg}$ membranes have methanol permeability values comparable with that of Nafion commercial; $NZrP_{exf}$ membranes show values one order magnitude lower than $NZrP_{isg}$ in all the range of temperature and filler content investigated.

The selectivity, defined as the ratio between proton conductivity and methanol permeability, is the term used to compare the membranes to each other. $NZrP_{exf}$ membranes with 1 wt.% filler content present the higher value of selectivity.

The swelling phenomenon, that influences the start-up and the operation of the DMFCs, has been also studied in the present work. The results show that it depends on the temperature, the methanol concentration and the filler content. The preparation method strongly affects methanol permeability and proton conductivity. The presence of the filler in Nafion-ZrP_{exf} membranes gives rise to lower swelling and tortuosity of the diffusion pathways than the same amount of ZrP_{isg} particles. These factors contribute to the lowering of the methanol permeability.

The new materials proposed have higher proton conductivity and lower methanol permeability than Nafion commercial, increasing the DMFC's performances. DMFC's efficiency higher than 30% is expected by the employment of such Nafion/ZrP_{exf} membranes.

1. INTRODUCTION

The current movement towards environmentally friendlier and more efficient power production has caused an increased interest in alternative fuels and power sources [1]. Fuel cells are one of the older energy conversion technologies, but only within the last decade have they been extensively studied for commercial use. The reliance upon the combustion of fossil fuels has resulted in severe air pollution, and extensive mining of the world's oil resources. In addition to being hazardous to the health of many species (including our own), the pollution is indirectly causing the atmosphere of the world to change (global warming). This global warming trend will become worse due to an increase in the combustion of fossil fuels for electricity because of the large increase in world population. In addition to health and environmental concerns, the world's fossil fuel reserves are decreasing rapidly [2]. The world needs a power source that has low pollutant emissions, is energy efficient, and has an unlimited supply of fuel for a growing world population. Fuel cells have been identified as one of the most promising technologies to accomplish these goals.

Many other alternative energy technologies have been researched and developed [2]. These include solar, wind, hydroelectric power, bio-energy, geothermal energy, and many others. Each of these alternative energy sources have their advantages and disadvantages, and are in varying stages of development. In addition, most of these energy technologies cannot be used for transportation or portable electronics. Other portable power technologies, such as batteries and supercapacitors also are not suitable for transportation technologies, military applications, and the long-term needs of future electronics. The ideal option for a wide variety of applications is using a hydrogen fuel cell combined with solar or hydroelectric power. Compared to other fuels, hydrogen does not produce any carbon monoxide or other pollutants. When it is fed into a fuel cell, the only by-products are oxygen and heat. The oxygen is recombined with hydrogen to form water when power is needed [1].

Fuel cells can utilize a variety of fuels to generate power–from hydrogen, methanol, and fossil fuels to biomass-derived materials. Using fossil fuels to generate hydrogen is regarded as an intermediate method of producing hydrogen, methane, methanol, or ethanol for utilization in a fuel cell before the hydrogen infrastructure has been set up. Fuels can also be derived from many sources of biomass, including methane from municipal wastes, sewage sludge, forestry residues, landfill sites, and agricultural and animal waste.

Fuel cells can also help provide electricity by working with large power plants to become more decentralized and increase efficiency. Most electricity produced by large fossil-fuel burning power plants is distributed through high voltage transmission wires over long distances [3]. These power plants seem to be highly efficient because of their large size; however, a 7 to 8 percent electric energy loss in Europe, and a 10 % energy loss in the United States occurs during long distance transmission [3]. One of the main issues with these transmission lines is that they do not function properly all the time. It would be safer for the population if electricity generation did not occur in several large plants, but is generated where the energy is needed. Fuel cells can be used wherever energy is required without the use of large transmission lines.

Fossil fuels are limited in supply, and are located in select regions throughout the world. This leads to regional conflicts and wars which threaten peace. The limited supply and large demand dries up the cost of fossil fuels tremendously. The end of low-cost oil is rapidly approaching.

Other types of alternative energy technology such as fuel cells, can last indefinitely when non-fossil fuel-based hydrogen is used.

1.1 Fuel Cells

Fuel cells are energy conversion devices that continuously transform the chemical energy of a fuel and an oxidant into electrical energy. The fuel and oxidant gases lick the anode and cathode and are continuously fed promoting the oxidation reaction of fuel and oxidant gas reduction. Fuel cells will continue to generate electricity as long as both fuel and oxidant are available [1].

There are different types of fuel cells, showing a flexibility that could replace most of the devices for production of electricity covering outputs ranging from a few W to several MW [1,6].

A first classification distinguishes cells in high temperature (HT) up to 1100 ° C, used in stationary systems for cogeneration processes, aerospace and marine applications, and low temperature (LT), from 60 to 120 ° C, for low-cost portable devices and automotive.

Power can be provided by fossil fuels, coal, biogas and biomass (for PAFC, PEMFC, MCFC, SOFC), by alcohol (DMFC) and hydrogen (PEMFC and AF).

A further classification of FCs is based on the electrolyte. In PEMFC and DMFC the electrolyte is a polymeric material with cation exchange capacity; Alkaline FCs have an

electrolyte solution with a KOH; MCFCs have electrolyte based on molten carbonate of lithium and potassium; SOFC are based on phosphoric acid etc etc.

The FCs are often presented as the solution to the problem of the future production of electricity and for transport vehicles.

Indeed, this technology presents several advantages:

- *low emissions, but depend on the fuel used, especially as regards the release of NOx, CO and particulate*
- *high energy efficiency, especially when compared to those of thermal machines*
- *weak noise*
- *different operating temperatures*
- *modular construction, so by putting in series or in parallel several elementary units you are covering the power range required*
- *more simple construction, and thus greater reliability and easier maintenance.*

These advantages justify the strong interest, particularly from many automotive companies, to develop the technology based on fuel cells for automotive.

Nevertheless, there are some problems should be solved in order that fuel cells can be competitive and penetrate the market:

- *the cost, due to the high value components*
- *The weight and volume, especially in the automotive*
- *the length of life, still very low (a few thousand hours for cars, about 40,000 for stationary systems)*
- *thermal management, for the large amount of heat exchange with an operative cooling system.*

Therefore, further studies are necessary because this method of generating energy supplements or replaces the current one.

1.1.1 Comparison with batteries

A fuel cell has many similar characteristics with batteries, but also differs in many respects. Both are electrochemical devices that produce energy directly from an electrochemical reaction between the fuel and the oxidant. The battery is an energy storage device. The maximum energy available is determined by the amount of chemical reactant stored in the battery itself. A battery has the fuel and oxidant reactants built into itself (onboard storage), in addition to being an energy conversion device. In a secondary battery, recharging regenerates the reactants. This involves putting energy into the battery from an external source. The fuel cell is an energy conversion device that theoretically has the capability of producing electrical energy for as long as the fuel and oxidant are supplied to the electrodes [7]. Figure 1.1.1-1 shows a comparison of a fuel cell and battery.

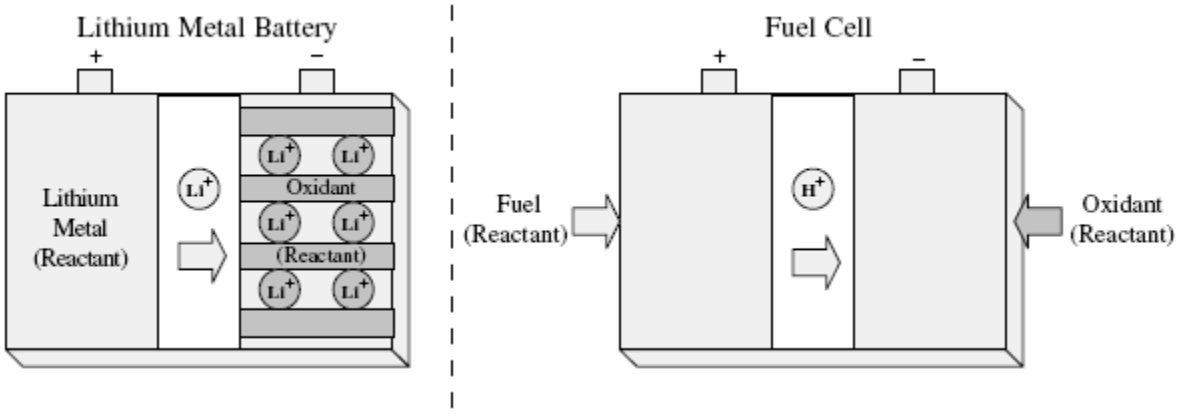

Figure 1.1.1-1 Comparison of a fuel cell and a battery.

The lifetime of a primary battery is limited because when the amount of chemical reactants stored in a battery runs out, the battery stops producing electricity. In addition, when a battery is not being used, a very slow electrochemical reaction takes place that limits the lifetime of the battery. The electrode of a battery is also used in the process; therefore, the lifetime of the battery is dependent on the lifetime of the electrode. In comparison, a fuel cell is an energy conversion device where the reactants are supplied. The fuels are stored outside the fuel cell. A fuel cell can supply electrical energy as long as fuel and oxidant are supplied [1]. The amount of energy that can be produced is theoretically unlimited as long as the fuel and oxidant are supplied. Also, no "leakage" occurs in a fuel cell, and no corrosion of cell components occurs when the system is not in use.

1.1.2 Comparison with heat engine

A heat engine converts chemical energy into electric energy likes fuel cells, but through intermediate steps. The chemical energy is first converted into thermal energy through combustion, then thermal energy is converted into mechanical energy by the heat engine, and finally the mechanical energy is converted into electric energy by an electric generator [1].

This multistep energy process requires several devices in order to obtain electricity. The maximum efficiency is limited by Carnot's law because the conversion process is based upon a heat engine, which operates between a low and high temperature [1]. The process also involves moving parts, which implies that they wear over time. Regular maintenance

of moving components is required for proper operation of the mechanical components. Figure 1.1.1-2 shows a comparison between a fuel cell and a heat engine/electrical generator.

Since fuel cells are free of moving parts during operation, they can work reliably and with less noise. This results in lower maintenance costs, which make them especially advantageous for space and underwater missions. Electrochemical processes in fuel cells are not governed by Carnot's law, therefore high operating temperatures are not necessary

for achieving high efficiency. In addition, the efficiency of fuel cells is not strongly dependent on operating power. It is their inherent high efficiency that makes fuel cells an attractive option for a wide range of applications, including road vehicle power sources, distributed electricity and heat production, and portable systems [6].

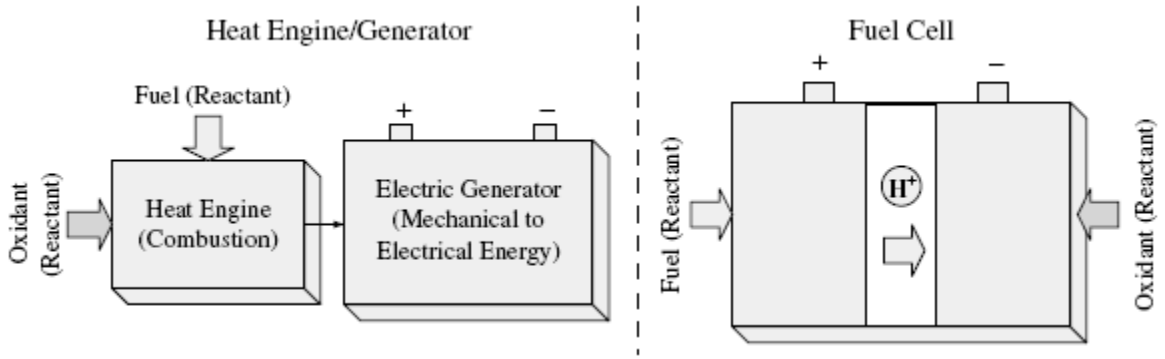

Figure 1.1.1-2 Comparison of a fuel cell to a heat generator.

1.2 Sectors of applications

Conventional power generation relies upon fossil fuels, which produce a significant amount of pollutants, and there is a limited supply. Many alternative energy approaches have been proposed, such as bio fuel, hydroelectric power, batteries, wind, solar, bio energy, and geothermal energy. All of these sources can provide energy, but every method has advantages and disadvantages. Fuel cells are needed because they provide electric power in applications that are currently energy-limited. For example, one of the most annoying things about a laptop computer is that the battery gives out after a couple of hours.

Each market needs fuel cells for varying reasons described as follow.

- *Portable sector*

In coming years, portable devices—such as laptops, cell phones, video recorders, and others—will need greater amounts of power for longer periods of time. Fuel cells are very scalable and have easy recharging capabilities compared to batteries. Cell phone technology is advancing rapidly, but the limiting factor for the new technology is the power. More power is required to provide consumers with all of the functions in devices they require and want. The military also has a need for long-term portable power for new soldier's equipment. In addition, fuel cells operate silently, and have low heat signatures, which are clear advantages for the military.

- *Transportation sector*

Many factors are contributing to the fuel cell push in the automotive market. The availability of fossil fuels is limited, and due to this, an inevitable price increase will occur. In addition, legislation is becoming stricter about controlling environmental emissions in many countries all over the world. One of the new pieces of legislation that will help introduce the fuel cell automobile market in the United States is the Californian zero emission vehicle (ZEV) mandate, which requires that a certain number of vehicles be sold annually in California. Fuel cell vehicles also have the ability to be more fuel efficient than vehicles powered by other fuels. This power technology allows a new range of power use in small two-wheeled and four-wheeled vehicles, boats, scooters, unmanned vehicles, and other utility vehicles.

- *Stationary sector*

Stationary fuel cells can produce enough electricity and heat to power an entire house or business, which can result in significant savings. These fuel cells may even make enough power to sell some of it back to the grid. Fuel cells can also power residences and businesses where no electricity is available. Sometimes it can be extremely expensive for a house not on the grid to have the grid connected to it. Fuel cells are also more reliable than other commercial generators used to power houses and businesses. This can benefit many companies, given how much money they can lose if the power goes down for even a short time.

1.3 History of Fuel Cells

Fuel cells have been known to science for about 150 years [4]. They were minimally explored in the 1800s and extensively researched in the second half of the twentieth century. Initial design concepts for fuel cells were explored in 1800, and William Grove is credited with inventing the first fuel cell in 1839 [4]. Various fuel cell theories were contemplated throughout the nineteenth century, and these concepts were studied for their practical uses during the twentieth century. Extensive fuel cell research was started by NASA in the 1960s, and much has been done since then. During the last decade, fuel cells were extensively researched, and are finally nearing commercialization. A summary of fuel cell history is shown in Figure 1.3-1.

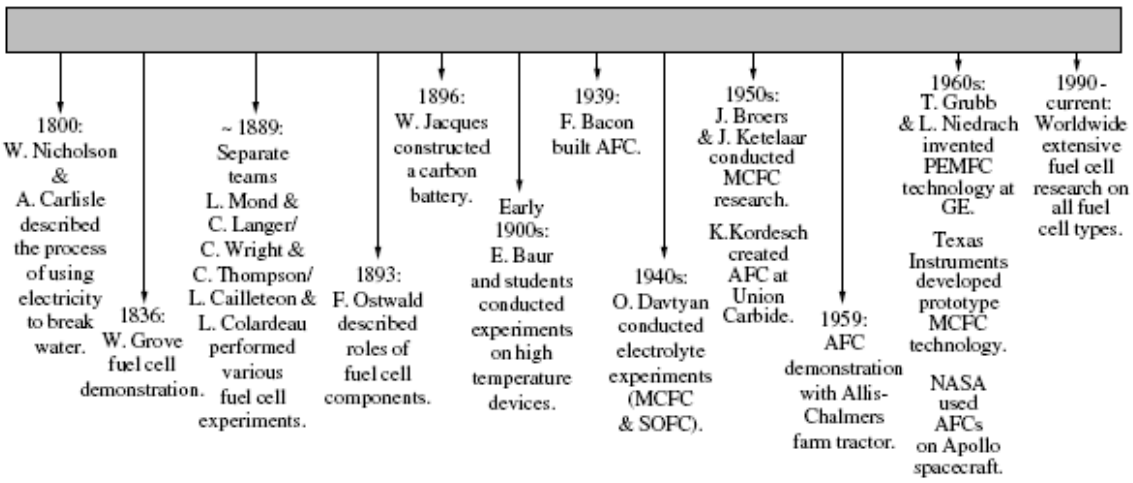

Figure 1.3.1 The history of fuel cells.

In 1800, William Nicholson and Anthony Carlisle described the process of using electricity to break water into hydrogen and oxygen [4]. William Grove is credited with the first known demonstration of the fuel cell in 1839. Grove saw notes from Nicholson and Carlisle and thought he might "recompose water" by combining electrodes in a series circuit, and soon accomplished this with a device called a "gas battery." It operated with separate platinum electrodes in oxygen and hydrogen submerged in a dilute sulphuric acid electrolyte solution. The sealed containers contained water and gases, and it was observed that the water level rose in both tubes as the current flowed. The "Grove cell," as it came to be called, used a platinum electrode immersed in nitric acid and a zinc electrode in zinc sulphate to generate about 12 amps of current at about 1.8 volts [4].

Friedrich Wilhelm Ostwald (1853-1932), one of the founders of physical chemistry, provided a large portion of the theoretical understanding of how fuel cells operate. In 1893, Ostwald experimentally determined the roles of many fuel cell components [4].

Ludwig Mond (1839-1909) was a chemist that spent most of his career developing soda manufacturing and nickel refining. In 1889, Mond and his assistant Carl Langer performed numerous experiments using a coal-derived gas. They used electrodes made of thin, perforated platinum, and had many difficulties with liquid electrolytes. They achieved 6 amps per square foot (the area of the electrode) at 0.73 volts [4].

Charles R. Alder Wright (1844-1894) and C. Thompson developed a similar fuel cell around the same time. They had difficulties in preventing gases from leaking from one chamber to another. This and other causes prevented the battery from reaching voltages as high as 1 volt. They felt that if they had more funding, they could create a better, robust cell that could provide adequate electricity for many applications [4].

The French team of Louis Paul Cailleteton (1832-1913) and Louis Joseph Colardeau came to a similar conclusion, but thought the process was not practical due to needing "precious metals." In addition, many papers were published during this time saying that coal was so inexpensive that a new system with a higher efficiency would not decrease the prices of electricity drastically [4].

William W. Jacques (1855-1932), an electrical engineer and chemist, did not pay attention to these critiques, and startled the scientific world by constructing a "carbon battery" in 1896 [4]. Air was injected into an alkali electrolyte to react with a carbon electrode. He thought he was achieving an efficiency of 82 percent, but actually obtained only an 8 percent efficiency [4].

Emil Baur (1873-1944) of Switzerland and several of his students conducted many experiments on different types of fuel cells during the early 1900s. His work included high-temperature devices, and a unit that used a solid electrolyte of clay and metal oxides [4].

O. K. Davtyan of the Soviet Union did many experiments to increase the conductivity and mechanical strength of the electrolyte in the 1940s. Many of the designs did not yield the desired results, but Davtyan's and Baur's work contributed to the necessary preliminary research for today's current molten carbonate and solid oxide fuel cell devices.

1.4 The choice of fuel cell

Currently, the most studied fuel cells use hydrogen as fuel (PEMFC). In these, the electrolyte is a polymeric membrane with proton exchange capacity, operating between 80-110 °C. H_2 can be fed as pure gas or come from a reactor for catalytic reforming placed upstream the FC.

Recent reports on direct methanol fuel cells (DMFCs), that use polymer electrolyte membranes and diluted aqueous methanol solutions fed at the anode, have demonstrated appreciable performance improvement, for potential portable power applications and for transport applications. There are still two major obstacles that hinder the introduction of current DMFC technology to widespread commercial applications: the low electro-activity of known catalyst for methanol electro-oxidation and the high permeation rate of methanol through commercially available polymer electrolyte membranes such as Nafion. The low catalyst activity would require a higher Pt loadings, and thus higher cost, in order to achieve appreciable anode performance. Methanol crossover through membrane from cell anode to the cathode causes a decrease in cell efficiency, up to now DMFC efficiency does not get over 20% [10]. The result of both these problems is that the performance of DMFC is markedly worse than other fuel cells, such as a hydrogen fuelled proton exchange membrane fuel cell (PEMFC). Nevertheless, if methanol can be used as fuel, then all the problems of hydrogen production and storing are swept aside. Methanol is a readily available and low cost liquid fuel that has an energy density not very different from gasoline. If it could be used directly in fuel cells, the resulting weight of any portable fuel cell system would be vastly

reduced. Table 1.4.1 shows how methanol compares with the main hydrogen storage technologies [15]:

Table 1.4.1 Energy density comparison for methanol and the most important hydrogen storage technologies

Storage method	*Energy density of fuel*	*Storage efficiency (%)*	*Net energy density*
- H_2 at 300 bar pressure in composite cylinders	*119.9 MJ kg^{-1} 33.3 kWh kg^{-1}*	*0.6*	*0.72 MJ kg^{-1} 0.20 kWh kg^{-1}*
- H_2 in metal hydride Cylinders	*119.9 MJ kg^{-1} 33.3 kWh kg^{-1}*	*0.65*	*0.78 MJ kg^{-1} 0.22 kWh kg^{-1}*
- H_2 from methanol (indirect methanol)	*119.9 MJ kg^{-1} 33.3 kWh kg^{-1}*	*6.9*	*8.27 MJ kg^{-1} 2.30 kWh kg^{-1}*
- Methanol for direct use as fuel	*19.9 MJ kg^{-1} 5.54 kWh kg^{-1}*	*95*	*18.9 MJ kg^{-1} 5.26 kWh kg^{-1}*

It can be observed that the main advantage of direct methanol system: the net energy density is much higher than any of other options. The fact that the system is simpler to use and very quick to refill are also important advantages.

Direct Methanol Fuel Cells can be considered as an evolution of PEMFC. These cells have the certain advantage of a simpler supply, as well as the absence of a cumbersome systems of reforming and purification for the reagent; furthermore, the storage of methanol is much simpler than that of hydrogen because it does not require high pressures or low temperatures, since methanol is liquid under normal conditions.
DMFC technology can be applied to various products. If the problems due to methanol crossover are solved, then the DMFC could be used in all mobile fuel cell applications, including such high-power applications as motor vehicles. The first applications of the DMFC will almost certainly be in cases where a power of only a few W is sufficient, but a high energy density is required. DMFCs could replace the use of batteries, such as the common rechargeable lithium-ion battery: cell phones, CD players, computers, the number of possible applications is unlimited. Good examples are third-generation (3G) mobile phones, or a high specification personal assistant (PDA), or digital movie cameras. The DMFC should be able to provide a better alternative to the rechargeable lithium-ion battery, which is the battery type almost universally used in such electronic equipment. This Li-ion battery provides a very clear target for DMFCs to compete with. In addition to a sensible use in the automotive field.

DMFC technology is a great source of alternative and clean energy. It represents the latest technology in the field of Fuel cells and it is a very versatile system, so the DMFC shows some interesting grounds for research in various fields.

First of all, the efficiency: DMFCs have still a low power density, about 180-250 mW / cm², but the research in this field is trying to overcome the 45% value of system efficiency and to increase the performances of the cell.

The development of this technology is linked to two issues: the slow kinetics of methanol oxidation and the diffusion of methanol through the polymeric membrane. The first problem can be overcome by using porous electrodes with high catalytic activity, the second is crucial in the realization of DMFC: the diffusion of methanol from the anode to the cathode (methanol crossover), which is directly oxidized by oxygen of the air, is the cause of the low efficiency currently obtained.

Therefore, the performance of the DMFC will be due to the characteristics of the electrolyte, the polymeric membrane, which on one side will ensure an excellent proton exchange and on the other it will hinder the phenomenon of methanol crossover.

2. DIRECT METHANOL FUEL CELL

A Direct Methanol Fuel Cell (DMFC) works creating an electric potential by the reaction between methanol and oxygen, specifically it produces electricity through an electrochemical process without combustion and without the need for a reformer system for the fuel.

The electric potential is created using a polymeric membrane that is selective to certain chemical molecules, in this case the membrane allows the passage of H^+ ions (proton conductivity). On one side of the membrane, an aqueous solution of methanol (CH_3OH) is feed to the anode catalyst where the catalytic decomposition of methanol molecules producing carbon dioxide (CO_2) and hydrogen (H_2) which is oxidized to H^+ ions at the anode. The protons produced can migrate to the cathode of the cell through the membrane where the electrons (e^-) produced to the anode, passing through an external circuit, reduce the oxygen (O_2) that is plugged in, allowing the formation of water (H_2O). The reactions occurring in the DMFC are as follows:

$$CH_3OH + H_2O \rightarrow CO_2 + 6\,H^+ + 6\,e^- \quad \text{anode}$$
$$6\,H^+ + 3/2\,O_2 + 6\,e^- \rightarrow 3\,H_2O \quad \text{cathode}$$

$$CH_3OH + 3/2\,O_2 \rightarrow CO_2 + 2\,H_2O \quad \text{global reaction}$$

It is noted that the reaction occurs in the DMFC is the same as the combustion of methanol.[1,21]

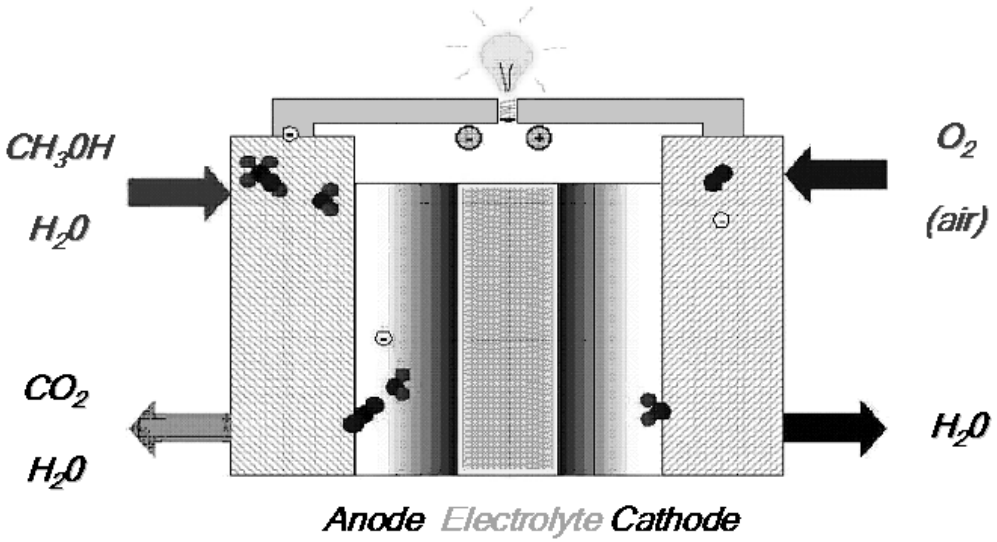

Fig. 2.1 Illustration of a direct methanol fuel cell

Unlike in ordinary batteries, fuel cells have the active material that is continually renewed and, therefore, the electric current can be provided indefinitely if you keep feeding fuel gas and oxidant.

Obviously, the faced areas must have a sufficient area to obtain the current intensity appropriate to the application needs. So, depending on the application and the length of the chain of cells, surfaces can be in the order of square meters. Individual cell is marked by tensions in the order of 0,5-1 volt, according to the technology used and the electrical load connected to it, It can be connected in series as well to obtain the overall voltage value required, forming the "stack". Generally, a fuel cell system also includes a power converter (inverter) and a transformer that converts direct current into alternating current at the voltage and frequency required.

- Reactions on the electrodes

The electrodes are typically made of Pt / Ru catalysts the anode, only Pt the cathode, mainly because the reactions that take place, oxygen reduction and oxidation of hydrogen occurs in the case of low temperatures (in this case less than 80 °C), at low speeds, so it must increase with the use of catalysts such as Pt. The phenomenon that slows down the main reaction is the reduction of oxygen at the cathode. The catalyst takes part in the chemical transformation combined with the reagents and giving rise to complex intermediate which subsequently decompose to form reaction products, and returning the catalyst unchanged. The role of platinum is very important but it is also very expensive, so we must try to increase as possible the adsorption surface. Porous carbon electrodes has been built with a small amount of platinum (0.2-0.4 mg/cm^2), the porous structure allows the diffusion through the electrode and, at the same time, the carbon allows a very good electron conductivity.

The oxidation reactions of methanol, due to the catalyst, have been extensively studied and they are described in much more detail in the literature [16,17,18]. The chart in figure 3.3.2 is an attempt to explain the stages and the different possibilities [18].

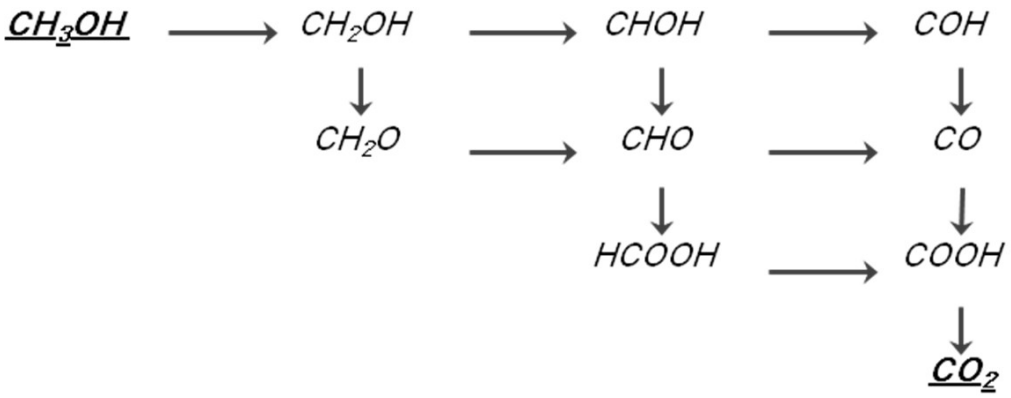

Fig. 2.2 Stages in the oxidation of methanol at a DMFC anode.

Referring to the figure 2.2, at the top left is methanol and at the bottom right is carbon dioxide. The right moving steps involve hydrogen stripping, the removal of hydrogen atom and the generation of a proton (H^+) and electron pair. The downward moving steps also involve the removal of hydrogen atom and the generation of a proton-electron pair, but these downward steps also involve the destruction of an OH group.

Any route through the compounds of figure 1.3.2 from top left to bottom right is possible, and all have the same results, three right steps, three down steps, producing carbon dioxide and six proton. However, the compound along the lower left edge (the hypotenuse) are the only stable compounds, and so this might be considered a preferred route. As evident, this route does not lead to the formation of CO stable, that could poison the Pt catalyst as it happens in PEMFC.

We can divide it neatly into three steps. First the methanal is oxidised to methanol (formaldehyde)

$$CH_3OH \rightarrow CH_2O + 2\,H^+ + 2\,e^-$$

The methanal then reacts to form methanoic (formic) acid via another right and another down steps:

$$CH_2O + H_2O \rightarrow HCOOH + 2\,H^+ + 2\,e^-$$

Finally, the formic acid is oxidised to carbon dioxide:

$$HCOOH \rightarrow CO_2 + 2\,H^+ + 2\,e^-$$

The sum of the reactions above is the same as the reaction at the anode.

2.1 Transport phenomena in the electrolyte membrane

To understand the performance of the electrolyte mebrane, transport phenomena (transport of protons, water, and methanol) must be considered.

Typically, the transport of small molecules across a dense (nonporous) polymer membrane follows a solution-diffusion mechanism [19]. Transport can be described as sorption of solutes into the membrane (upstream or high concentration side), diffusion across the membrane (concentration gradient is the driving force), and desorption of solutes out of the

membrane (downstream or low concentration side). Overall, the transport rate is determined by a permeability coefficient (P), which is a product of the solubility (S) and the diffusion coefficient (D).

$$P = SD$$

Solubility is the equilibrium parameter based on solute-polymer thermodynamics, while the diffusion coefficient is a kinetic parameter based on the free-volume or structure of the polymer. The ratio of desired (1) to undesired (2) solute permeabilities is referred to as selectivity (α).

$$\alpha_{1/2} = \frac{P_1}{P_2} = \frac{S_1 D_1}{S_2 D_2}$$

Overall, this generally describes selectivity for solute-polymer systems (e.g., gases or organic vapor/liquid diffusion in nonionic dense polymer membranes). However, for transport phenomena in proton exchange membranes, there are a number of additional parameters to consider, such as ion transport, the ionic structure of the polymer, and a potential difference (for fuel cell tests).

Experimentally for the separate proton conductivity and methanol permeability measurements, the transport of protons (desired) and methanol (undesired) are the two primary diffusing solutes of interest. The steady-state flux of protons in a membrane can be described by the Nernst-Planck equation [20]:

$$-j_1 = D_1 C_1 \left(\frac{\Delta C_1}{C_1} + z_1 \frac{F \Delta \psi}{RT} \right)$$

where D_1, C_1, and z_1 are the diffusion coefficient, concentration, and charge, respectively, for protons; F is Faraday's constant, R is the gas constant, T is the temperature, and ψ is the electrostatic potential. With the aid of the Nernst- Einstein relation, proton conductivity (z_1 = +1) can be related to its diffusion coefficient [20]:

$$\sigma_1 = \frac{D_1 C_1 F^2}{RT}$$

For methanol, the steady-state flux can be described by Fick's law as

$$-j_2 = D_2 \Delta C_2$$

where D_2 and C_2 are the diffusion coefficient and concentration, respectively, for methanol. When the concentration of methanol on the upstreamside of the membrane, C_{2o}, is constant and there is a zero-sink boundary condition for concentration on the downstream side, then the equation above can be represented as

$$j_2 = \frac{D_2 K_2 C_2}{\delta}$$

where K_2 is the partition coefficient (the ratio ofmethanol concentration inside the membrane to that in the adjacent solution) and the product D_2K_2 is the methanol permeability, P_2. Selectivity for protons to methanol can be defined as the ratio of proton conductivity to methanol permeability:

$$\alpha_{1/2} = \frac{\sigma_1}{P_2} = \frac{D_1 C_1 F^2}{D_2 C_2 RT}$$

Note that conductivity and permeability are both proportional to their respective diffusion coefficients, and are the two separate quantities that are experimentally measured for the polymeric electrolyte membranes.

Aside from temperature effects, the driving factors that affect selectivity are the diffusion coefficient of protons, D_1, the concentration of protons in the membrane or concentration of fixed ion sites in the membrane, C_1, the diffusion coefficient of methanol, D_2, and the partition coefficient of methanol in the membrane, K_2. Increasing membrane selectivity

is a difficult problem since several of these factors are interdependent and also a function of several other parameters. For instance, D_2 is a function of both water and methanol concentration in the membrane, but also a function of molecular size and polymer free volume, and K_2 is a function of C_1 and also a function of water/methanol uptake and the solute-polymer interaction parameter. Also, D_1 is a function of C_1 and also hydration (water uptake) and membrane structure.

2.2 DMFC's performances

The passage of methanol through the membrane appears to be the main problem of loss of efficiency in the DMFC. Therefore, to improve the performance of the DMFC is necessary to reduce or eliminate the methanol crossover. Following this line we try to improve the technology of the membrane.

In general, the problem of methanol crossover is influenced by the following factors:

- *Concentration of methanol. It is noted that the electromotive force (EMF). decreases with increasing concentration of methanol, and this is attributed mainly to the permeability of the membrane to methanol, which reduces the performance of the cathode catalyst in the contact. Therefore, It must find the optimal value of concentration as a function of operating conditions.*
- *Pressure. Literature data [22] indicate that there is a significant effect on the performance of the cell increasing the pressure of the current oxidant that can not be predicted by thermodynamic and dynamic behaviour of the system. Is found that the pressurization of oxygen reduces the permeability of the membrane to methanol, leading to a higher voltage of the cell.*
- *Temperature. The ionic conductivity of membranes increases with increasing temperature, but also increases the permeability of methanol. The first effect is dominant so that the cell performance improved with increasing temperature.*
- *Thickness of the membrane. The permeability of methanol decreases with increasing thickness of the membrane and increases the EMF. However, this behaviour changes at higher current density, because the resistance of the membrane to the transport becomes dominant. Indeed, the overall performance of the fuel cell considers the combined effect of ion exchange between the anode and cathode and methanol crossover. The electrical performance of the DMFC*

decreases with increasing the specific weight of the membrane, although less markedly.

As mentioned, the performance of the DMFC will depend on the characteristics of the polymeric membrane, which on one hand it must ensure a good proton exchange on the other prevent the phenomenon of methanol crossover. Ultimately, it is necessary to optimize the ratio:

Methanol permeability / Proton conductivity

Recently, hybrid membranes have been proposed, they are prepared by dispersing inorganic nanoparticles into the polymer matrix, resulting in nanocomposite materials, in order to improve DMFC performances.
The study of proton conductivity and methanol permeability of these nanocomposite materials appears to be the crucial step for the application of DMFC technology on a large scale.

2.3 Efficiency and the electromotive force

In some electrical power-generating devices, the electrical power and energy output are calculated from the equations

$$P = V*I$$

and

$$E = V*I*t$$

However, the energy of the chemical input and output is not easily defined, so we must use the "Gibbs free energy".
In the case of fuel cells, the Gibbs free energy can be defined as the "energy available to do external work, neglecting any work done by changes in pressure and/or volume". In a fuel cell, the external work involves moving electrons round an external circuit and any work done by a change volume between the input and output is not involved in the fuel cell.
The Gibbs function for a system is defined in terms of the enthalpy and the entropy.

$$G = H - T S$$

Similarly, the molar Gibbs energy of formation, the molar enthalpy of formation, and the molar entropy are connected by the equation

$$g_f = h_f - T\,S$$

In a fuel cell the temperature is constant. So, we can say that

$$\Delta g_f = \Delta h_f - T\,\Delta S$$

The value of ∆hf is the difference between hf of the products and hf for the reactants. Thus, for the reaction

$$CH_3OH + 3/2\ (O_2) \rightarrow CO_2 + 2\ H_2O$$

We have:

$$\Delta hf = (hf)CO_2 + 2\ (hf)H_2O - (hf)CH_3OH - 3/2\ (hf)O_2 \qquad 1$$

Similarly, ∆s is the difference between s of the product and s of the reactants:

$$\Delta s = (s)CO_2 + 2\ (s)H_2O - (s)CH_3OH - 3/2\ (s)O_2 \qquad 2$$

The value of hf and s vary with the temperature according to the equations given below: The molar enthalpy of formation at temperature T is given by

$$h_T = h298.15 + int(298.15 - T)\ cp\ dT$$

The molar entropy is given by

$$s_T = s298.15 + int(298.15 - T)1/T\ cp\ dT$$

cp is the molar heat capacity at constant pressure; 298.15 K is the standard temperature.

The value for the molar entropy and enthalpy of formation at 298.15 K are obtainable from thermodynamics tables and are given in table 2.3.1. These values are at the standard pressure (0.1 MPa) [23]

Table 2.3.1 Thermodynamics values

	N	$\Delta H°$ (Kcal/mol)	$\Delta G°$ (Kcal/mol)
CH_4O	-1	-57.041	-39.822
CO_2	+1	-94.052	-94.261
O_2	-1.5	0	0
H_2O	2	-68.317	-56.690
Tot.		-173.647	-167.841

To use equations 1 and 2, we need to know the value of the molar heat capacity at constant pressure cp. Fortunately, over the range of temperature used in DMFCs, cp is approximately constant. Cp is in J g mole-1 K.

If there are no losses in the fuel cell, or as we should more properly say, if the process is reversible, then all Gibbs free energy is converted into electrical energy. So, we shall use this to find the reversible open circuit voltage of a fuel cell.
For the DMFC, six electrons pass round the external circuit for each molecule of methanol and water used. So, for one mole of methanol used, 6N electrons pass round the external circuit, where N is Avogadro's number. If "-e" is the charge on one electron, then the charge that flows is

$$-6Ne = -6F \text{ [coulombs]}$$

F being the Faraday constant or the charge of one mole of electrons (F = 96485.3 C/mol).
If E is the voltage of the fuel cell, then the electrical work done moving this charge round the circuit is

$$\text{Electrical work done} = \text{charge} \times \text{voltage} = -6FE \text{ [joules]}$$

If the system is reversible or has no losses, then this electrical work done will be equal to the Gibbs free energy released Δg_f

$$\Delta gf = -6FE$$

thus

$$E = -\Delta gf / 6F$$

This fundamental equation gives the electromotive force (EMF) or reversible open circuit voltage of the fuel cell.
DMFC operating at room temperature (or at standard conditions) has Δgf = -698,2 kJ/mol, so

$$E \approx 1.21 \text{ [volt]}$$

This value is slightly higher than that of PEMFC ($E \approx 1.18$) as well as compared to the voltage obtained from a common alkali battery used in portable appliances ($E \approx 1.44$). [21,25]

2.4 Efficiency Limits

It is quite well known that the fuel cells are not subjected to the Carnot efficiency limit

$$\text{Carnot limit} = (T_1 - T_2)/T_1$$

Where T_1 and T_2 are the maximum and the minimum temperatures (in Kelvin) of the heat engine.
It is commonly supposed that if there were no irreversibilities then the efficiency could be 100%. We said that the Gibbs free energy is converted into electrical energy, all this energy would be converted into electrical energy and the efficiency could be 100%. However, the Gibbs free energy changes with temperature, pressure and other factors (see par. 2.5)
Since a fuel cell uses materials that are usually burnt released their energy, it would make sense to compare the electrical energy produced with the heat that would be produced by burning the fuel. This is called the calorific value, though a more precise description is the change in enthalpy of formation, Δhf. As with the Gibbs free energy, the convention is that Δhf is negative when energy is released. So to get a good comparison with other fuel-using technologies, the efficiency of the fuel cell is usually defined as

$$\text{Electrical energy produced per mole of fuel} / -\Delta hf$$

We can now see that there is a limit to the efficiency, so

$$\text{Maximum efficiency possible} = \Delta gf / \Delta hf * 100\%$$

This maximum efficiency limit is known as "thermodynamic efficiency".

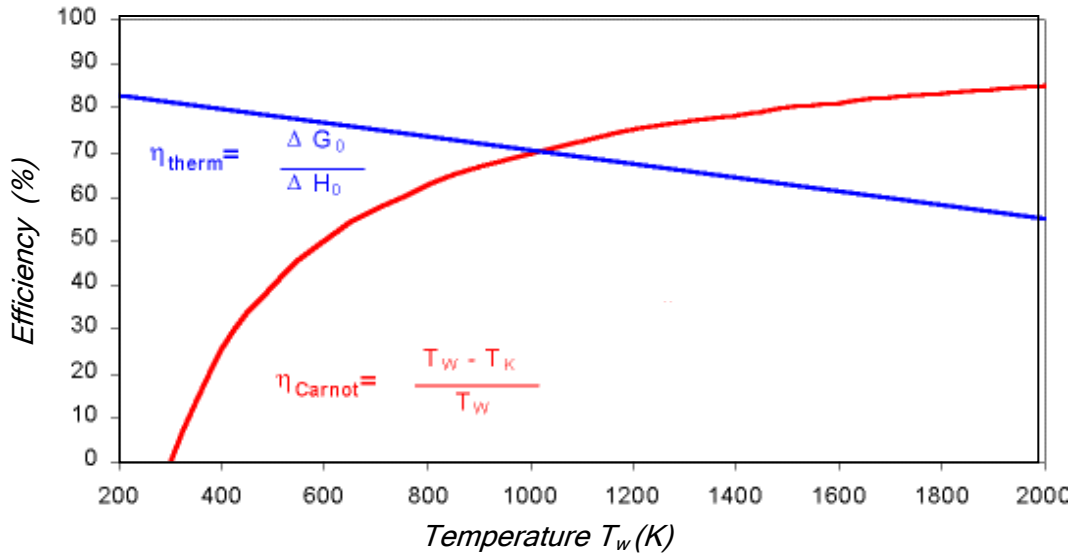

Fig. 2.4.1 Thermodynamic efficiency for H_2 fuel cell and Carnot efficiency for heat engines

The graph in figure 2.4.1 shows how these values vary with temperature, and how they compare with the Carnot limit. Three important points should be noted:

- *Although the graph would suggest that lower temperatures are better, the voltage losses are nearly always less at higher temperature. So in practice fuel cell voltages are usually higher at higher temperatures*
- *The waste heat from the higher temperature cells is more useful than that from lower temperature cells*
- *Contrary to statements often made by their supporters, fuel cells do not always have a higher efficiency limit than heat engines.*

It is clearly that there is a connection between the maximum EMF of a cell and its maximum efficiency. The operating voltage of a fuel cell can be related to its efficiency. If all the energy from the fuel, its calorific value, or heating value or enthalpy of formation, were transformed into electrical energy, then the EMF would given by

$$E = -\Delta hf / 6F$$

The theoretical value of the open circuit voltage (OCV) of a DMFC is given by the formula

$$E = -\Delta g_f / 6F$$

However, when a fuel cell is made and put to use, it is found that the voltage is less than this. Figure 2.4.2 shows the performance of a typical single cell operating at about 70°C, at normal pressure. The key points to notice about this graph of the cell voltage against the current density are as follows:

- *Even the open circuit voltage is less than the theoretical value*
- *There is a rapid initial fall in voltage*
- *The voltage then falls less rapidly and more linearly*
- *There is sometimes a higher current density at which the voltage falls rapidly.*

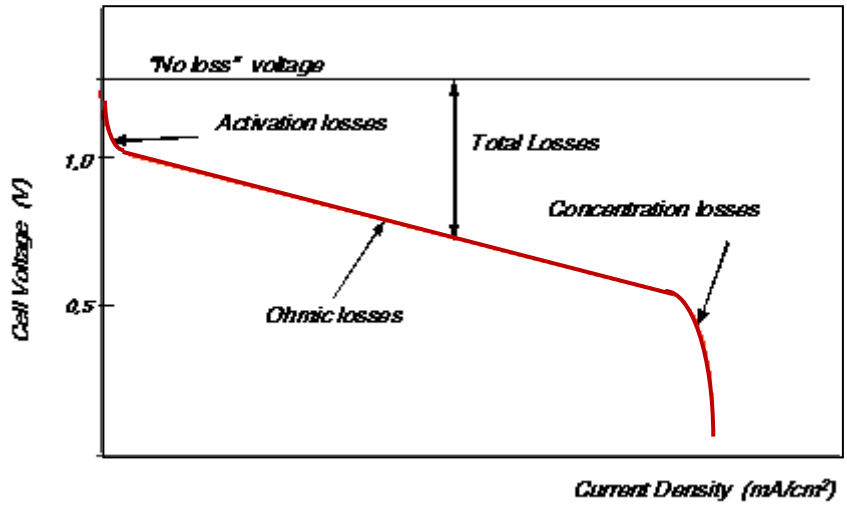

Fig. 2.4.2 Voltage for a typical low temperature, air pressure, fuel cell

If the cell is operating at higher temperatures, the shape of the voltage/current density graph changes. The difference between the actual operating voltage and the no loss value usually becomes less. In particular, the initial fall in voltage as current is drawn from the cell is markedly less.

The characteristic shape of the voltage/current density graphs results from four major irreversibilities: activation losses, fuel crossover and internal currents, ohmic losses, mass transport or concentration losses.

So, we can calculate the operating voltage of a fuel cell, at current density i, with the following equation

$$V = E - \Delta V_{ohm} - \Delta V_{act} - \Delta V_{trans}$$

The terms of this equation will be described in the next paragraphs. [24]

2.4.1 Activation losses

The overvoltage or overpotential at the surface of an electrode followed a similar pattern, in a great variety of electrochemical reactions, as shown in figure 2.4.1.1. It shows that if a graph of overvoltage against log *of current density is plotted, then the graph approximates to a straight line. Such plots are known as "Tafel plots". The diagram shows two typical plots.*

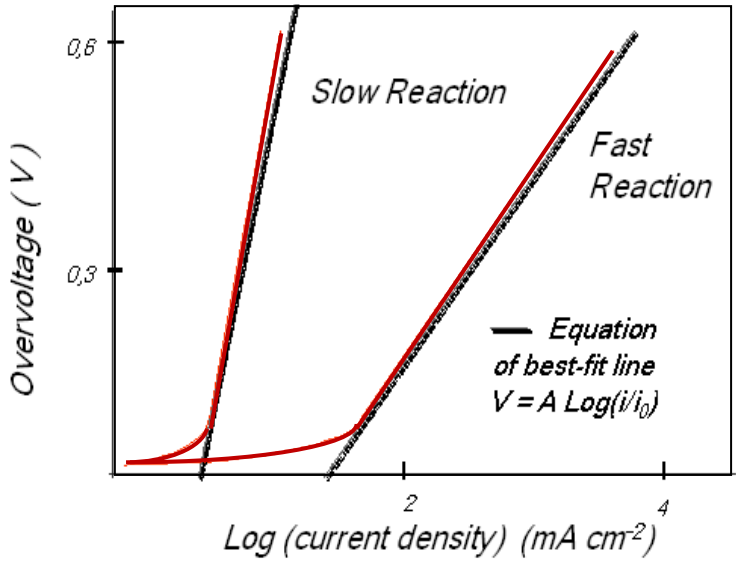

Fig 2.4.1.1 Tafel plots for slow and fast electrochemical reactions.

For most values of overvoltage its value is given by the equation

$$\Delta V_{act} = A \ln (i/i_0) \quad (1)$$

This equation is known as the "Tafel equation". The constant A is higher for an electrochemical reaction that is slow. The constant i_0 is higher if the reaction is faster. The current density i_0 can be considered as the current density at which the overvoltage begins to move from zero, it is usually called the "exchange current density".

For a fuel cell, the constant A is given by

$$A = RT/n\alpha F$$

Where n is the electrons mole transferred, the constant α is called the "charge transfer coefficient" and is proportional to the electrical energy applied that is harnessed in changing the rate of electrochemical reactions. Its value depends on the reaction involved and the material the electrode is made from, but it must be in range 0 to 1.0 .

The appearance of T might give the impression that rising the temperature increases the overvoltage. In fact this is very rarely the case, as the effect of temperature increases in i_0 with temperature far outweigh any increase in A. Indeed, we shall see that the key to making the activation overvotage as low as possible is this i_0, which can vary by several orders of magnitude. Furthermore, it is affected by several parameters other than the material used for the electrode.

There is a continual backwards and forwards flow of electrons from and to the electrolyte, this current density is i_0, the exchange current density. It is evident that if this current density is high, then the surface of the electrode is more active and a current in one particular direction is more likely to flow. This exchange current density i_0 is crucial in controlling the performance of a fuel cell electrode, it is vital to make its value as high as possible.

Imagine a fuel cell that has no losses at all except for this activation overvoltage on one electrode, its voltage would then be given by the equation

$$V = E - A \ln (i/i_o) \qquad (2)$$

Where E is the reversible OCV.

The importance of i_0 can be seen. The effect is to reduce the cell voltage by fairly fixed amount, as we could predict from the Tafel equation. The smaller the i_0, the greater is this voltage drop.

It is possible to measure this overvoltage at each electrode, either using reference electrodes within a working fuel cell or using half-cells. Table B.2.1 below gives the values of i_0 for hydrogen electrode at 25°C for various materials. The measurements are for flat smooth electrodes.

Metal	i_0 (A cm^{-2})
Pb	2.5×10^{-13}
Zn	3×10^{-11}
Ag	4×10^{-7}
Ni	6×10^{-6}
Pt	5×10^{-4}
Pd	4×10^{-3}

Table 2.4.1.1 i_0 for an acid electrolyte for various materials [23]

The most striking thing about these values is their great variation, indicating a strong catalytic effect.

However, the value of i_0 for real fuel cell electrode is much higher that values in Table 2.4.1.1, because of the roughness of the electrode. This makes the real surface area many times bigger, typically at least 10^3 times lager than the nominal length x width.

Moreover, i_0 at the cathode is much smaller than that at the anode, sometimes 10^5 times smaller. Indeed, it is generally reckoned that the overvoltage at the anode is negligible compared to that of the cathode, at least in the case of hydrogen fuel cells. For a low temperature, a typical value for i_0 would be about 0.1 $mAcm^{-2}$ at the cathode and about 200 $mAcm^{-2}$ at the anode.

Nevertheless, in direct methanol fuel cell, the anode overvoltage is by no means negligible. In these cases, the equation for the total activation overvoltage would combine the overvoltage at both anode and cathode, giving

$$\text{Activation Voltage drop} = A_a \ln(i/i_{0a}) + A_c \ln(i/i_{0c})$$

However, it is proved that this equation can be expressed as

$$\Delta V_{act} = A \ln (i/b)$$

where

$$A = Aa + Ac$$

And

$$b = (i_0a)^{(Aa/A)} + (i_0c)^{(Ac/A)}$$

this is exactly the same form as the equation (1). [25]

We have seen that the exchange current density i_0 is the crucial factor in reducing the activation overvoltage. A crucial factor in improving fuel cell performance is, therefore, to increase the value of i_0 especially at the cathode. This can be done in the following ways:

- *Raising the cell temperature. For a low-temperature cell, i_0 at the cathode will be about 0.1 $mAcm^{-2}$, whereas for a typical 800°C cell, it will be about 10 $mAcm^{-2}$.*
- *Using more effective catalysts. The effect of different metals in the electrode is shown in table 2.4.1.1*

- *Increasing the roughness of the electrodes. This increase the real surface area of each nominal 1 cm^2 and this increase i_0*
- *Increasing reactant concentration. For example using pure O_2 instead of air, this works because the catalyst sites are more effectively occupied by reactants.*
- *Increasing the pressure. This is also presumed to work by increasing catalyst site occupancy.*

Increasing the value of i_0 has the effect raising the cell voltage by a constant amount at most current and raising the open circuit voltage (OCV).

2.4.2 Fuel Crossover and Internal Current

Although the electrolyte of a fuel cell would have been chosen for its ion conducting properties, it will always be able to support very small amount of electron conduction.

In a practical fuel cell, some fuel diffuse from the anode through the electrolyte to the cathode. Here, because the catalyst, it react directly with the oxygen producing no current from the cell. This amount of wasted fuel that migrates through the electrolyte is known as fuel crossover.

These effect, internal currents and fuel crossover, are essentially equivalent. Although these two phenomena cause the same effect on the cell, in DMFC fuel crossover is more important. Nevertheless the effect on the cell voltage is easier to understand if we just consider the internal current.

In low-temperature cells, the flow of fuel and electrons cause a very noticeable voltage drop at open circuit. Users of fuel cell can readily accept that the working voltage of a cell will be less than the theoretical 'no loss' reversible voltage. However, at open circuit, when no work is being done, surely it should be the same. In DMFC, if operating on air at ambient pressure, the voltage will usually be at least ≈0.2 V less than the 1.21 V reversible voltage that might be expected.

Because of the internal current density, the cell current density is not zero, even if the cell is open circuit. So, the open circuit voltage will be lower than the theoretical OCV. This large deviation from reversible voltage is caused by the very steep initial fall in voltage that we can see in the curves of figure 2.4.2.1

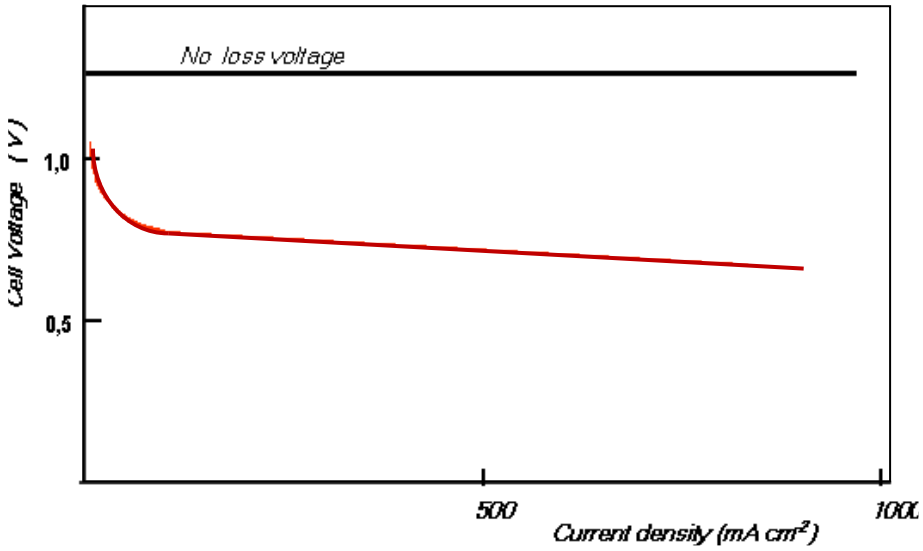

Fig 2.4.2.1 Fuel cell voltage modelled using activation and fuel crossover/internal current losses only

The graph tell us that a small change in fuel crossover and/or internal current, caused, for example, by a change in humidity of the electrolyte, can cause a large change in OVC.

The fuel crossover and internal current are obviously not easy to measure, an ammeter cannot be inserted in the circuit (one way of measuring it, could be to measure the consumption of reactant gases at open circuit).

In i_n is the value of this internal current density, then the equation for cell voltage that we have been using, equation (2), can be refined to

$$V = E - A \ln((i + i_n)/i_0)$$

The importance of this internal current is much less in the case of higher-temperature cells, because the exchange current density i_0 is so much higher and so the initial fall in voltage is not nearly so marked. On the contrary, in the case of low-temperature cells, it has a very marked effect on the open circuit voltage.

2.4.3 Ohmic Losses

Ohimic losses are due to the electrical resistance of the electrodes and the resistance to the flow of ions in the electrolyte. The size of the voltage drop is simply proportional to the current

$$V = I R$$

In most fuel cells the resistance is mainly caused by the electrolyte, though the cell interconnects or bipolar plates can also be important.

To be consistent with the other equation for voltage loss, the equation should be expressed in terms of current density. To do this we need to bring in the idea of the resistance corresponding to 1 cm2 of the cell, this quantity is called the area-specific resistance, for which we use the symbol r. The equation for the voltage drop the becomes

$$\Delta V = i\, r$$

where i is the current density. If i is given in mA cm^{-2}, then the area-specific resistance should be given in $k\Omega\ cm^2$.

Three ways of reducing the internal resistance of the cell are as follows:

- *the use of electrodes with the highest possible conductivity*
- *good design and use appropriate materials for the bipolar plates or cell interconnects*
- *making the electrolyte as thin as possible*

In DMFC, there is a large activation overvoltage at both electrodes, as a result, the activation overvotage is much grater than the ohmic (and so it dominates at all times).

2.4.4 Mass Transport or Concentration Losses

If the oxygen at the cathode of a fuel cell is supplied in the form of air, then it is self-evident that during fuel cell operation there will be a slight reduction in the concentration of the oxygen in the region of cathode, as the oxygen is extracted. The extent oj this change in concentration will depend on the current being taken from the fuel cell, and on physical factors relating to how well the air around the cathode can circulate and how quickly the oxygen can be replenished. This change in concentration will cause a reduction in the partial pressure of the oxygen.

Similarly, the same reasoning can be repeated for the fuel on the anode.

In both cases, the reduction in gas pressure will result in a reduction in voltage.

The following equation gives the change in OCV caused by a change in pressure of the oxygen [27]

$$\Delta V = RT/4F \ln (P_2/P_1)$$

We postulate a limiting current density i1 at which the fuel is used up at a rate equal to its maximum supply speed. The current density cannot rise above this value, because the fuel gas cannot be supplied at a greater rate. At this current density the pressure would have just reached zero. If P_1 is the pressure when the current density is zero, and we assume that the pressure falls linearly down to zero at the current density i1, then the pressure P_2 at any current density I is given by the formula

$$P_2 = P_1(1-i/i1)$$

So, we obtain

$$\Delta V = RT/4F \ln(1-i/i_1)$$

This give us the voltage change due to the mass transport losses. Nevertheless, if we want an equation for voltage drop, we should write it as

$$\Delta V_{trans} = -RT/4F \ln(1-i/i_1)$$

The term RT/4F is related to oxygen, but it will be different for different reactants, for example, for hydrogen in PEM it will be RT/2F.
In general, we may say that the concentration or mass transport losses are given by the equation

$$\Delta V_{trans} = -B \ln(1-i/i_1)$$

where B is a constant that depends on the fuel cell and its operating state.

Another approach that has no claim for a theoretical basis, but is entirely empirical, has become more favoured and yields an equation that fits the results very well [27]. This approach uses equation below, it gives a very good fit to the results, provided the constants m and n chosen properly.

$$\Delta V_{trans} = m \exp(n\, i)$$

The value of m will typically be about $3x10^{-5}$ V, and n about $8x10^{-3}$ cm^2 mA^{-1}.
The mass transport or concentration overvoltage is particularly important in cases where the air supply is not well circulated at the cathode. A particular problem is that the

nitrogen that is left behind after the oxygen is consumed can cause a mass transport problem at high currents, it effectively blocks the oxygen supply.

2.4.5 The Charge Double Layer

The charge double layer is a phenomenon which affects electrodes. Whenever two different materials are in contact, there is a build-up of charge on the surfaces or a charge transfer from one to other. In electrochemical systems, the charge double layer forms in part due to diffusion effects, as in semicoductors, and also because of the reactions between the electrons in the electrodes and the ions in the electrolyte, and also as a result of applied voltages. In the figure 2.4.5.1 might arise at the cathode of an acid electrolyte fuel cell.

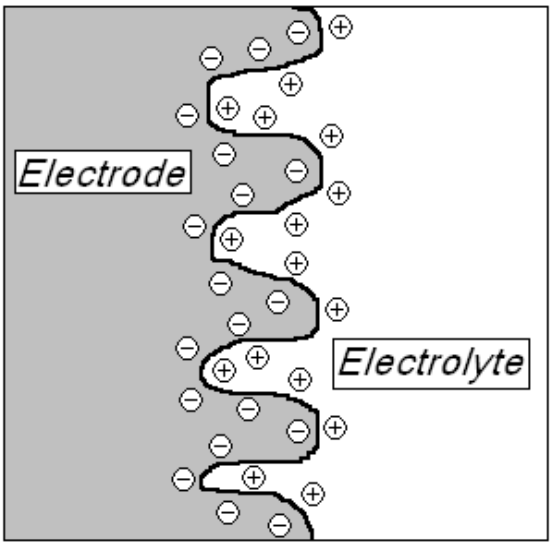

Fig pag 2.4.5.1 The charge double layer at the surface of a fuel cell cathode

Electrons will collect at the surface of electrode and H^+ ions will be attracted to the surface of the electrolyte. Certainly, these electrons and ions will take part in the electrode reaction.The probability of the reaction taking place obviously depends on the density of the charges, electrons and H^+ on the electrode and electrolyte surfaces. The more the charge the greater is the current. However, any collection of charge, such as of these electrons and H^+ ions at the electrode/electrolyte inteface will generate an electrical voltage. The voltage in this case is the activation overvotage we have been considering before. So the charge double layer gives an explanation of why the

activation overvoltage accurs. It shows that a charge double layer needs to be present for a reaction to occur, that more charge is needed if the current is higher and so the overvoltage. We can also see that the catalytic effect of the electrode is important, as an effective catalyst will also increase the probability of a reaction, so that an higher current can flow without such a build-up of charge.

The layer of charge on or near the elctrode/electrolyte interface is a store of electrical charge and energy, and as such behaves much like an electrical capacitor. If the current changes, it will take some time for this charge, and its associate voltage, to dissipate or build up, if the current reduces or increases respectively. So, the activation overvoltage does not immediately follow the current in the way that the ohmic voltage drop does. The result is that if the current suddenly changes, the operating voltage shows an immediate change due to internal resistance, but moves fairly slowly to its final equilibrium value. One way of modelling this is by using an equivalent circuit with the charge double layer rapresented by an electrical capacitor. The capacitance of a capacitor is given the equation

$$C = \varepsilon A / d$$

Where ε *is the electrical permittivity,* A *is the surface area, and* d *is the separation of the plates. In this case, A is the real surface area of the electrode, which is several thousand times grater than its length x width. Also* d *is very small, typically only a few nanometres. The result is that the capacitance will be of the order of a few Farads, wich is high in terms of capacitance values. The connection between this capacitance, the charge stored in it, and the resulting activation overvoltage, leads to an equivalent circuit as shown in figure 2.4.5.2*

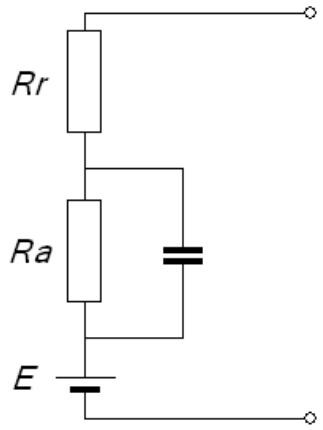

Fig 2.4.5.2 Simple equivalent circuit model of a fuel cell

The resitor Rr models the ohmic losses. A charge in current gives an immediate change in the voltage drop across the resistor. The resistor Ra models the activationovervoltage and the capacitor smoothes any voltage drop across this resistor. If we were to include the concetration overvoltage this would be incorporated into this resitor too.
Generally speaking, the effect of this capacitance resulting from the charge double layer gives the fuel cell a good dynamic performance in that the voltage moves gently and smoothly to a new value in response to a charge in current demand. It also permits a simple way to distinguish between the main types of voltage drop, and hence to analyze the performance of a fuel cell. [21,185]

2.5 The effect of pressure

he Gibbs free energy changes in a chemical reaction vary with the temperature. Equally important are the changes in Gibbs free energy with reactant pressure and concentration.
Consider a general reaction such as

$$rR \rightarrow mM$$

where r moles of R react produce m moles of M. Each of the reactants and products has and associated activity. This activity is designated by a, a_R being the activity of reactants and a_M the activity of the product. In case of gases behaving as ideal gases, it can be shown that

$$\text{activity } a = P / P^0$$

where P is the pressure or partial pressure of the gases and P0 is the standard pressure, 1 bar. Since fuel cells are generally gas reactors, this simple equation is very useful. We can say that activity is proportional to partial pressure. In the case of dissolved chemicals, the activity is linked to the molarity of the solution. For example, in the case of the water produced in fuel cells, it is can be either as steam or a liquid. For steam, we can say that

$$a_{H2O} = P_{H2O}/P^0_{H2O}$$

where P^0_{H2O} is the vapour pressure of the steam at the temperature concerned. This has to be found from the tables. In the case of liquid water product, it is reasonable approximation to assume that $a_{H2O} = 1$.

The activities of reactants and products modify the Gibbs free energy change of a reaction. Using thermodynamic arguments, it can be shown that in a chemical reaction such as that given before

$$\Delta gf = \Delta g^0_f - RT \ln (a^r_R / a^m_M)$$

where Δg^0_f is the change in molar Gibbs free energy of formation at standard pressure.

In case of the direct methanol fuel cell reaction, operating at room temperature

$$CH_3OH + 3/2\ (O_2) \rightarrow CO_2 + 2\ H_2O$$

The equation becomes

$$\Delta gf = \Delta g^0_f - RT \ln (a^{3/2}_{O2} / a_{CO2})$$

We can see that if the activity of reactants increases, Δgf becomes more negative, that is, more energy is released. On the other hand. If the activity of the product increases, Δgf increases, so becomes less negative, and less energy is released.

To see how this equation affects voltage, we can consider the following equation as resulted

$$E = -\Delta gf/ 6F + RT/6F \ln (a^{3/2}_{O2} / a_{CO2}) = E^0 + RT/6F \ln (a^{3/2}_{O2} / a_{CO2})$$

Where E^0 is the EMF at standard pressure. The equation shown precisely how raising the activity of the reactants increases the voltage. The equation which given an EMF in terms of product and/or reactant activity, is called "Nernst equation". The EMF calculated from such equation is known as the "Nernst voltage" and is the reversible cell voltage that would exist at a given temperature and pressure. [21,186]

2.6 Membranes

The research and development of novel proton exchange membranes (PEMs) is known to be one of the most challenging issues regarding the direct methanol fuel cell technology [28,30,31]. The PEM is usually designated as the heart of the DMFC, and should ideally combine high proton conductivity (electrolyte properties) with low permeability towards DMFC species. Additionally, it should have a very high chemical and thermal stability in order to enable the DMFC operation at up to ~150 °C. For this reason, a variety of PEMs have been developed by various researchers using different preparation methods. Some of the most common PEMs studied are listed in the table 3.1. The proton conductivity and the methanol permeability are indicated for each PEM [28,29].

The different companies producing polymer electrolyte membranes have their specific patents. However, a common theme is the use a sulphonated fluoro-polymers, usually fluoroethylene. The most well known and well established of these is Nafion (®Dupont), which has been developed through several variants since 1960s.

Polymer Electrolyte Membranes	Proton Conductivity (S/cm)	Methanol Permeability (cm^2/s) ($*10^{-6}$)	Reference
Blends of sulfonated poly[bis(phenoxy)phosphazene] and polybenzimidazole	0.060[a]	1.300	45
Nafion/montmorillonite nanocomposite	0.087[b]	0.770	46
Crosslinked poly(vinyl alcohol)/poly(acrylic acid)/silica hybrid	0.012[b]	0.210	50
poly(vinylidene fluoride-hexafluoropropylene) copolymer/Nafion blend	0.002[a]	0.200	52
Nitrile-functional, disulfonated poly(arylene ether sulfone)	0.090[b]	0.870	53
Nafion[1]/ORMOSILS composite	0.019[a]	1.750	54
Sulfonated poly(ether ether ketone ketone)	0.040[b]	0.575	55
Sulfonated poly(styrene-b-ethylene-r-butadiene-b-styrene) block copolymer	0.023[a]	0.820	56
Sulfonated poly(styrene)/poly(tetrafluoroethylene) composite	0.110[b]	0.670	57
Sulfonated co-polyimide	0.082[b]	0.480	58
4-Dodecylbenzene sulfonic acid-doped polyethylene glycol/silica hybrid	0.004[a]	0.020	59
Sulfonated poly(ethersulfone)-Cardo	0.004[a]	0.210	60
Sulfonated poly[(aryloxy)phosphazene]	0.035[b]	0.148	62
Sulfonated poly(styrene)	0.050[b]	0.520	63
Sputter coated palladium on Nafion[1]	0.016[a]	2.230	64
Phosphotungstic acid/poly(vinyl alcohol) composite	0.006[a]	0.454	65
IonClad[1] R-1010	0.080[b]	0.590	66
Nano-silica layered Nafion[1] composite	0.077[b]	0.920	67
Sulfonated poly(ether ether ketone)/zirconium oxide composite	0.005[a]	0.091	68
Palladium deposited on Nafion[1]	0.003[a]	0.430	69
4-Dodecylbenzene sulfonic acid-doped poly(ethylene glycol)/silica hybrid	0.004[a]	0.022	70
Nafion[1]/H-substituted montmorillonite composite	0.087[b]	0.800	71
Polypropylene-g-poly(styrene sulfonic acid)/Nafion[1] laminate	0.075[b]	2.800	73
Sulfonated poly(phthalazinone ether sulfone ketone)/silica hybrid	0.034[b]	0.415	74
IPN of crosslinked poly(2-acrylamido-2-methyl-1-propanesulfonic acid) and Nafion[1]	0.019[a]	1.120	75
Sulfonated naphthalene dianhydride based polyimide copolymer	0.120[b]	0.800	76
Sulfonated poly(arylene ether) copolymer	0.100[b]	0.810	77
Sulfonated poly(styrene-b-ethylene-r-butadiene-b-styrene) block copolymer	0.045[a]	2.600	78
Sulfonated polyimide	0.120[b]	0.570	79
Nafion[1]/montmorillonite nanocomposite	0.078[b]	0.100	64
Sulfonated poly(ether ether ketone)	0.070[b]	0.300	80
Chemically crosslinked poly(vinyl alcohol)/ poly(2-acrylamido-2-methyl-1-propanesulfonic acid)/poly(vinylpyrrolidone) blend	0.090[b]	0.600	81
IPN of Nafion[1] and polypyrrole	0.017[a]	0.600	82
Sulfonated polystyrene and sulfonated poly(2,6-dimethyl-1,4-phenylene oxide) blend	0.034[b]	2.350	83
Poly(styrene sulfonic acid) grafted onto poly(vinylidene fluoride)	0.102[a]	1.500	84
Crosslinked poly(vinyl alcohol) using sulfosuccinic acid	0.015[b]	0.330	85
Poly(vinyl alcohol)/poly(styrene sulfonic acid) blend	0.004[a]	1.00	86
Nafion[1] 117	0.026[a]	1.980	79
Nafion[1] 117	0.067[b]	1.980	87
Sulfonated poly(styrene-b-isobutylene-b-styrene) block copolymer	0.004[a]	0.090	79
Sulfonated poly(styrene-b-isobutylene-b-styrene) block copolymer	0.019[b]	0.150	87
Nafion[1]/poly(vinyl alcohol) blend	0.020[a]	0.650	88
Poly(vinyl alcohol)/poly(styrene sulfonic acid-co-maleic acid) blend	0.095[b]	0.266	88

a Through the plane of themembrane (two-electrode technique).
b Along the plane of the membrane (four-electrode technique).

Table 3.1 PEMs developed for DMFC

It is clear from table 3.1 that there are a number of PEMs that possess lower methanol permeability at similar or even higher proton conductivity when compared with Nafion. Other companies, such as Dow Chemical, Aciplex, Pall RAI, Asahi Chemical, and Solvay Solexis, have developed similar perfluorinated polymer membranes to Nafion [33,34]. However, most of these PEMs possess similar transport properties to Nafion. Other PEMs developed in the literature for the DMFC constitute a variety of design approaches, such as the synthesis of new ionic (sulfonic acid) random and block copolymers [53, 55,56,58,60,62,63,68,76-79,80,83,89-98], graft copolymerization of ionic polymers unto hydrophobic membranes [47,48,66,84,99], blending ionic and non-ionic polymers [45,52,49,81,85,86,88,100-114], the synthesis of interpenetrating networks of ionic and nonionic polymers[75,82,115-125], incorporating a variety of fillers (e.g., silica, montmorillonite) into ionic polymer membranes [44,46,50,51,54,57,59,61,65,69-71,74, 118,126-144], and coating ionic polymer membranes with thin barrier coatings [44,64,67,73,106,126-152].

- Random Copolymers

A number of sulfonic acid containing random copolymers have been synthesized for the DMFC [53,55,58,62,63,68,77,79,80,83,89,91-93]. Sulfonated poly(styrene) (SPS), a random copolymer of poly (styrene) and poly (styrene sulfonic acid) (PSSA) has been investigated for its use in the DMFC [63,83].

Interestingly, crosslinked PSSA membranes were one of the first PEMs used in fuel cells for the Gemini space program [153]. Additionally, sulfonated crosslinked polystyrene has been used in ion exchange columns and as water purification membranes [171]. SPS can be synthesized either by copolymerizing styrene and styrene sulfonic acid monomers or by postsulfonation [154] of poly(styrene) with a variety of sulfonating agents (e.g., acetyl sulfate, sulfur trioxide). Postsulfonation results in an electrophilic substitution of sulfonic acid to the aromatic group along the backbone of poly(styrene), and is a commonly used procedure to sulfonate polymers containing aromatic groups. This results in random copolymers, where the ion exchange capacity (IEC) or sulfonic acid content can be controlled by reaction conditions. Results show a simultaneous increase of both proton conductivity and methanol permeability with increasing sulfonic acid content in SPS membranes. A sharp increase in both aforementioned transport properties was observed at 14 mol % sulfonation. Selectivity is higher than Nafion; however, the chemical stability and durability of SPS membranes is not ensure for fuel cell applications.

Sulfonated poly(ether ether ketone) (SPEEK) and sulfonated poly(ether ether ketone ketone) (SPEEKK) have been synthesized through either Polymerization [32,60] or postsulfonation [68,93] techniques producing random copolymers with sulfonic acid substituted directly to the aromatic backbone.

These copolymers possess a number of beneficial attributes for the DMFC: good thermal stability, mechanical strength, and adequate conductivity [55,68,80,93]. Random copolymers synthesized by polymerization reveal that proton conductivity and methanol crossover both increase with increasing IEC of the membrane. However, selectivity ~7 times higher than Nafion were observed at the highest IEC synthesized. Postsulfonated copolymers were less selective than these membranes, but an improved DMFC performance was demonstrated compared to the copolymers synthesized by polymerization. Poly(imide)s have received considerable interest because they are both thermally and oxidatively stable [58,76,91,92].

Ultimately, these membranes were found to be unstable under fuel cell conditions.

Another polymer of interest is poly(phosphazene), because of its thermal and chemical stability and the ease at which side chains can be attached to the --P=N–backbone [89]. These polymers can also be easily sulfonated to control IEC and therefore proton conductivity. For example, it is sulfonated and crosslinked (using gamma radiation) poly[(aryloxy)phosphazene [62] and obtained proton conductivities approximately half of Nafion, but selectivity ~7 times higher. Another study sulfonated and crosslinked (with UV light) poly[bis(3-methylphenoxy)phosphazene] and demonstrated conductivities and crossover rates that were comparable with Nafion in a temperature range of 21 – 72 °C. These membranes exhibit good thermo-mechanical strength up to 173 °C [89].

Overall, selectivity of these membranes were approximately twice that of Nafion with methanol permeability 3-20 times lower than Nafion. Slightly lower DMFC voltages compared to Nafion were reported. Stability tests showed a cell voltage loss of ~0.8 mV/h,

which was attributed to growing contact resistance between the SPOP – PBI membrane and the Nafion binder in the catalyst layer.

A membrane of sulfonated poly(ether sulfone) [a polymer with six-membered aromatic rings linked with sulfide bonds] and 9,9-bis(4-aminophenyl fluorene) (CARDO) exhibited high mechanical, thermal, and chemical stability [60]. These membranes have proton conductivities and methanol permeability approximately one order of magnitude lower than Nafion at room temperature. Another study on sulfonated poly(ether sulfone)

demonstrated 10 times lower methanol permeabilities than Nafion [152]. Sulfonated poly(arylene ether sulfone) and sulfonated poly(arylene ether benzonitrile) random copolymers have been synthesized [53,77]. Both copolymers have similar aromatic backbones, which are attractive due to their thermal, mechanical, and oxidative stabilities. Transport properties of the sulfonated poly(arylene ether sulfone) membranes yielded selectivity ~3 times higher than Nafion, while the selectivity of the poly(arylene ether benzonitrile) membranes were ~4 times higher than Nafion. Polarization curves from DMFC tests for the poly(arylene ether benzonitrile) membranes showed higher cell voltages at corresponding current densities compared to Nafion.

- Graft Copolymer

Several investigators have grafted SPS or PSSA on a variety of hydrophobic polymers, such as poly(ethylene-tetrafluoroethylene) (ETFE), poly(vinylidene fluoride) (PVDF), and low-density poly(ethylene) (LDPE) [47,48,66,84,99]. Graft copolymerization usually consist of exposing the hydrophobic polymer membrane to a radiation source, which promotes the formation of radicals and functional groups on the membrane. This was followed by an in situ graft copolymerization of styrene or styrene sulfonic acid monomers. In the case of grafting styrene, copolymerization is followed by post-sulfonation of the membrane.

The relationship between the degree of grafting and proton conductivity for membranes consisting of PSSA grafted on ETFE [48]. At low degrees of grafting (< 30 wt %), conductivity was significantly lower than Nafion. At 30 wt % grafting, the conductivity showed an abrupt increase to values approximately double that of Nafion, and the conductivity continued to increase linearly up to 50 wt% grafting. Methanol and water uptakes increased linearly with the degree of grafting, and the selectivity for water to methanol was higher compared with Nafion. Methanol permeability experiments showed a 30% decrease compared with Nafion, however, the fuel cell performance of these graft copolymer membranes was lower than Nafion. The investigators attribute this to poor bonding between the catalyst layer and the membrane.

Generally, these membranes exhibited higher fuel cell voltages at higher current densities.

However, the stability of the MEA, specifically, adhesion of the catalyst layer to the membrane was an issue (delamination was observed when removing the MEA from the fuel cell). Further work [84] on PSSA grafted on ETFE, PVDF, and LDPE demonstrated approximately three times higher selectivity compared to Nafion with lower methanol

crossover and higher proton conductivity than Nafion. DMFC performance tests showed decreased performance with grafted ETFE and PVDF over time, but grafted LDPE membranes improved with time.

- Block Copolymers

A number of sulfonic acid containing block copolymers (i.e. ionic block copolymers) have been synthesized for the DMFC [56,78,81,87,90,94-98]. Ionic block copolymers are attractive because they chemically conjoin both ionic and nonionic monomers on the same polymer backbone in an ordered sequence. Block copolymers provide a unique template, where microphase separation occurs on a nanometer scale because of the thermodynamic incompatibility between unlike blocks forming a variety of self-assembled morphologies including spheres arranged on a cubic lattice, hexagonally packed cylinders, interpenetrating gyroids, and alternating lamellae [155]. This provides the potential for unique ordered morphologies, where transport properties can be tailored [98].

Initial studies on sulfonated block copolymers focused only on the sulfonation and the structural and thermal characterization of styrene-based block copolymers at low ion exchange capacities (IECs) [155-161]. These reports did not address transport properties. Recently, a number of investigators have examined the transport properties of sulfonated block copolymers at higher IECs (~1 – 2meq/g), and have shown comparable conductivities to Nafion (0.9 meq/g) [162-165].

Various research groups have examined sulfonated poly(styrene-b-ethylene-r-butylene-b-styrene) (S-SEBS) [56,78,95,96]. The styrene block of SEBS was sulfonated with a standard postsulfonation process in all of these studies. Similar to studies with SPS, both proton conductivity and methanol permeability increased simultaneously with increasing sulfonation levels [56,78]. Another study investigated the effect of casting solvent choice on morphology and transport properties in S-SEBS membranes [56,96]. Both proton conductivity and methanol permeability increased by an order of magnitude when the casting solvent was changed from tetrahydrofuran (THF) to a THF/methanol mixture. Small-angle Xray scattering (SAXS) results revealed a morphological transition from a preferentially ordered lamellar structure to a nonperiodic structure coinciding with the increased transport rates [96]. However, these morphological transitions did not significantly change the selectivity of the membrane.

A similar block copolymer, sulfonated poly(styrene-b-isobutylene-b-styrene) (S-SIBS), has been investigated [87,94,97]. Similar to S-SEBS, both proton conductivity and methanol permeability increased as IEC increased. However, the selectivity are similar to Nafion at all IECs.

Other block copolymers such as sulfonated poly (styrene-b-ethylene) (S-SE) [97] and sulfonated hydrogenated poly(styrene-b-butadiene) rubber (HSBR) [98] have been investigated as alternative PEMs. S-SE has proton conductivities as high as 0.11 S/cm (four-electrode), and a bi-continuous structure was observed with small-angle neutron scattering (SANS). For sulfonated HSBR, the SBR was hydrogenated to eliminate the double bonds in the butadiene block and then the styrene blocks were sulfonated. After sulfonation, the membranes exhibited lower proton conductivities and methanol permeability compared with Nafion.

Poly(arylene ether sulfone-b-polybutadiene) block copolymers are synthesized by a polycondensation reaction of poly(arylene ether sulfone) and poly(butadiene) and then postsulfonated [90].

Relatively high conductivities were achieved at low IECs. This result suggests that sulfonic acid groups on the flexible segments of the block copolymer can arrange into a more favorable morphology for transport.

- Blends

Research on polymer blends includes polyvinyl(alcohol) (PVA) and Nafion PVA and PSSA [86], PVA and poly(styrene sulfonic acid-co-maleic acid) (PSSA-MA) [88,100], PVA crosslinked with sulfosuccinic acid [85], PVA and poly(2-acrylamido-2-methyl-1-propanesulfonic acid) (PAMPS) [88,101], PAMPS and poly(2-hydroxyethyl methacrylate) (PHEMA) [102], sulfonated poly(sulfone) and acid-doped PBI [103], sulfonated poly(ether ketone) and PBI [49], and sulfonated poly(sulfone)/poly(ether sulfone) and SPEEK/poly(ether sulfone) [104]. These polymers have previously been investigated as it applies to pervaporation (liquid/vapor separation of binary mixtures) of ethanol/water mixtures (ethanol dehydration). The chemical selectivity of water over ethanol suggests that these polymers may increase proton/methanol selectivity. Since these polymer membranes alone are not proton conductors, it is difficult to project clear conclusions from their data.

The transport properties of Nafion/PVA blends have been investigated as a function of composition and annealing temperature. One key observation was the trends in proton and methanol transport in the Nafion/PVA blend membrane at 50 wt % PVA. As

annealing temperature increased, proton conductivity remained relatively constant, while methanol permeability decreased by almost an order of magnitude. These trends differ from most investigations, where proton and methanol transport usually increase or decrease simultaneously in sulfonic acid containing polymers with changes in polymer properties.

Also, the Nafion/PVA blend membrane at 5 wt % PVA and 230 °C annealing temperature had a similar proton conductivity, but three times lower methanol permeability when compared with Nafion. This increased selectivity was not observed in Nafion/PVA blend membranes (5 wt% PVA) at other annealing temperatures.

Blends of PVA with other sulfonic acid containing polymers have also been studied. PVA/PSSA blend membranes were investigated at various PSSA contents and annealing temperatures [86]. At 17 wt % PSSA and an annealing temperature of 110 °C, methanol crossover was half of Nafion, but proton conductivity was an order of magnitude lower.

*Similarly, polymer blends of PVA and PSSA-MA were investigated, where introducing maleic acid reduced membrane swelling when compared with pure PSSA [88,100]. PVA crosslinked with sulfosuccinic acid revealed similar transport property trends when compared with PVA/PSSA blends. A maximum in selectivity was observed at 17 wt % sulfosuccinic acid and an annealing temperature of 130 °C (0.015 S/cm; 3.3 *10^{-7} cm^2/s) [85]. Although this is technically not a polymer blend, this polymer is similar in concept to crosslinked blends that have both a sulfonic acid containing polymer and PVA.*

Polymer blends containing PAMPS and PHEMA [102]. Nafion (5 wt %) was added to this blend to increase flexibility in the dry state. At small PAMPS content (4 wt %), conductivities similar to Nafion were reported, but the membranes were still too brittle in the dry state. Methanol crossover experiments were not measured in this study.

Polymer blends of sulfonated poly(sulfone) and acid-doped PBI were investigated [103]. These membranes did not show any significant improvements for use in a DMFC, but proton conductivities were comparable to Nafion at 80 °C.

A number of investigators have explored PBI in PEMs for the DMFC [106-114,166-173]. PBI is interesting because it possesses both donor and acceptor hydrogen bonding sites, high thermal stabilities, chemical resistance, and mechanical strength. It has been used in acid-base blend membranes with PEEK and polysulfone [106], and it has been N-substituted with methyl and ethyl groups and doped with phosphoric acid [107]. The former study shows a 10-fold decrease in methanol permeability, but does not include

conductivity experiments. In the latter study, methanol crossover was less than Nafion, but proton conductivities were not comparable (3 orders of magnitude lower).

- Impregnated Membranes

A number of researchers have impregnated polymers within membranes using several strategies, including in situ polymerization and sorption within both swollen dense membranes and porous membranes.

An example is in situ polymerization of poly(pyrrole) within a Nafion membrane. This procedure entailed immersing Nafion in an acid electrolyte containing the monomer and then polymerizing within the membrane galvanostatically in an electrochemical cell. Results show a decrease in methanol permeability when compared with Nafion.

Another study incorporates poly(pyrrole) within a Nafion membrane with in situ polymerization, where peroxide was used as the free-radical initiator [116]. A decrease in methanol and water sorption compared to Nafion was reported.

Nafion membranes impregnated with poly(pyrrole) using in situ polymerization [82] and observed ~5 times increase in selectivity compared to Nafion. A sulfonic acid containing polymer, poly(2-acrylamido-2-methyl-1-propanesulfonic acid-co-1,6-hexanediol propylate diacrylate-co-ethyl methacrylate), (i.e. crosslinked PAMPS), was polymerized withina Nafion membrane and then subsequently crosslinked [121]. A reduction in methanol permeability compared to Nafion was observed, while a high proton conductivity was maintained.

A variety of methods are used to incorporate acid-doped PBI into a Nafion membrane [119], such as spin coating, dipping, and screen printing. Spin coated membranes reduced methanol permeability by 58% when compared with Nafion. Dipped membranes produced varied results over a range of PBI contents, but the best data reported a 50% reduction in methanol permeability compared to Nafion. Both of these methods, however, resulted in low proton conductivities.

Another study polymerized and crosslinked styrene monomers within a PVDF matrix followed by sulfonation of the impregnated polystyrene [120]. The authors refer to this membrane as a 'semi' interpenetrating network (IPN) and suggest that these membranes do not follow the same transport mechanisms as Nafion and grafted PSSA systems; this is prescribed to differences in water flux properties and distribution of sulfonic acid moieties. These membranes resulted in lower methanol permeabilities (95% less) and higher DMFC power densities when compared with Nafion [143].

IPN membranes of crosslinked P(AMPS-co-HEMA) and PVA has been developed [121]. Free-radical copolymerization and crosslinking of AMPS and HEMA were performed in a PVA matrix. PVA was crosslinked in a subsequent step with glutaraldehyde. Since the two crosslinking reactions were independent of one another. The crosslinking of AMPS and HEMA can be tailored to achieve high proton conductivities, and the crosslinking reaction of PVA can be optimized to induce the lowest methanol permeability. This concept was initially confirmed with water and methanol sorption experiments.

The benefits of polymer-filled microporous membranes in comparison to crosslinked polymers in both experiment and theory demonstrate that polymer-filled microporous membranes can effectively suppress the same amount of swelling compared to a highly crosslinked polymer, while increasing selectivity. At last, polymer-filled microporous membranes demonstrated an increase in proton conductivity without a significant increase in methanol crossover.

- Composite Membranes

Polymer membranes containing micrometer to nanometer size fillers (composite membranes) have been explored intensely for the DMFC [44,74,126-144,175,177,178]. A variety of fillers, including silica [50,51,70,74,82,131,141], zirconium phosphate [135,175,178], phosphotungstic acid [126], molybdophosphoric acid [138], Aerosil (silicon dioxide powder) [138], ORMOSILS (organically modified silicates) [54], silane-based fillers [54], titanium oxide [135], hydroxyapatite [130], laponite [143], montmorillonite [46,70,136], zeolites [140], and palladium [142], have been incorporated in a number of different polymer membranes including Nafion.

Silica has been frequently used as a filler, and these composite membranes demonstrate improved thermal [126] and mechanical stability [59], and maintain adequate water uptakes at elevated temperatures [59]. Silica has been incorporated within PVA/phosphotungstic acid (PWA) [126] polyethylene glycol (PEG) membranes doped with 4-dodecylbenzene sulfonic acid (DBSA) (via sol–gel process) [59,70], crosslinked PVA/poly(acrylic acid) (PAA) blends [50], Nafion/PWA (via sol–gel process) [51], sulfonated poly(phthalazinone ether sulfone ketone) (SPPESK) [74], macroporous silica matrix [131], and S-SEBS [141]. In all studies, introducing silica leads to decreased methanol permeability when compared with the parent polymer. Several problems were encountered, such as decreased water transport (resulting in lower proton conductivities), membranes becoming too brittle when the inorganic phase

*loading reached a critical level, and decreased fuel cell performance. These silica composite membranes generally shared similar trends and ranges with respect to proton conductivity (~0.01 – 0.03 S/cm) and methanol permeability (~ 1 – 5 *10^{-7} cm^2/s) [50,51,59,70,74,126,131,141]. The membranes containing PEG and DBSA exhibited permeabilities an order of magnitude lower than Nafion, while its conductivity was only half the value (selectivity ~double compared with other silica composite membranes).*

A number of investigators have also explored heteropolyacids as fillers in polymer membranes [128,132,133,137,139]. Heteropolyacids are strong acids composed of heteropolyanions and protons as the counterions and are good proton conductors in their crystalline form [137,162]. A heteropolyanion is a self-assembled structure that consists of one or more heteroatoms (e.g., phosphorus) surrounded by several additional metal-oxygen polyhedrons (metals include zirconium, tungsten, molybdenum). Composite membranes with heteropolyacids include zirconium oxide in SPEEK [128,133,137], boron phosphate within a perfluorosulfonic acid ionomer, organosilyl derivatives of divacant tungstosilicates in SPEEK [132], and zirconium phosphate sulfophenylenphosphonate in sulfonated polyetherketone (SPEK) [139]. Several researchers suggest that this strategy will reduce methanol crossover because of increased tortuosity (impermeable fillers), while increasing proton conductivity (heteropolyacid enhances proton mobility). Conductivity tests on these membranes were often measured at high temperatures (70 – 110 °C). Conductivities up to 0.035 S/cm (two-electrode) were observed at 110 °C [132]. An important issue regarding these composites is the potential for the heteropolyacids to leach out of the membrane in methanol/water solutions, which can result in lower conductivities.

Incorporating layered silicate nanoparticles (e.g., montmorillonite, Laponite, and modified montmorillonite) into polymers, such as Nafion and SPEEK, is another strategy researchers have explored to make nanocomposite membranes for the DMFC [46,72 ,136,143]. Montmorillonite and its derivatives were chosen as fillers because they enhance the mechanical properties of the membrane [71,143], improve barrier properties [46], prevent excessive swelling [143], and can conduct ions [136].

Interestingly, three different research groups prepared nanocomposite membranes of montmorillonite in Nafion using different techniques [46,71,136]. The most promising results were obtained from the solvent cast membranes in which proton conductivity was~20% higher than Nafion and methanol permeability was ~20 times less than Nafion [72]. In this study, permeability experiments were inconclusive as their methods were

incomparable to other standard experimental techniques. Significant differences between composites of Nafion and montmorillonite vs. Nafion and modified montmorillonite were not observed. Some samples containing montmorillonite were found to have increased methanol permeability when loading increased [46].

When Cloisite 30B was dispersed in Nafion1, methanol permeability decreased ~33% with only a 0.5 wt % filler content. When DMFC tests were performed on the Cloisite 30B nanocomposites, performance dropped ~50% when compared with Nafion [46]. Data from the SPEEK nanocomposites showed decreased proton conductivities (~300%), methanol permeabilities (~75%), and fuel cell performance (~25%) compared to Nafion [143].

Other researchers developed composite membranes of PVDF filled with nanoparticles, such as silica, zirconia, and aqueous mixtures of acids [144]. These membranes exhibited lower methanol crossover compared to Nafion, but due to the use of aqueous acids, corrosion-resistant materials for the fuel cell would be required in the fuel cell assembly. Palladium nanoscale agglomerates were impregnated into Nafion membranes to decrease

methanol diffusion by increasing toruosity [69]. These membranes were an order of magnitude lower in methanol permeability compared to Nafion, but conductivity also decreased significantly.

- Coated membranes

Coating PEMs with thin barrier layers is a technique that a number of investigators have pursued through a variety of deposition techniques [44,64,67,73,145-152]. One study coated a Nafion membrane with charged palladium particles via self-assembly, where a layer-by-layer technique was employed to achieve 1 – 5 double layers of palladium [146]. A methanol crossover two orders of magnitude lower than uncoated Nafion was observed at three self-assembling double layers, while the conductivity continually decreased as more double layers were formed on the surface. In addition to this study, other researchers have deposited thin palladium layers on Nafion membranes [64,147,150]. Other researchers used an electroless plating technique, in which Nafion was submerged in a palladium sulfate solution, followed by submersion in a hydrazine solution to coat Nafion membranes with palladium. Only a slight decrease in methanol crossover was observed [147]. However, DMFC tests reveal a lower performance compared to Nafion.

Another study used hexane/hydrogen plasma irradiation to deposit a thin barrier layer on the surface of a Nafion membrane [106]. This resulted in a lower methanol crossover with only~ 0.3 μm barrier layer. Low-dose electron beam (e-beam) exposure has also been used to modify the surface of Nafion membrane resulting in a thin barrier layer (~ 1.5 μm) [145]. This technique mainly affects the hydrophilic side chains and not the fluorine rich backbone. DMFC tests confirm higher power densities after e-beam exposure.

A multilayer composite have been developed with a Nafion membrane coated on both sides with PVA using an immersion technique. These membranes were exposed to post treatments, sulfonation followed by crosslinking with glutaraldehyde. Three immersions resulted in a 61% increase in selectivity. For MEA preparation, a PVA-coated Nafion membrane (1:1 wt ratio) was sandwiched between two Nafion membranes. The Nafion layers were placed on the outside of the multilayer composite in an effort to enhance catalyst adhesion to the membrane and increase conductivity. A 5 – 10% increase in cell voltage at all current densities was observed for the multilayer composite of Nafion and PVA.

Other polymers, such as poly(1-methyl pyrrole), have also been coated on Nafion membranes [152]. Methanol permeability showed a ~1000 times decrease compared to uncoated Nafion but proton conductivity showed a similar decrease. In addition, several other studies have used lamination techniques to coat Nafion [73,148,149]. A 37% reduction in methanol crossover was exhibited in multilayer membranes consisting of 44 μm thickness SPEEK membrane sandwiched between two Nafion membranes [149]. Laminated membranes consisting of poly(propylene)-g-PSSA and Nafion showed a consistent decrease in methanol permeability with increased crosslinking density. Also, DMFC tests showed a 22% increase in voltage compared to Nafion [73].

2.6.1 Nafion membrane

Nafion is a perfluorosulfonate ionomer membrane.

The preparation procedure of the electrolyte material is described in the following.

The starting point is polyethylene. Its molecular structure based on ethylene is shown in figure 2.6.1.1

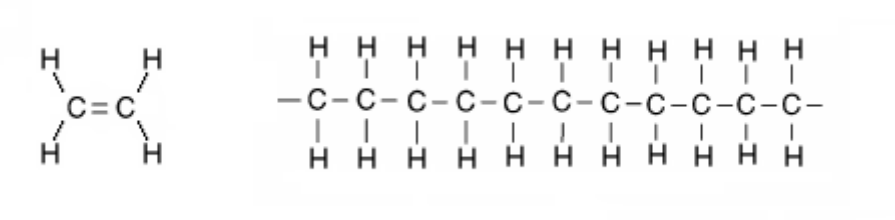

Fig. 2.6.1.1 Structure of ethylene and polyethylene

This basic polymer is modified by substituting fluorine for the hydrogen. This process is called perfluorination and the product is called tetrafluoroethylene. The modified polymer, shown in figure 2.6.1.2 is polytetrafluoroethylene or PTFE, commonly named Teflon, the registered trademarked of ICI.

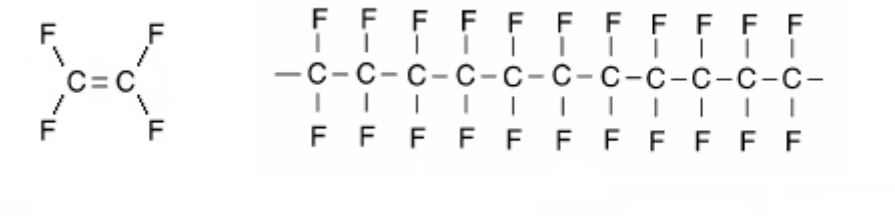

Fig. 2.6.1.2 Structure of tetrafluoroethylene and polytetrafluoroethylene (PTFE)

This materials has a very important role in the development of fuel cells. The strong bonds between the fluorine and the carbon make it durable to chemical attack. Another important property is the strongly hydrophobic and so it is used in fuel cell electrodes to drive the product water out of electrode, and thus it prevents flooding.

However, to make an electrolyte, a further stage is needed. The basic PTFE polymer is sulphonated, a side chain is added, ending with sulphonic acid HSO_3. One possible side chain structure is shown in figure 2.6.1.3.

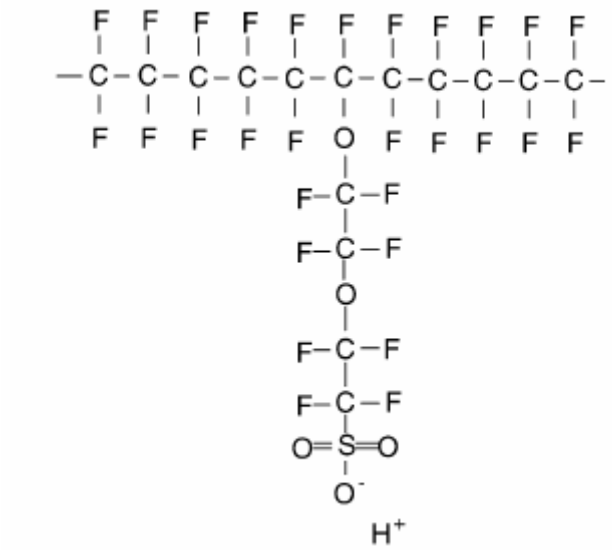

Fig. 2.6.1.3 Example structure of a sulphonated fluoroethylene

The HSO_3 group is ionically bonded, and so the end of the side chain is SO_3^- ion. For this reason, the resulting structure is called an ionomer. The result of these SO_3^- and H^+ ions is that there is a strong mutual attraction between positive and negative ions from each molecule. The result is that side chain molecules tend to cluster within the material. The sulphonic group is highly hydrophyllic and attracts water molecules. This gives rise to the formation of hydrophyllic regions within a generally hydrophobic matrix. The hydrophyllic regions around the clusters of sulphonated side chain lead to the absorpition of large quantities of water, increasing the weight and the volume of the material, this phonomenon is known as swelling. Whitin these hydrated regions, the H^+ ions are relatively weakly attracted to the SO_3^- group and are able to move. [174,187]
The resulting material has different phases, diluted acid regions within a tough and strong hydrophobic structure, as shown in figure 2.6.1.4 .

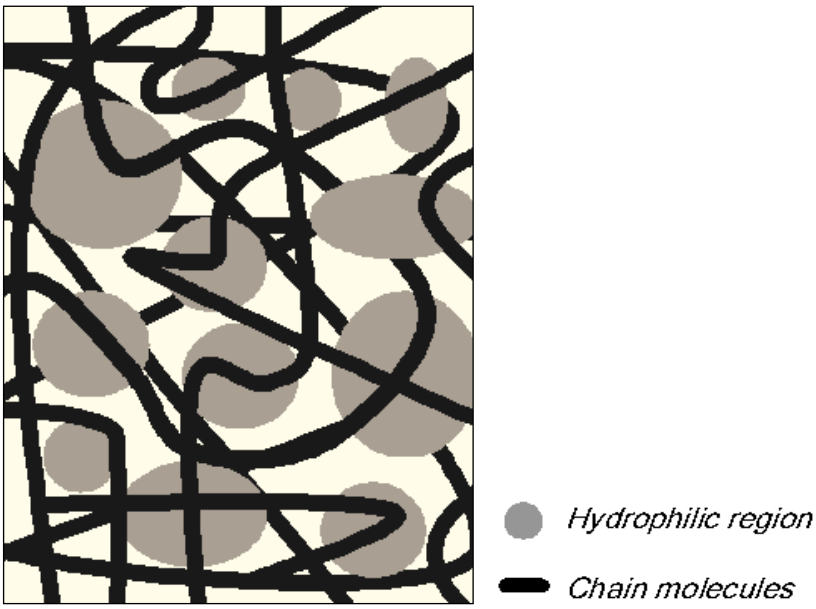

Fig. 2.6.1.4 The structure of Nafion-type membrane materials.
Long chain molecules containing hydrated regions around the sulphonated side chain

Although the hydrated regions are somewhat separated, it is still possible for H^+ ions to move through the supporting long molecule structure. In a well hydrated electrolyte, there will be about 20 water molecules for each SO_3^- group side chain. This will typically give a conductivity of about 0.1 S cm^{-1}. By decreasing the water content, the conductivity decreases.

From the point of view of fuel cell use, the main features of Nafion are that:

- *It is chemically highly resistant*
- *It is strong (mechanically), and so can be made into very thin films*
- *It is acid*
- *It can absorb large quantities of water*
- *If it is well hydrated, it is a good proton conductors*

3. AIM OF RESEARCH ACTIVITY

The development of the DMFCs technology requires increasing the performance of the polymer electrolyte membrane. At the present, the most widely used electrolyte is based on Nafion (®Dupont), which has been developed for PEMFCs, because it has an high proton conductivity, good thermal and mechanical properties, low cost. However, Nafion membranes present a high methanol crossover causing a drastic reduction in efficiency.

The problem to obtain polymeric proton conducting membranes retaining high proton conductivity and good mechanical stability above 100°C, and having low methanol permeability, can be overcome by the development of hybrid membranes containing a nano-dispersed proton conductor which above 100°C is able to facilitate (or even increase) the membrane hydration and to reduce the membrane permeability to methanol.

The aim of the present research activity is to study new polymeric electrolyte membranes suitable for DMFCs based on Nafion modified with the addition of nano-composite inorganic materials.

The nano-composite materials proposed are based on a layered inorganic proton conductor, α-zirconium phosphate (α-$Zr(HPO_4)_2$ H_2O), which is inserted in the Nafion matrix by two different techniques, obtaining Nafion composite membranes containing high aspect ratio particles of exfoliated α-zirconium phosphate ($NZrP_{exf}$) and Nafion composite membranes with loadings of in situ grown α-zirconium phosphate ($NZrP_{isg}$).

This study deals with the measurement of methanol permeability of these membranes, changing the temperature, the mixing rate and the methanol concentration. The swelling phenomenon, that affects the behaviour of the membrane, was also investigated.

A new laboratory apparatus and experimental procedure are employed for the measurement of methanol permeability. This procedure allows an easy calculation of the permeability. On the other hand, the determination of the diffusivity is not considered due to difficulty in the measurement of the partition coefficient.

To compare the performance of different membranes, it is also required to determinate the through-plane and in-plane proton conductivity of the NZrP membranes as a function of the filler loading at 40 °C and 100% RH.

The selectivity, defined as methanol permeability / proton conductivity ratio is used to identify the best membrane.

Summarizing, the research program is developed by following these steps:

1) *characterization of membranes*
2) *development of an experimental procedure for permeability measurement*
3) *measuring the methanol permeability of different membranes*
4) *correlation of data acquired*
5) *study of the swelling phenomenon of the membranes*

4. EXPERIMENTAL

4.1 Nafion Modified

Nafion is a highly versatile material. The specific structure allows to modify physical and chemical properties by the introduction of inorganic nanoparticles in the polymeric matrix encouraged the development of composite membranes in order to increase the proton conductivity and to reduce the methanol permeability.

Layered zirconium phosphate α–$Zr(HPO_4)_2\,H_2O$ (ZrP) can be used as filler of polymeric membranes, because of ion exchange properties and good chemical and thermal stability [174,176]. Consequently, the presence of ZrP nanoparticles improves the Nafion mechanical properties and the fuel cell performances, at temperatures above 100 °C, moreover reducing methanol cross-over [177,178].

In this work, the methanol permeability of Nafion/ZrP membranes obtained by two different techniques was studied:

- *Nafion composite membranes containing high aspect ratio particles of exfoliated α-zirconium phosphate ($NZrP_{exf}$) [175]*
- *Nafion composite membranes with loadings of in situ grown α-zirconium phosphate ($NZrP_{isg}$) [175]*

4.2 Preparation of the membranes

- Preparation of a Gel of ZrP in dymethylformamide

At first, a crystalline ZrP was prepared by the direct precipitation method in the presence of hydrofluoric acid [16]. A colloidal dispersion of ZrP intercalated with propylamine in water was prepared by slowly adding 16.6 mL of 0.1 M propylamine to a suspension of 0.5 g microcrystalline ZrP in 33 mL water [184]. The dispersion was left under stirring at room temperature for 24 h and then treated with 6 mL of 1 M HCl (pH <2) to regenerate the hydrogen form of zirconium phosphate. The solid was separated from the solution and washed with water under vigorous stirring. A gelatinous precipitate was settled by centrifugation at 3,000 rpm. The washing was repeated till the elimination of chloride ions, which were detected by precipitation with 1 M AgNO3. An amount of the ZrP gel in water, containing 1.5-2.5 wt.% anhydrous ZrP and x mL water, was washed thrice with

4x mL of dymethylformamide (DMF). After each washing, the ZrP gel was separated from the solution by centrifuging at 3,000 rpm. The final gelatinous product contained 2 wt. % anhydrous ZrP in DMF [182].

- Preparation of $NZrP_{exf}$

The commercial Nafion (5 g) dispersion was concentrated at 80 °C to reduce the volume by 90%. About 10 mL of DMF was added to the remaining solution and the volume was reduced again. The procedure was repeated several times in order to ensure the complete removal of water and alcohols. The final dispersion contained about 15 wt.% Nafion in DMF. A weighed amount of ZrP gel in DMF was added to the polymer solution and the mixture was held under stirring at room temperature for about 5 h and cast on a Petri dish. The solvent was evaporated at 100 °C overnight. Finally, the composite membranes were washed with a 1 M HCl solution at room temperature for 24 h and then heated at 100 °C for 4 h. Composite membranes with filler contents in the range 0.25 - 7 wt.% and thickness between 75 and 100 nm were prepared. Neat recast Nafion membranes, to be used as reference, were also prepared by the same synthetic procedure.

- Preparation of $NZrP_{isg}$

Recast Nafion membranes with loadings of in situ grown ZrP in the range 5 - 20 wt.% were prepared as described in [185,186]. A solution of ZrP precursors in DMF was prepared as follows: 0.10 g of zirconyl propionate was dissolved in 4.3 mL of DMF; separately, 0.18 g of phosphoric acid was dissolved in 4.3 mL of DMF. The first solution was added to the second one under stirring at room temperature, thus obtaining a clear solution (P/Zr = 4, [Zr] ≈ 0.05 M). A weighed amount of the ZrP precursor solution in DMF was added to a 15 wt.% Nafion dispersion in the same solvent so that the ratio between the Zr moles and the Nafion equivalents was in the range 0.2 - 1.7. The mixture was held under stirring at room temperature for about 15 min and cast on a Petri dish. The solvent was evaporated at 100°C overnight. The samples were then equilibrated with a 1 M NaCl solution at 80 °C for 4 h, rinsed in water at room temperature and then heated at 140 °C for 4 h. Finally, the membranes underwent the following standard treatment: 1 h in boiling 3% H_2O_2, 1 h in boiling 0.5 M H_2SO_4, 1 h in boiling H_2O, three washings with H_2O followed by drying in air. The thickness of these membranes was in the range 90-100 nm [175].

4.2 Basic Characterisation

The structure of α-layered ZrP is built up by the packing of layers made of planes of zirconium ions bonded, on both plane sides, to monohydrogen phosphate groups [22]. ZrP undergoes infinite swelling when propylamine is intercalated from aqueous solutions with loadings in the range 40-60% of the ZrP ion exchange capacity [184]. The resulting colloidal

dispersion contains single solvated layers. As the intercalation does not significantly modify the covalent structure of the layers [182], the size of the solvated layers depends on the morphology of the ZrP microcrystals. Therefore, it is possible to obtain dispersions containing high aspect ratio lamellar particles if sufficiently large ZrP microcrystals are used as a starting material. Treatment of the dispersion with hydrochloric acid leads to the regeneration of the ZrP hydrogen form and to partial layer reaggregation with the formation of gels of ZrP/H_2O. The gel water can be replaced with solvents miscible with water. Due to the presence of hydroxyl groups on the surface of ZrP particles, stable gels are obtained with solvents that are polar and, preferably, capable of forming hydrogen bonds. In this work, gels of ZrP in DMF were used to prepare $NZrP_{exf}$ membranes with filler loadings up to 7 wt.%.

Particles of exfoliated ZrP have the largest dimension in the range 100-200 nm and thickness of few nanometers with aspect ratio of at least 20. Such morphology is completely different from that observed for $NZrP_{isg}$ membranes [185] where the filler consists of low aspect ratio particles of some tens of nanometers.

The presence of the exfoliated filler also has a strong influence on the thermal behaviour and on the elastic modulus of the membranes. Figure 4.2.1 shows that in comparison to neat Nafion, the beginning of thermal decomposition is delayed to a great extent for a sample of $NZrP_{exf}$ 2 wt.% and to a much smaller extent for a sample of $NZrP_{isg}$ 15 wt.%: more specifically a weight loss of 2% occurs at 295 °C for neat Nafion, at 307 °C for $NZrP_{isg}$ 15 wt.-% and at 368 °C for $NZrP_{exf}$ 2 wt.%. The large decomposition delay observed for $NZrP_{exf}$ 2 wt.% is typical of composites filled with high aspect ratio particles, being associated with the barrier effect of the filler particles towards the diffusion of the gaseous species involved in the thermal decomposition of the membrane.

The elastic modulus of $NZrP_{exf}$ membranes, previously conditioned at 53% RH, was determined by stress-strain mechanical tests at room temperature. Figure 4.3.1 shows

the modulus proportional changes, %DE = 100[E(NZrP$_{exf}$)/E(Nafion) -1], as a function of the filler loading.*

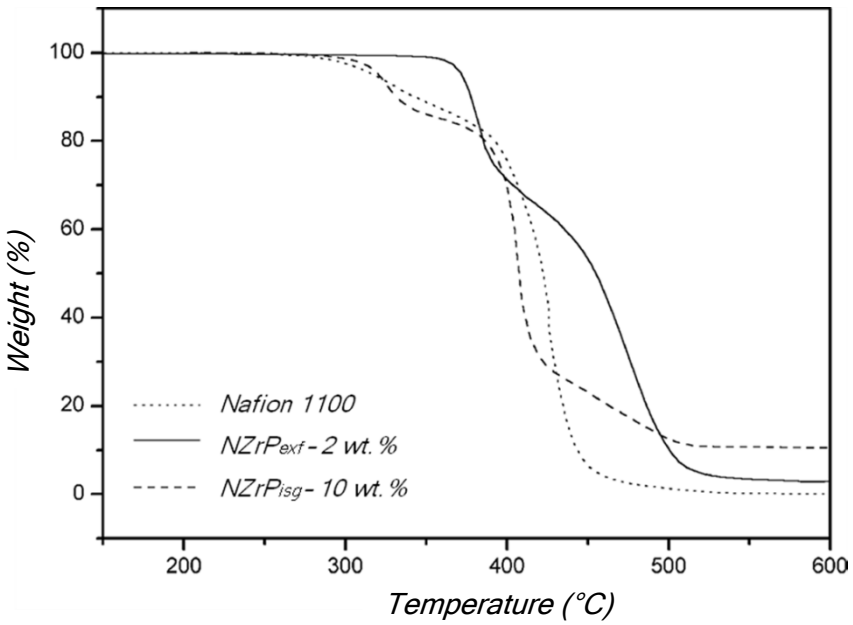

Fig. 4.3.1 Weight loss curves in air for the indicated membranes (heating rate 10 °C min^{-1})

The %DE values of NZrP$_{isg}$ membranes, calculated from the data of ref. [185], are reported for comparison. It is clearly seen that the modulus enhancement determined by the presence of the filler is much higher for the membranes filled with ZrP$_{exf}$ and that the same %DE value is reached with ZrPi$_{sg}$ loadings, which are about four times higher than the ZrP$_{exf}$ loadings.

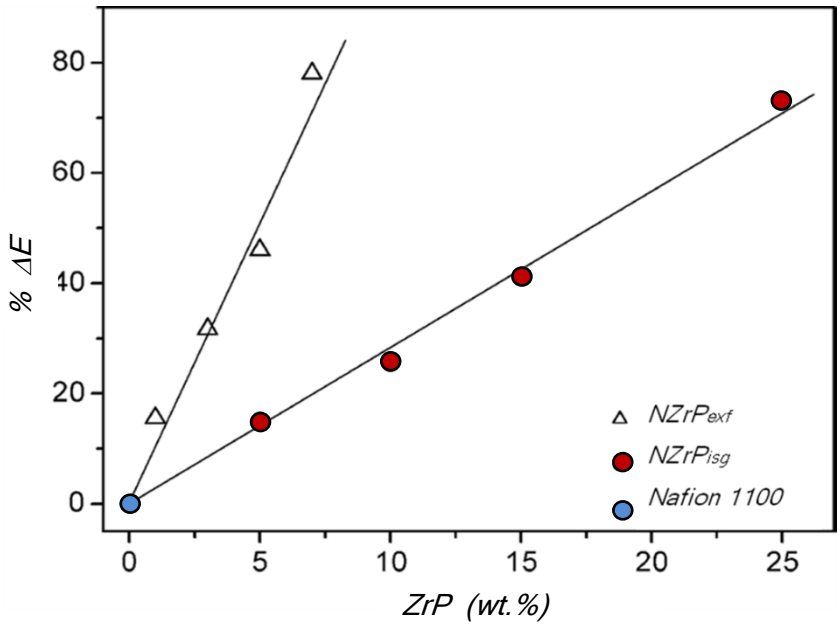

Fig. 4.3.2 Elastic modulus proportional changes, %DE = 100[E(NZrP$_{exf}$)/ E(Nafion) -1], as a function of filler loading for NZrP$_{exf}$, NZrP$_{isg}$ membranes.*

4.4 Experimental Apparatus

Fig. 4.4.1 Experimental apparatus

The figure 4.4.1 shows the experimental apparatus used for the methanol permeability measurements of the proton exchange membranes

Following, a detailed description of the various components:

- *outside pyrex flask, figure 4.3.2. It contains a solution of water-methanol-isopropanol, the volume is approximately one litre. It has three openings arranged respectively to insert the thermometer, the vessel containing the membrane and the opening that allows to keep a sample for the measurements. Inside the container there is also magnet that allows, if necessary, to obtain the required mixing rate.*

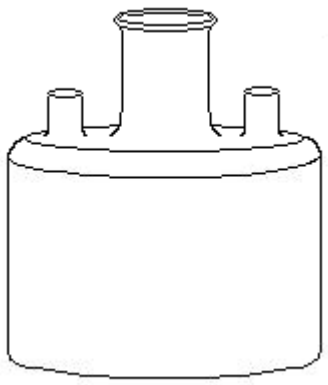

Fig. 4.4.2 Outside pyrex flask

- *Figure 4.4.3 shows a pyrex cylindrical cell, the measuring cell, with a volume of about 0.4 litres, containing the solution of water and isopropanol 0.5 wt. The upper end is arranged to support the mechanic mixer, while the bottom has a flange that allows to fix the membrane under test, by an aluminium ring, shaped according to the diameter of the ring. The cell also has an opening with a cap that allows to keep the sample of solution by microsyringe.*

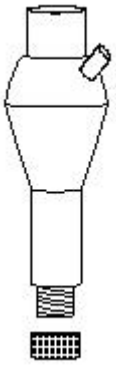

Fig. 4.4.3 Measuring cell in which the membrane is fixed by a flange

- *The mechanic mixer, showed in figure 4.4.4, consists of electric motor that rotates the pyrex arm with fins that is put inside the measuring cell, in order to stir the solution.*

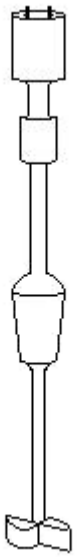

Fig. 4.4.4 Mechanic mixer

- *Magnetic mixer, figure 4.4.5 . It consists in a magnet located into the outside flask which is put in rotation by compressed air sent in a turbine.*

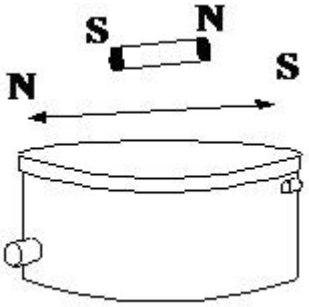

Fig. 4.4.5 Magnetic mixer

Moreover, are used the following devices (not showed):

- *Water bath, that surrounds the measuring device and allows to perform the tests at the desired temperature.*

- *Gas-Chromatograph HP5890 equipped with a capillary column SPB-1 and FID detector using isopropanol (0.5 wt %) as internal standard. It allows to carry out the analysis of the sample of the solution withdrawn from the measuring cell at different times.*

- *Flowmeter. It allows to adjust the air flow entering the turbine and therefore adjust the degree of mixing of the solution that depends on the speed of rotation of the magnet.*

At t = 0 in the internal volume, the measuring cell, there is only distilled water and isopropanol 0.5 wt %, while in the external volume, the flask, there is an aqueous solution of methanol 5 wt % and isopropanol 0.5 wt % .

The experimental apparatus allows to properly vary the operating conditions

- Temperature regulation

The water bath allows to operate at the chosen temperature. The adjustment of the water bath temperature is through by a PID controller.

- Concentration regulation

it can be done changing the concentration of methanol in the solution in the outside flask. In all tests, the concentration of methanol is set at 5 wt %, in order to obtain the same driving force for the different membranes and facilitate the comparison operation.

- Mixing rate regulation

The flowmeter allows to control the air flow it in the turbine, therefore, it will adjust the speed of rotation of the magnet and with it the degree of mixing of the solution.

The solution in the measuring cell is always stirred in order to ensure a more accurate measurements which are not influenced by diffusion resistances.

4.5 Analytical Method

Experimental analysis for methanol (CH_3OH) permeability of proton exchange membranes, through the device described in paragraph 4.4, needs the use of a gas-chromatograph.

A sample of solution, about 0.2-0.5 μl, is withdrawn from the measuring cell by microsyringe at different times (t), it is vaporized and analyzed for the methanol content using Helium as carrier flow. The analysis is carried out using isopropanol (C_3H_7OH) 0.5 wt % as internal standard. For that reason, in both in the flask and in the internal volume of the measuring cell, there will be the same concentration of isopropanol, 0,5 wt % ,in order to avoid its flow through the membrane.

We compared the effect that the isopropanol has on the swelling phenomenon to that of methanol.

Identified the internal standard, we proceed to calibrate the gas-chromatograph by injecting known amounts of solution with isopropanol 0.5 wt % of and varying percentages of methanol.

The gas chromatograph will provide a chromatogram with peaks of isopropanol approximately constant, since its weight percentage in the sample is always the same, and peaks of methanol, which vary depending on the composition.

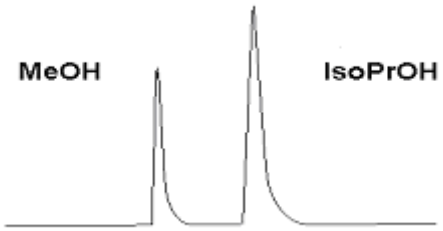

Fig. 4.5.1 A sample chromatogram

The relationship between the peak of isopropanol and methanol is directly proportional to the ratio between their concentrations. This will allow us to calculate a calibration curve (regression line) to which we will use to identify the unknown quantity of methanol present in the samples.

4.5.1 Mass balance

The flow of methanol through the proton exchange membrane must be derived from the well know Fick's equation:

$$N = -D\frac{d(C^*)}{dx}$$

The flow N is measured in mol/(s cm^2)

C : methanol concentration in the membrane C* = K* C [=] mol/l*

C : methanol concentration in the liquid bulk [=] mol/l

K: partition equilibrium constant between the membrane and the adjacent solution*

x : coordinate along the direction of diffusion [=] cm

D: methanol diffusion coefficient in the membrane [=] cm^2/se

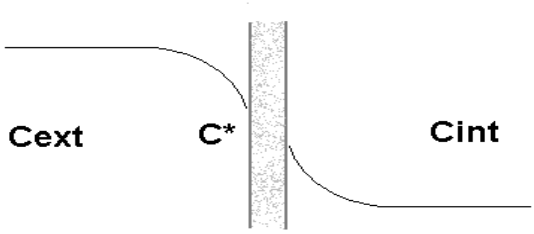

Fig. 4.5.1.1 Concentration profile near the membrane

Since the partition coefficient is not easily measurable, should use the concept of permeability. The permeability of methanol through the membrane is defined in the following equation:

$$N = P\frac{\Delta C}{\delta}$$

where

P : Permeability P = f(D, K) [=] cm²/s*

ΔC = Cext - Cint(t) Driving force for the concentration [=] mol/lt

δ : thickness of the membrane [=] cm

The mass bilance for the internal volume will be:

$$V\frac{d\Delta C}{dt} = -\frac{S * P * \Delta C}{\delta}$$

S : surface S = πD²/4 [=] cm²

V : internal volume of measuring cell [=] l

δ : thickness of the membrane [=] cm

ΔC = Cext - Cint(t) [=] mol/l

Resolution of the differential equation:

$$\frac{d\Delta C}{\Delta C} = -\frac{S * P}{V * \delta}dt$$

$$\ln(\Delta C) = -\frac{S * P}{V * \delta}t + Cost$$

If the initial conditions are t = 0 and ΔC = Cext, the solution is:

$$\Delta C = Cest * \exp\left[-\frac{S * P}{V * \delta} t \right]$$

at last, we obtain

$$C\text{int}(t) = Cest - Cest * \exp\left[-\frac{S * P}{V * \delta} t \right]$$

The solution of the differential equation, obtained from the global mass bilance in transient conditions, shows an exponential trend with time of the methanol concentration in the internal volume, Cint (t).
Nevertheless, if we assume that the concentration remains constant on time, due to the large volume of the flask, and Cest >> Cint (t), and assuming t_0 = 0, we obtain the following equation:

$$C\text{int}(t) = Cest\left(\frac{S * P}{V * \delta} \right) t$$

that describes a linear trend of the methanol concentration with time.
Knowing the flow of methanol from the experimental measurements

$$N = \frac{n_{CH3OH}}{t * S}$$

we can calculate the permeability of proton exchange membrane:

$$P = N \frac{\delta}{\Delta C}$$

4.6 Experimental procedure

The methanol permeability of a given proton-exchange membrane is measured in the range of temperature between 20 °C and 80 °C, that is the temperature range of interest for DMFC.

The experimental apparatus also allows to evaluate the influence of the mixing rate on the methanol flow through the membrane and then revealed the presence of possible diffusion resistance through the boundary layer.

An adequate stirring in the flask allows the system to approximate a perfectly mixed. Differently, we would have a gradient of concentration in close proximity to of the membrane and than a different methanol concentration in the bulk of the liquid. It happens when the magnet is unmoving.

It is important to emphasize that the stirring in the internal volume of 0.2 litres, using the mechanic mixer, is always present as necessary for a more precise measurement. In fact, the stirring ensures that the sample is not influenced by any diffusion resistances, if they are present.

Moreover, the experimental apparatus, in comparison with the other apparatus described in literature, shows the advantages of simple operation and a more accurate control of measurements conditions. [179,180]

In paragraph 4.5.1 we report in detail the procedure employed for measurement of methanol permeability of commercial Nafion, as an example.

4.6.1 Commercial Nafion membrane

We propose to evaluate the methanol permeability as function of temperature, mixing rate and constant methanol concentration in the external volume.

The initial conditions are reported in table 4.6.1.1:

Table 4.6.1.1 Initial conditions

	CH_3OH	C_3H_7OH	Volume	T	Stirring
Ext	5%	0.50 wt%	1000 ml	25 °C	450 rpm
Int	0	0.50 wt%	20 ml	25°C	450 rpm

In this sample we choose to take the samples after 4 min, 10 min, 18 min, and then every 8 min. For each sample there will be a corresponding chromatogram whereby we

can determine the methanol concentration through the ratio between the area of two peaks corresponding to methanol and isopropanol 0.5 wt % .
In this case, we obtain the following values grouped in table 4.6.1.2:

Table 4.6.1.2 Values of the area of the peaks

t (min)	Area 1 MeOH	Area 2 IsoPrOH	Area1/Area2
4	627	17075	0.036
10	1591	17463	0.091
18	2710	16691	0.162
26	3511	15479	0.226
34	4410	15051	0.293
42	5602	15660	0.357
50	6150	14500	0.424
58	10564	20246	0.521

Knowing the slope of the calibration curve (0.72032) will allow us to calculate the methanol concentration (wt %):

$$\frac{MeOH}{Iso\mathrm{Pr}OH} = \frac{Area1}{Area2} * 0.72032$$

Table 4.6.1.3 Experimental Cint calculated for Commercial Nafionat 25°C and 450 rpm

t (min)	Area1 / Area 2	MeOH / IsoPrOH	% MeOH
4	0.036	0.051	**0.025**
10	0.091	0.126	**0.063**
18	0.162	0.225	**0.112**
26	0.226	0.314	**0.157**
34	0.293	0.406	**0.203**
42	0.357	0.496	**0.248**
50	0.424	0.588	**0.294**
58	0.521	0.724	**0.362**

Plotting the values obtained we find an approximately linear trend of concentration with time:

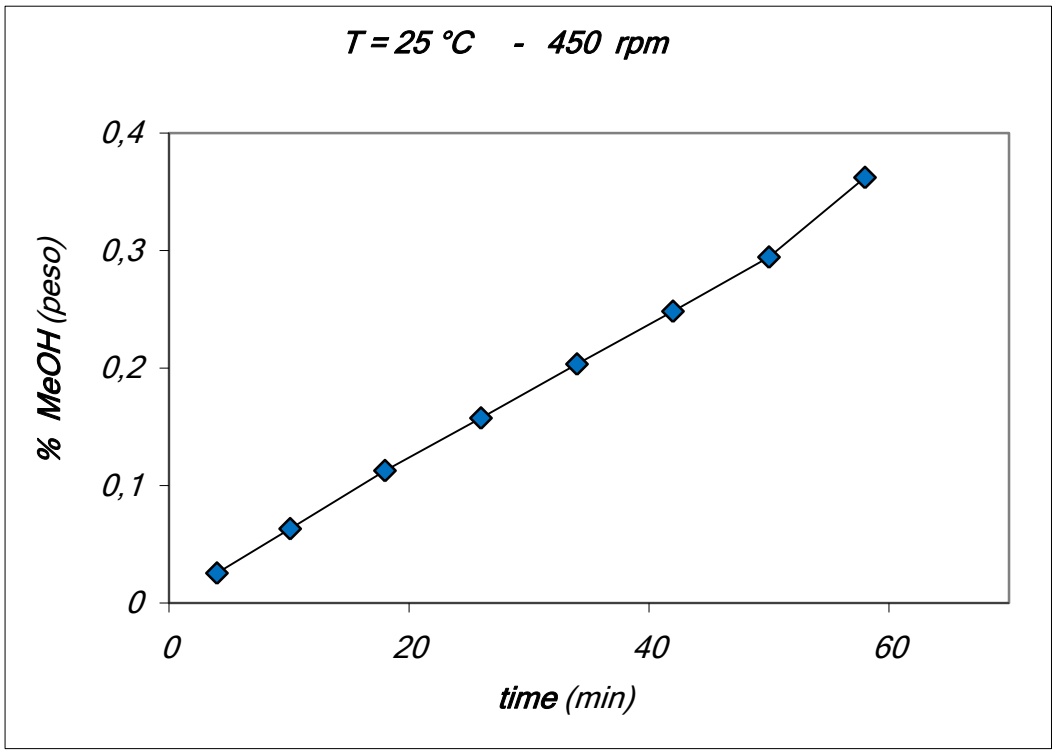

Fig 4.6.1.1 Methanol concentration as function of time at 25°C and 450 rpm

Now, to determine the methanol permeability through the following equation

$$P = \frac{n_{CH3OH}}{t} \frac{\delta}{\Delta C}$$

we must determine the moles of methanol that pass through the membrane per unit time. Knowing the molecular weight of methanol (32,042 AMU) and the internal volume (0.2 litres) can calculate the moles of methanol (n) reported in table 4.5.1.4:

Table 4.6.1.4 Moles of methanol calculated for Commercial Nafionat 25°C and 450 rpm

t (min)	*Wt %*	*gram*	*mol*	*M*
4	*0.025*	*0.0051*	*0.00016*	*0.00799*
10	*0.0632*	*0.0126*	*0.00039*	*0.01983*
18	*0.1127*	*0.0225*	*0.00070*	*0.03532*
26	*0.1574*	*0.0314*	*0.00098*	*0.04935*
34	*0.2033*	*0.0406*	*0.00127*	*0.06375*
42	*0.2483*	*0.0496*	*0.00155*	*0.07783*
50	*0.2944*	*0.0588*	*0.00184*	*0.09229*
58	*0.3621*	*0.0724*	*0.00227*	*0.11355*

The moles of methanol obtained are corrected considering the amount of methanol that, inevitably with the measuring device used, pass into the vapour phase. This amount is negligible at 25 °C, if compared with the methanol content in the measuring cell, but it is important if the temperature increases.
The calculation was conducted by considering the equilibrium conditions expressed by Raoult's law for the non-ideal mixture water-methanol in liquid phase.

Table 4.6.1.5 Effect of water and methanol evaporation in the measurementcell during the test at 25°C

CH_3OH	H_2O
mole $*10^6$	mole $*10^4$
6.85	1.41
1.71	1.41
3.01	1.41
4.22	1.40
5.42	1.40
6.62	1.40
7.86	1.40
9.61	1.40

So, the value of permeability can be found by knowing the values of thickness, surface area and molar concentration of methanol in the flask. The thickness of the membrane is measured using a micrometer (precision ± 10 μm), whereas the effect of swelling that leads to an increase in thickness after the absorption of water and methanol molecules in the molecular structure of the membrane.

C est	1.537	mole/l
Thickness	0.0215	cm
Surface	4.240	cm^2

therefore, recalling that

$$N = \frac{n_{CH3OH}}{t * S}$$

and

$$P = N * S \frac{\delta}{\Delta C}$$

we have the following results summarized in table 4.6.1.6

Table 4.6.1.6 Methanol permeability, flow and concentration for Commercial Nafionat 25°C and 450 rpm

t (min)	N *10^{-7} (mol/cm^2 s)	Cint (M)	ΔC (mol/cm^3)	Permeability *10^{-6} (cm^2/s)
4	1.578	0.0079	1.529	**2.201**
10	1.541	0.0198	1.517	**2.182**
18	1.540	0.0353	1.501	**2.201**
26	1.492	0.0495	1.487	**2.151**
34	1.471	0.0635	1.473	**2.156**
42	1.459	0.0778	1.459	**2.139**
50	1.450	0.0921	1.444	**2.148**
58	1.543	0.1135	1.423	**2.161**

Plotting the values of permeability calculated as a function of time we obtain the trend shown in the figure 4.6.1.2:

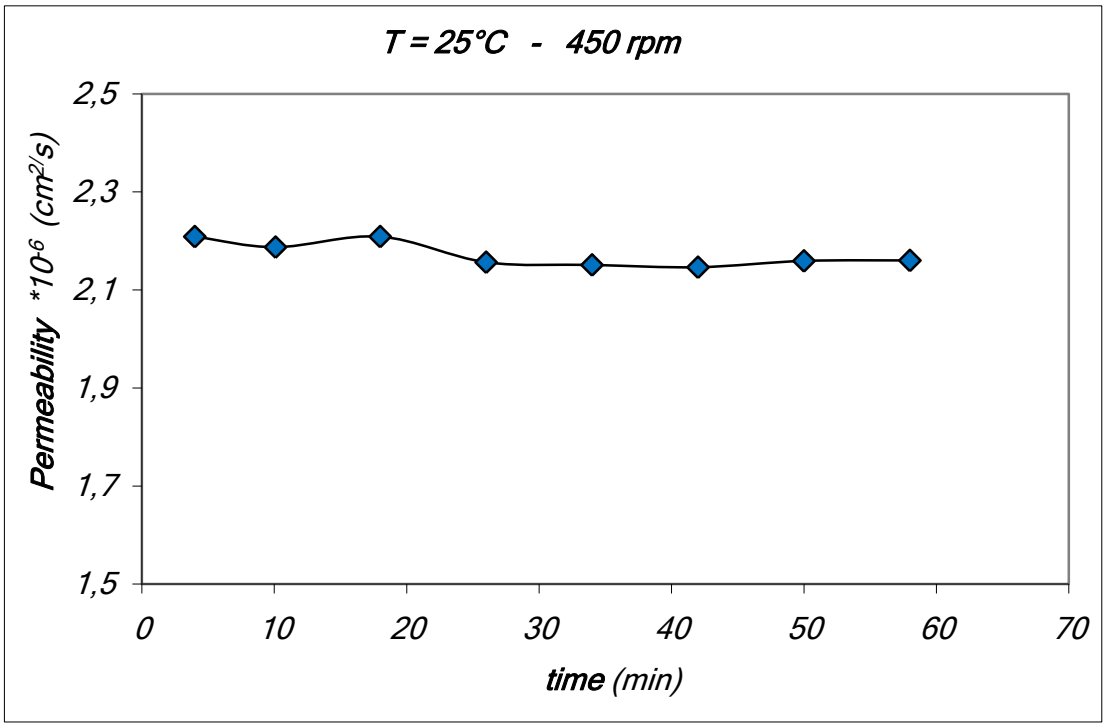

Fig. 4.6.1.2 Permeability as a function of time of Nafion

Not considering the first three, four experimental points, we get an almost constant trend that allows to draw the following conclusions:

- *We have overcome, or at least reduced, in an acceptable way the problem of the unsteady state that the membrane shows in the opening minutes because of swelling.*
- *We can identify an average value of permeability*

In this sample, at T = 25°C, 450 rpm, Cest 5 wt 5 for Nafion commercial, the avarage valuer of permeability is

$P = 2.153*10^{-6}$ *[=]* cm^2/s

4.7 The mixing rate

The mixing rate in the flask is controlled regulating the compressed air flow that is sent to the turbine. It drives a cylindrical magnet (length 2 cm) according to an appropriate speed.

The following figure 4.7.1 relates the rotating speed depending on the compressed air flow measured by the flowmeter:

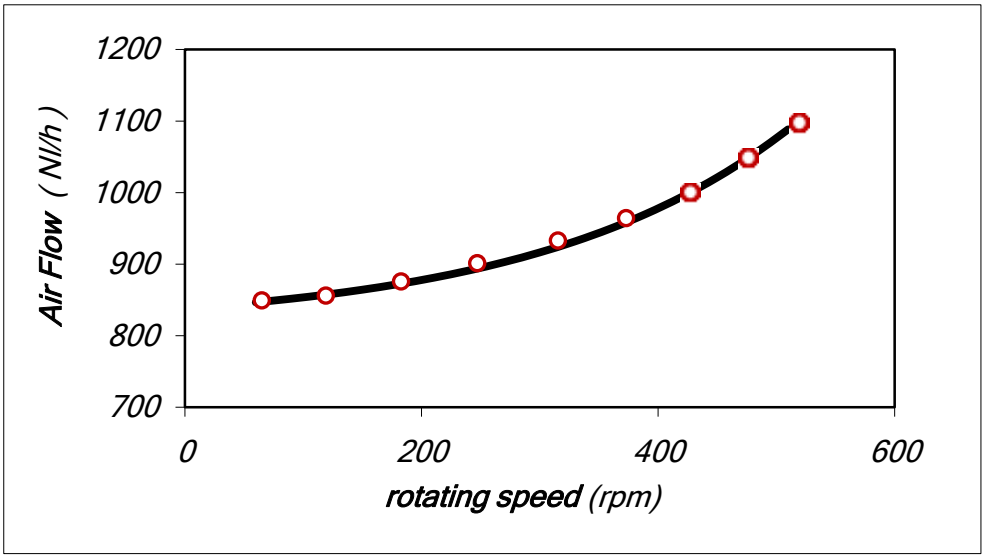

Fig. 4.7.1 Rotating speed of the magnet measured as function of the air flow

We consider negligible the effect that the variation in temperature can have on the physical properties of the mixture, density and viscosity, and thus generalize this trend over the entire temperature range (20 - 80 °C) considered in experimental tests.

The maximum value for the rotating speed used in the experimental measurement is 450 rpm. If the rotating speed increases, the magnet is unable to follow the rotation of the turbine and consequently there is a departure from the same axis of rotation.
However, this speed can fall into a state of turbulent regime for the system, as is apparent from the figure 4.6.2, obtained considering the flow of methanol through the membrane experimentally measured and calculated as the Reynolds number:

$$\mathrm{Re} = \frac{d^2 \rho n}{\mu}$$

where

d: length of the magnet [=] cm

ρ: density of the solution [=] gr/cm^3

μ: viscosity of the solution [=] gr/s cm

n: rate per second of the magnet

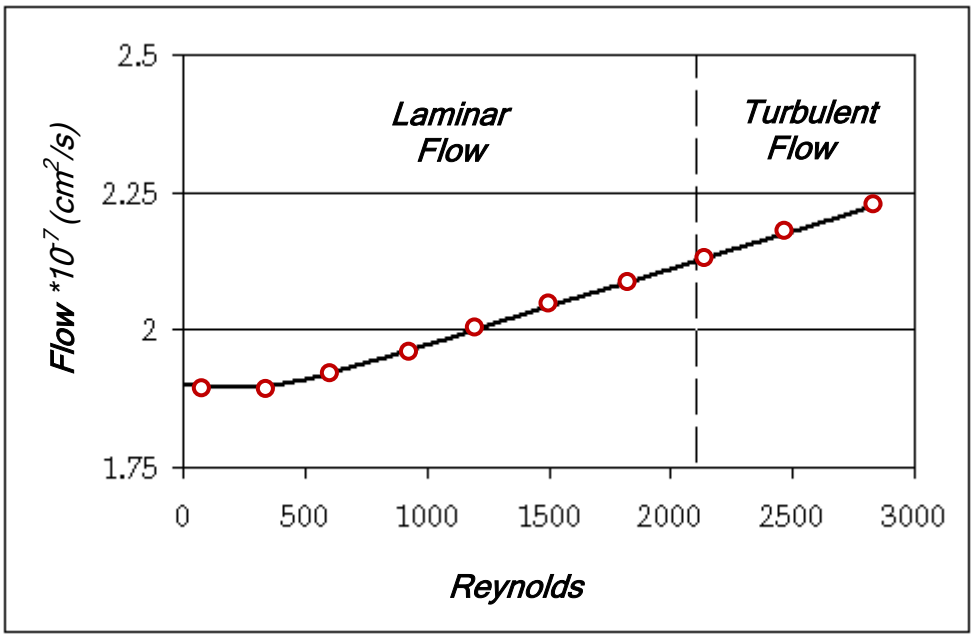

Fig. 4.7.2 Methanol flow as function of Reynolds number

5. RESULTS AND DISCUSSION

5.1 Nafion Commercial

The experimental measurement starts testing the commercial Nafion membrane in order to compare the measurements obtained with the literature and therefore the correctness of the experimental procedure adopted. Moreover, the commercial Nafion is assumed as a term of comparison for the other membrane tested.

Fixed the operating conditions, temperature, mixing rate and methanol concentration in the flask, the gas-chromatograph allows to avaluate the methanol concentration in the measuring cell as function of time, as shown in figure 5.1.1

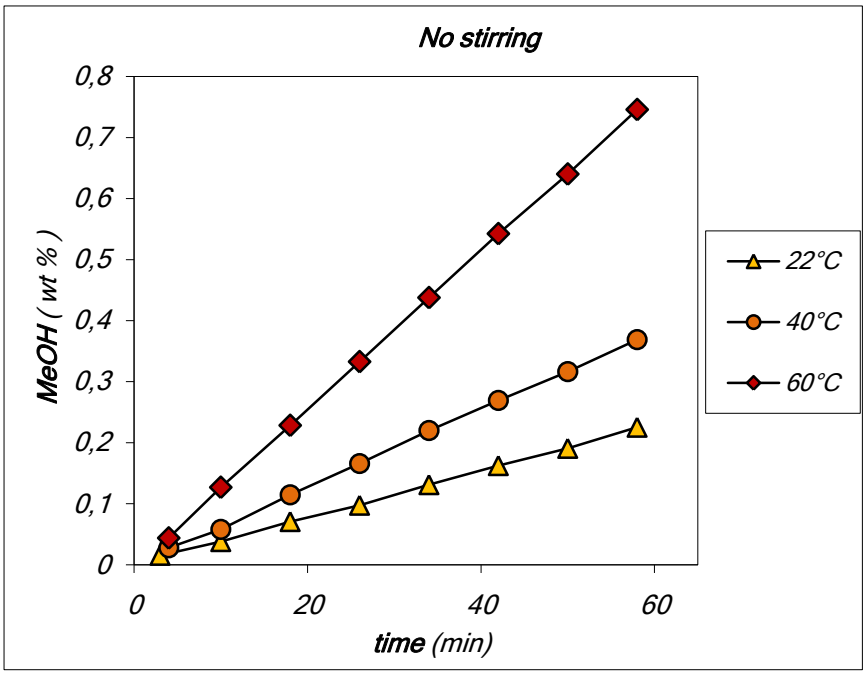

Fig. 5.1.1 Methanol concentration as function of time at different temperatures

Knowing the moles of methanol that crossed the membrane (n_{CH3OH}), the thickness (δ) and driving force (ΔC), the permeability is calculated by the following equation:

$$P = \frac{n_{CH3OH}}{t} * \frac{\delta}{\Delta C}$$

Some values of permeability for Nafion commercial, obtained at different condition of temperature (22 - 40 - 60 °C) and mixing rate (0- 450 rpm), are shown in table 5.1.1

Table 5.1.1 Permeability of Nafion commercial at 22 - 40 - 60 °C and 0 - 450 rpm

Permeability *$*10^{6}$*	*Tempearure (°C)*		
Mixing rate (rpm)	*22*	*40*	*60*
0	*1.4*	*2.9*	*4.7*
450	*2.2*	*3.4*	*5.7*

It is clearly the effect of temperature and mixing rate on the permeability values measured. The figure 5.1.2 below shows the effect of temperature on the methanol permeability of Nafion membrane.

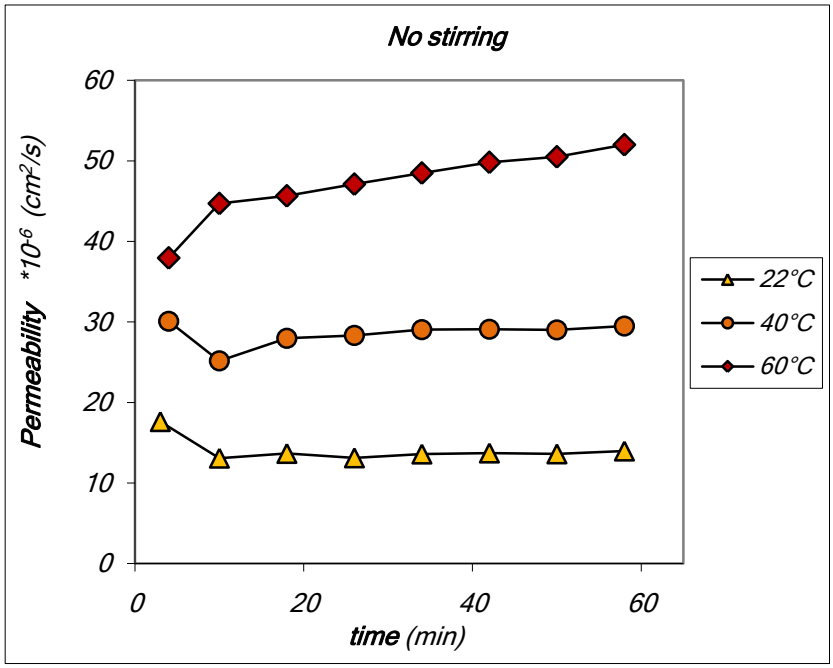

Fig. 5.1.2 Permeability as function of time at different temperatures

The following figures 5.1.3-4 put out the differences between the values observed with a maximum rotating speed of the magnet, about 450 rpm, and those without stirring, both reported at 40 °C:

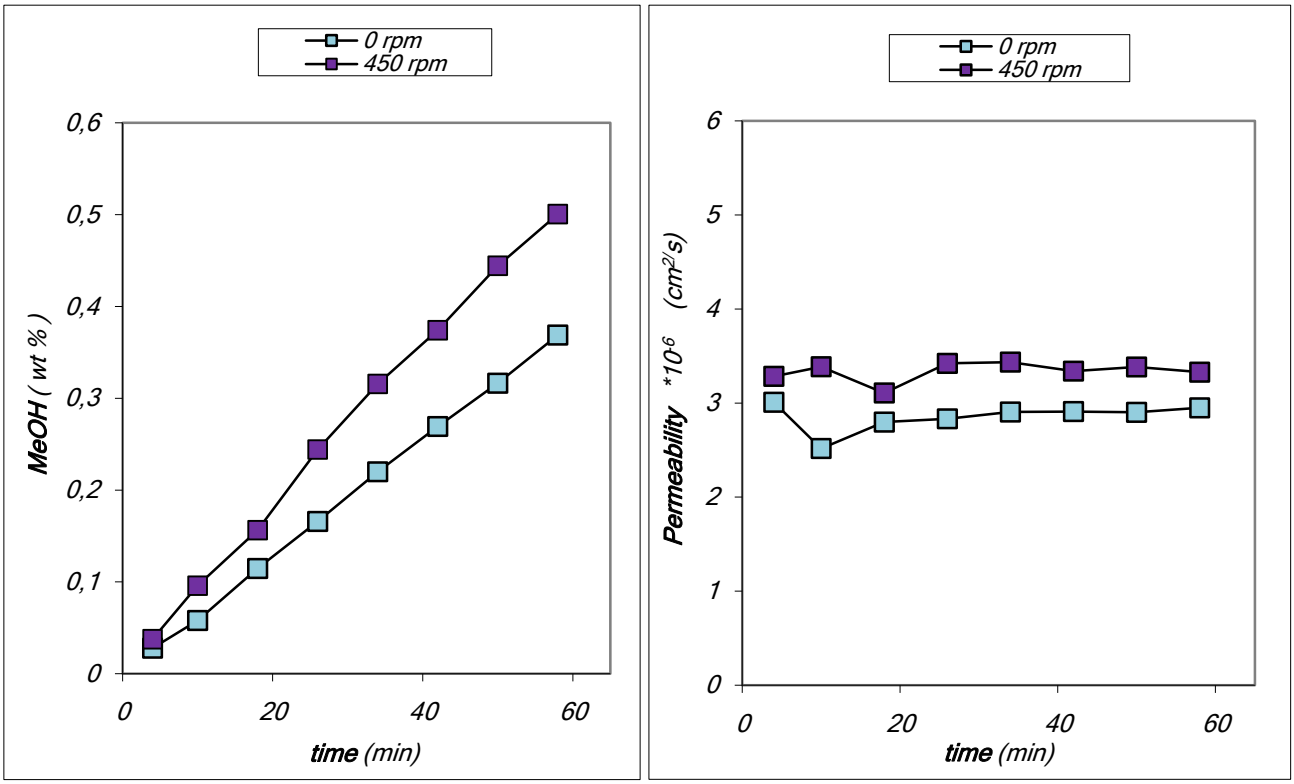

Fig 5.1.3-4 Comparison between the methanol concentration and permeability as function of time, at 40 °C without mixing rate and at 450 rpm

5.2 Nafion modified

Methanol permeability measurements for each membranes were performed in the experimental apparatus that was described in chapter 4.3 . It allows to measure the mass flow of methanol, as a function of time, under fixed measurements conditions, such as methanol concentration, temperature and mixing rate. The permeability (P) can be obtained by the following equation:

$$P = \frac{n_{CH3OH}}{t} * \frac{\delta}{\Delta C}$$

where

n_{CH3OH} *= moles of methanol (mol)*

t = time (sec)

δ *= thickness (cm)*

ΔC *= driving force for the concentration (M)*

This equation allows to calculate the methanol permeability unknowing the partition constant and the diffusivity of the solution through the membrane, that are not easy to determinate. A that point, the comparison between the different membranes can be done by the values at steady state.

Nevertheless, the permeability does not varies linearly with the thickness because of Nafion is a polymeric material, it is not homogeneous. For this reason, the mass flow, and in the same way the calculated permeability, will be as a function of the thickness of the membrane. So, in order to compare the membranes, we must consider the methanol flow (N) given by the following equation:

$$N = \frac{P}{\delta} \Delta C$$

where the term P/δ means like a global transport coefficient. If ΔC is constant, N varies linearly with P/δ.

- ***T = 40°C, static conditions***

For each Nafion/ZrP composite membranes studied at different temperature and mixing rate conditions, it is useful to calculate, in the same conditions, the permeability and the flow of methanol from the experimental measurements of Nafion commercial, assumed as the reference, in order to compare the values obtained.
Starting in comparison between Nafion commercial and Nafion obtained by casting for two different thickness values, Nafion commercial thermally treated at 180 °C (A), Nafion by casting thermally treated at 180 °C (B) and Nafion/ZrP composite membranes with 4.7 and 10 wt.% filler content:

Membrane	***Permeability*** *(cm^2/s)*	***P/δ*** *(cm/s)*	***Flow*** *($mol/cm^2 s$)*	***Thickness*** *(μm)*
Nafion commercial	*2.94E-06* *2.58E-06*	*1.37E-04* *2.58E-04*	*1.96E-07* *3.45E-07*	*185* *100*
Nafion by casting	*2.58E-06* *2.66E-06*	*3.04E-04* *1.56E-04*	*4.03E-07* *2.26E-07*	*75* *170*
Nafion/ZrP_{isg} 4.7wt% from prec *Nafion/ZrP_{isg} 10wt% from prec*	*2.94E-06* *2.58E-06*	*1.37E-04* *3.04E-04*	*1.96E-07* *4.03E-07*	*105* *215*
Nafion thermally treated (A) *Nafion thermally treated (B)*	*3.73E-06* *2.26E-06*	*1.59E-04* *1.03E-04*	*2.25E-07* *1.50E-07*	*200* *210*

(A), (B) mean two different thermal treatments

Obviously, the values obtained for methanol flow, permeability and P/δ are quite different. The values of methanol concentration in the test cell are reported in figure 5.2.1 as a function of time. It can be observed that for each tested membrane, methanol concentration increases quite linearly with time, as expected from the above assumption. The points are fitted by lines with different slopes and not appreciable intercepts with the axes.

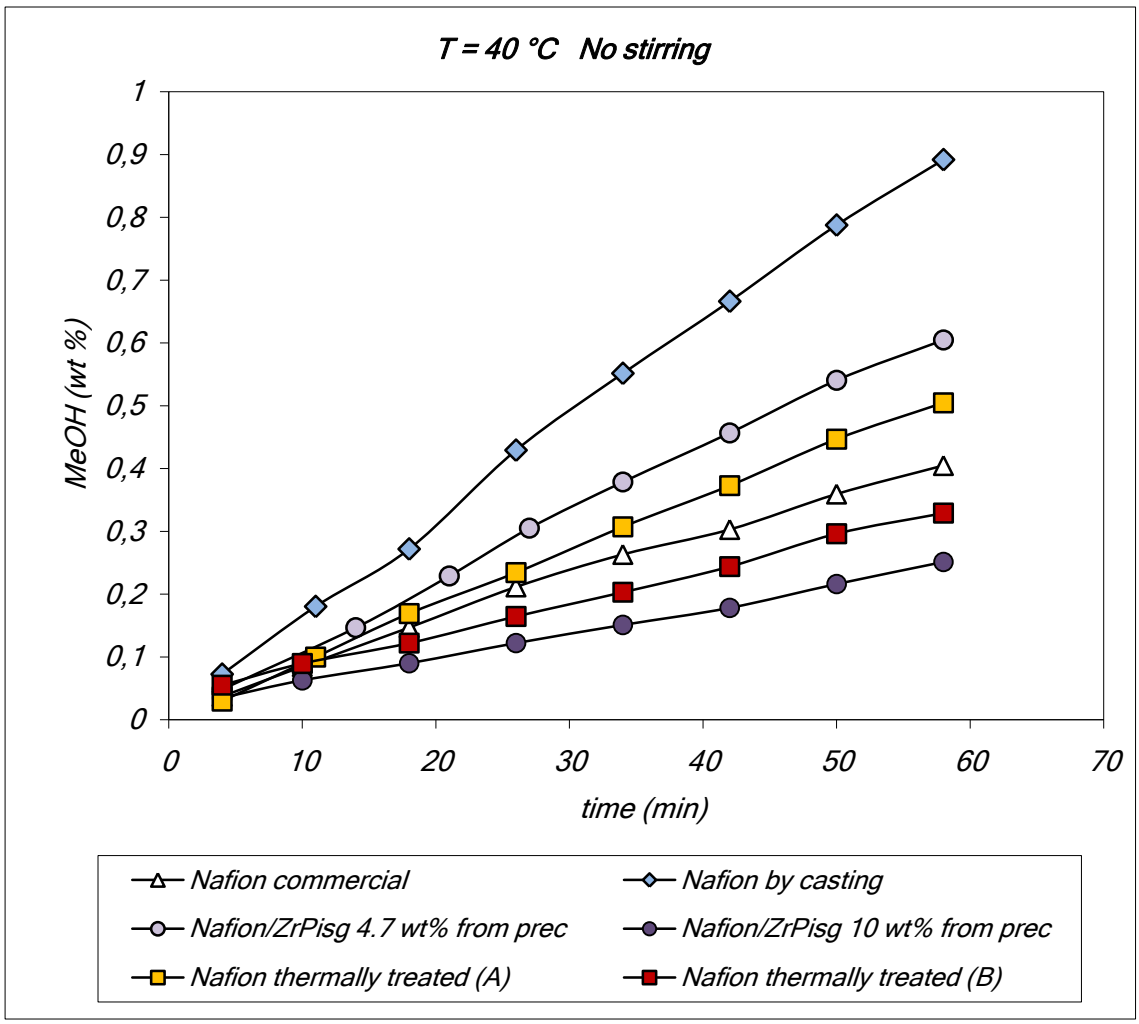

Fig. 5.2.1 Methanol concentration as function of time of different membranes

The values of methanol concentration at different times is used for the calculation of the flow (N) and then of the methanol permeability (P). Such calculation needs the knowledge of the membrane thickness, which is always reported next to the column of the methanol flow values in each table. The thickness varies among the different membranes from 75 to 215 μm.

In the figure 5.2.2 are showed the permeability values calculated for the different membranes described before. Not considering the first three experimental points, we get an almost constant trend for each curves that allows to validate the values obtained above.

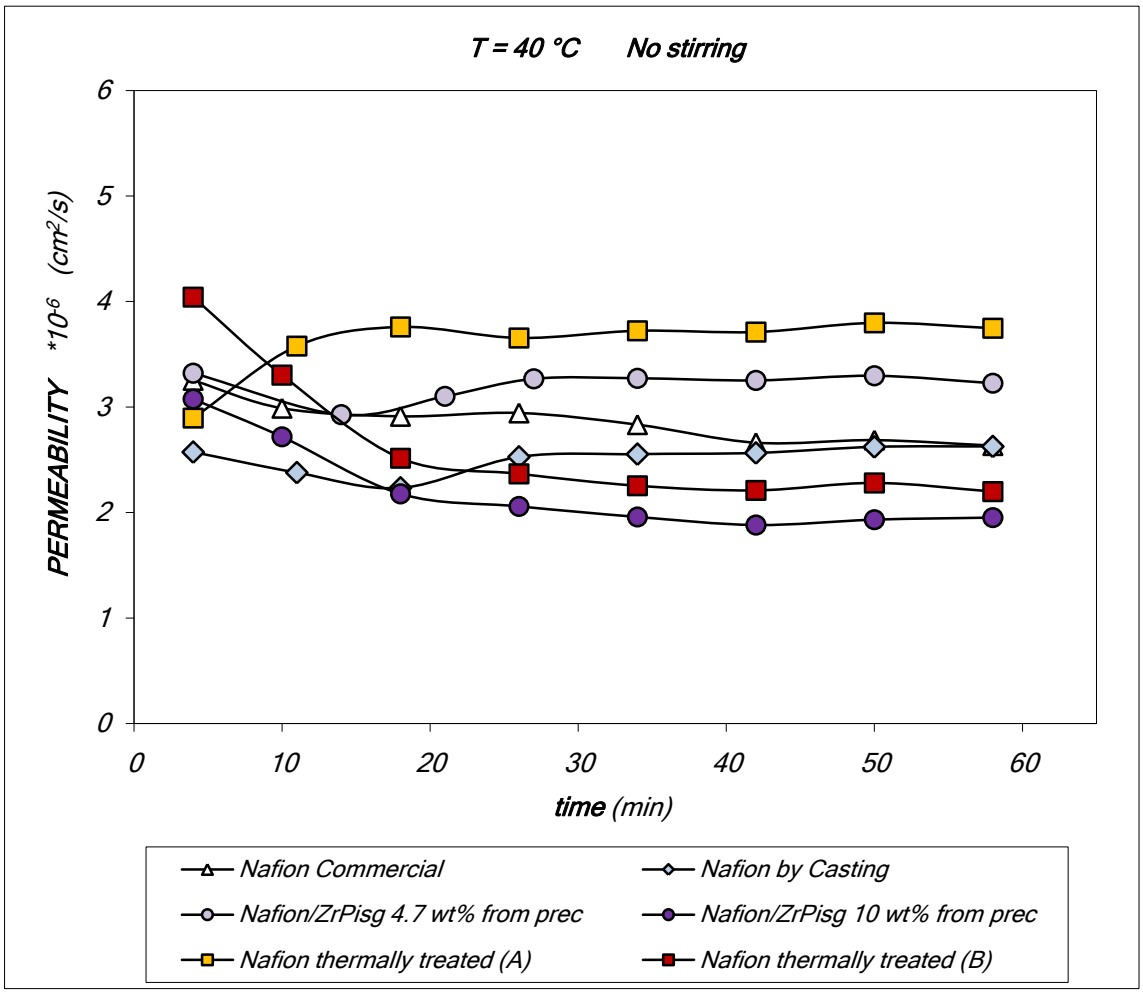

Fig. 5.2.2 Permeability of different membranes

Nafion composite membranes with loadings of in situ grown α-zirconium phosphate ($NZrP_{isg}$) have been studied. The filler content varies from 5 wt.% to 20 wt.%.

Membrane	*Permeability* (cm^2/s)	*P/δ* (cm/s)	*Flow* ($mol/cm^2 s$)	*Thickness* (μm)
Nafion commercial	*2.94E-06*	*1.37E-04*	*1.96E-07*	*185*
Nafion/ZrP_{isg} 5 wt%	*3.95E-06*	*2.72E-04*	*3.58E-07*	*101*
Nafion/ZrP_{isg} 10 wt%	*4.04E-06*	*2.38E-04*	*3.18E-07*	*108*
Nafion/ZrP_{isg} 15 wt%	*4.30E-06*	*2.32E-04*	*3.15E-07*	*111*
Nafion/ZrP_{isg} 20 wt%	*4.08E-06*	*1.94E-04*	*2.66E-07*	*114*

The data above and the figures 5.2.3-4, that show the methanol concentration and permeability as a function of time for different ZrP_{isg} content, indicate that the presence of the filler increases the permeability and the methanol flow, although the thickness of the composite membranes are quite smaller than the thickness of Nafion commercial.

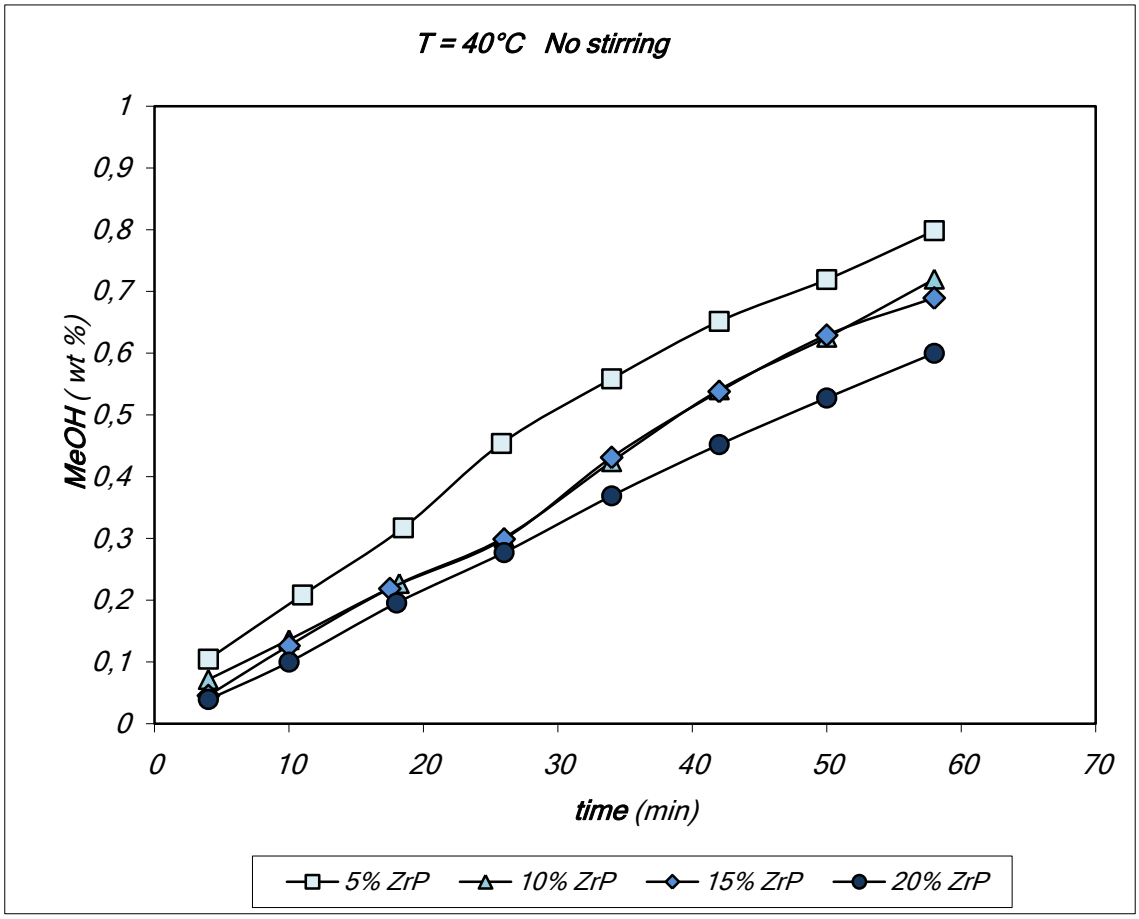

Fig. 5.2.3 Methanol concentration as function of time for Nafion/ZrP_{isg} at different ZrP contents

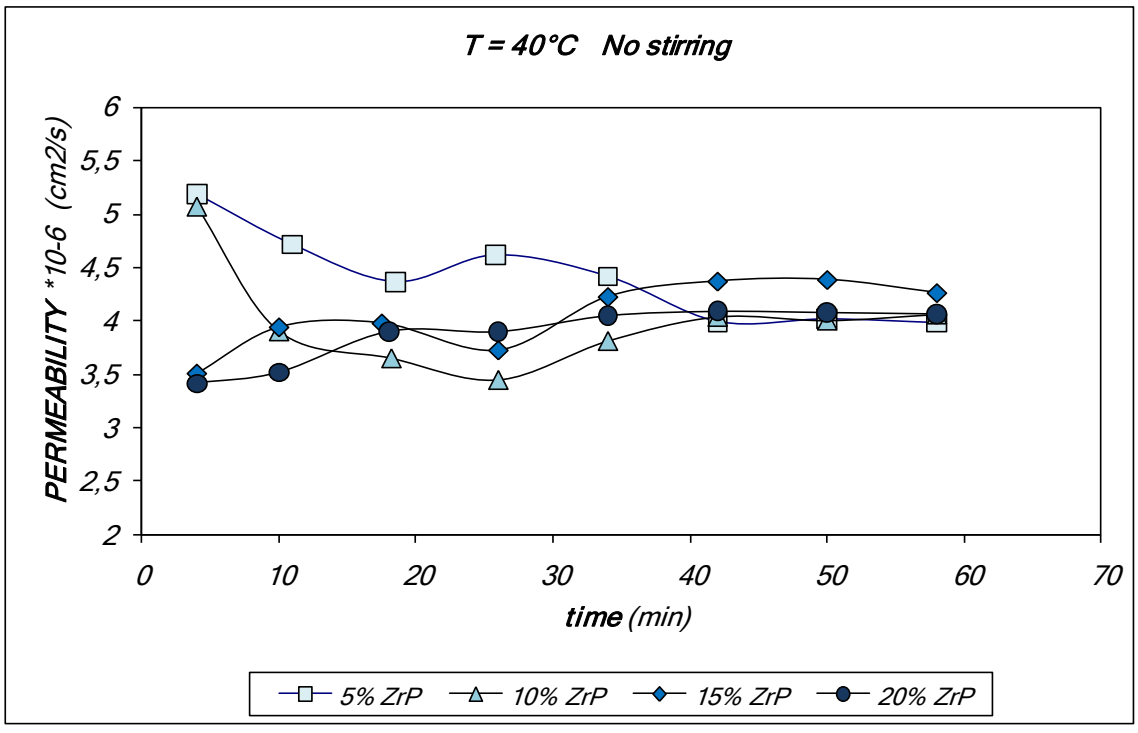

Fig. 5.2.4 Permeability for Nafion/ZrP_{isg} at different ZrP contents

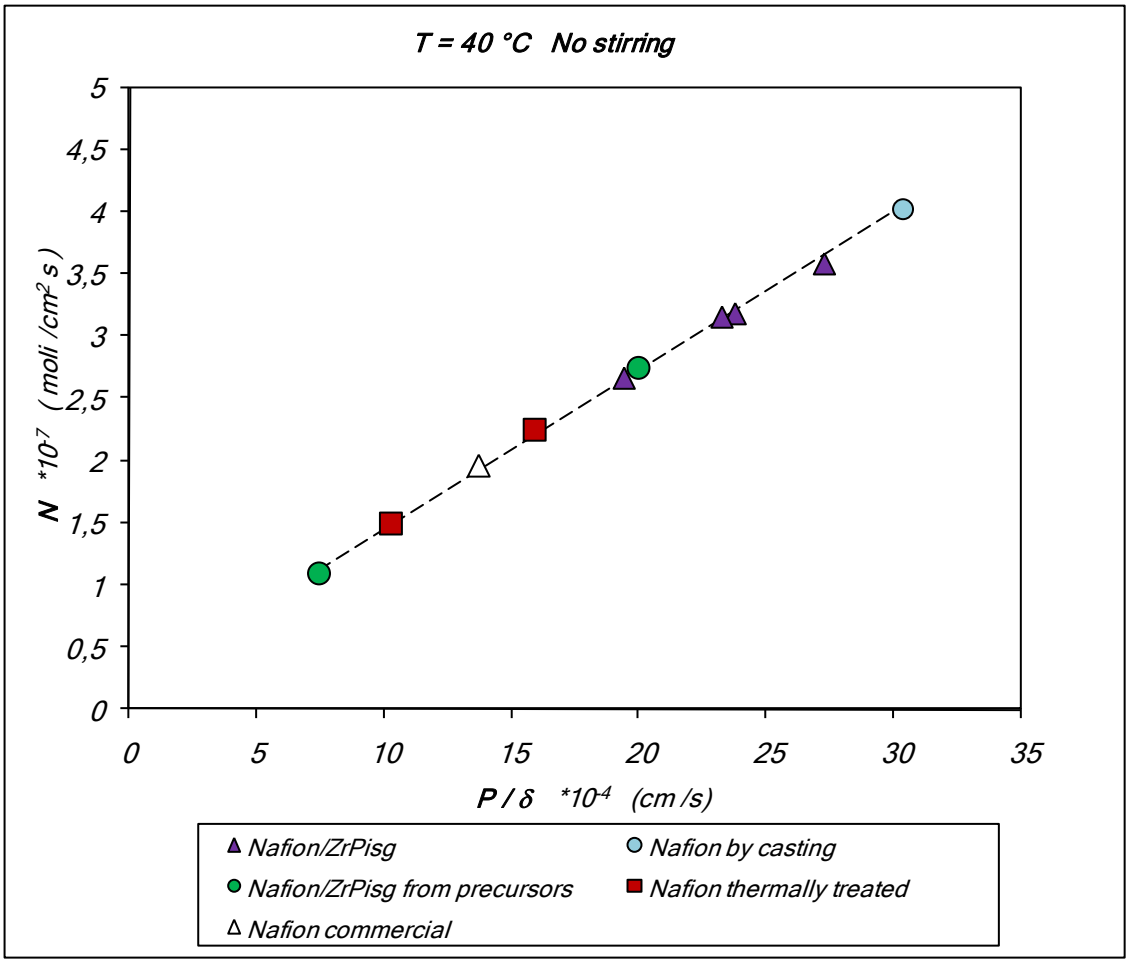

Fig. 5.2.5 Methanol flow as a function of P/δ coefficient for the studied membranes

Nafion/ZrP$_{isg}$ membranes and Nafion modified with thermal treatments have a unpredictable behavior. Considering the methanol flow as a function of P/δ coefficient in figure 5.2.5, it is seen that only two membranes have lower values than Nafion reference.

Nafion composite membranes containing high aspect ratio particles of exfoliated α-zirconium phosphate ($NZrP_{exf}$) have been studied. The filler content varies from 0.25 wt.% to 7 wt.%. There are two groups for the membranes, (1) and (2), it indicates two different preparation methods for the membranes with the same techniques.[10], [11]

Membrane	*Permeability* (cm^2/s)	*P/δ* (cm/s)	*Flow* ($mol/cm^2 s$)	*Thickness* (μm)
Nafion/ZrP_{exf} 1 wt% (1)	*2.27E-07*	*2.27E-05*	*3.44E-08*	*100*
Nafion/ZrP_{exf} 2 wt% (1)	*2.26E-07*	*2.83E-05*	*4.27E-08*	*80*
Nafion/ZrP_{exf} 3 wt% (1)	*3.31E-07*	*4.41E-05*	*6.59E-08*	*75*
Nafion/ZrP_{exf} 4 wt% (1)	*5.03E-07*	*4.79E-05*	*7.15E-08*	*105*
Nafion/ZrP_{exf} 5 wt% (1)	*3.99E-07*	*3.62E-05*	*5.46E-08*	*110*
Nafion/ZrP_{exf} 0.25 wt% (1)	*2.07E-06*	*1.25E-04*	*1.79E-07*	*165*
Nafion/ZrP_{exf} 0.5 wt% (1)	*2.03E-06*	*1.50E-04*	*2.11E-07*	*135*
Nafion/ZrP_{exf} 7 wt% (1)	*1.50E-06*	*1.36E-04*	*1.93E-07*	*110*
Nafion/ZrP_{exf} 1 wt% (2)	*2.68E-07*	*4.13E-05*	*6.20E-08*	*65*
Nafion/ZrP_{exf} 2 wt% (2)	*3.12E-07*	*2.60E-05*	*3.93E-08*	*120*
Nafion/ZrP_{exf} 3 wt% (2)	*3.26E-07*	*3.43E-05*	*5.18E-08*	*95*
Nafion/ZrP_{exf} 4 wt% (2)	*4.24E-07*	*5.30E-05*	*7.89E-08*	*80*
Nafion/ZrP_{exf} 5 wt% (2)	*1.86E-07*	*1.62E-05*	*2.46E-08*	*115*
Nafion/ZrP_{exf} 0.25 wt% (2)	*1.64E-06*	*1.82E-04*	*2.51E-07*	*90*
Nafion/ZrP_{exf} 0.5 wt% (2)	*1.54E-06*	*2.05E-04*	*2.85E-07*	*75*

(1), (2) mean two different preparation methods for the membranes

The Nafion/ZrP_{exf} membranes show a completely different behaviour than the Nafion/ZrP_{isg}: the presence of the filler gives rise to low permeability and methanol flow, with thickness always lower than the reference.

In figures 5.2.6-7 the flow values are reported as a function of P/δ coefficient for different ZrP content. It is clearly that Nafion/ZrP_{exf} membranes have values with a order of magnitude lower than the reference. Apparently, it is seen that there is a linear inverse-relationship between the permeability and the ZrP content: the lower permeability value is obtained from Nafion/ZrP_{exf} 7 wt% (1), while the higher value from the membrane with lowest filler content, Nafion/ZrP_{exf} 0.25 wt% (1). Nevertheless, ZrP content from 0.25 wt.% to 7 wt.% gives intermediate permeability values with unpredictable behaviour.

Like the permeability, the thickness does not increase proportionally with the filler content.

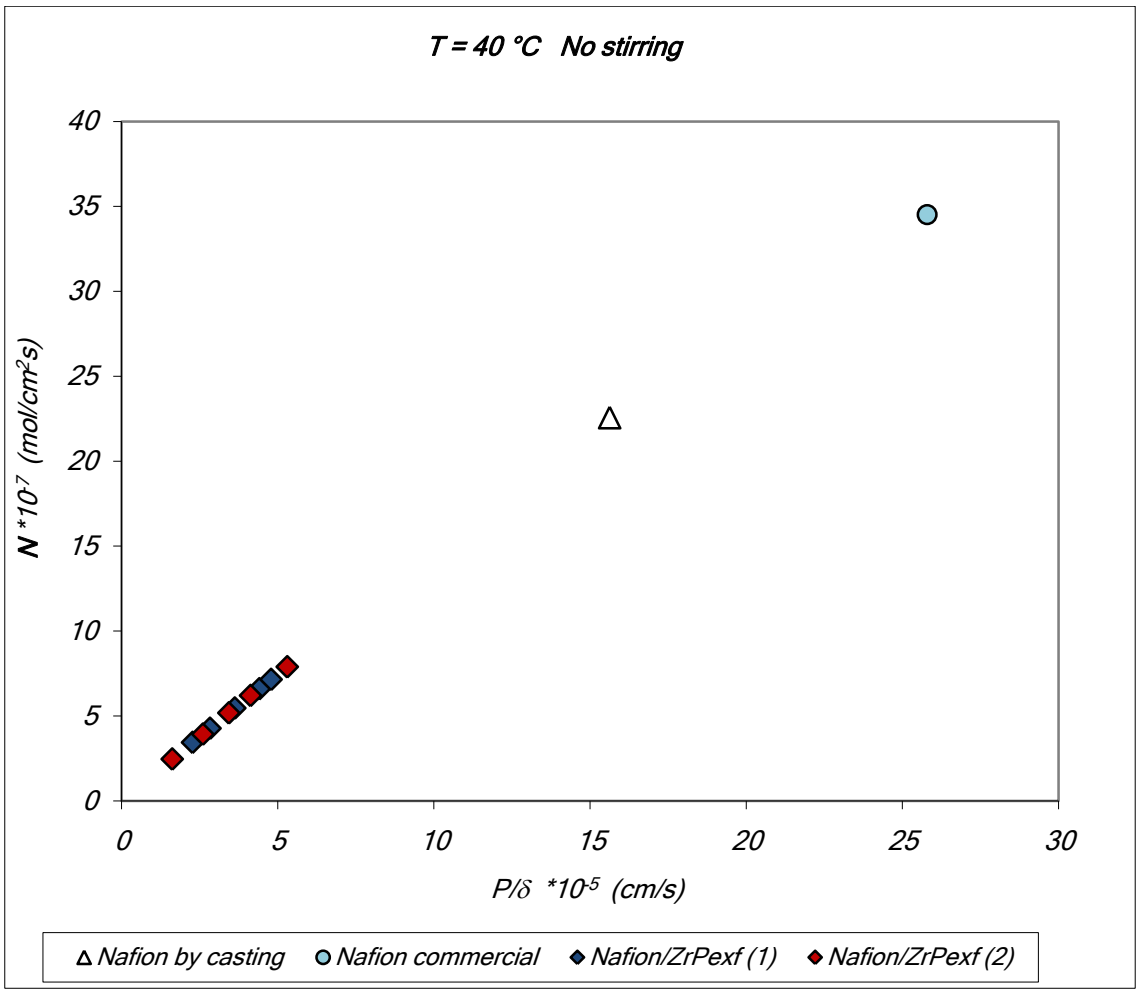

Fig. 5.2.6 Methanol flow as a function of P/δ coefficient for the studied membranes. Comparison of the performances of the Nafion/ZrP$_{exf}$ with the commercial Nafion and Nafion by casting

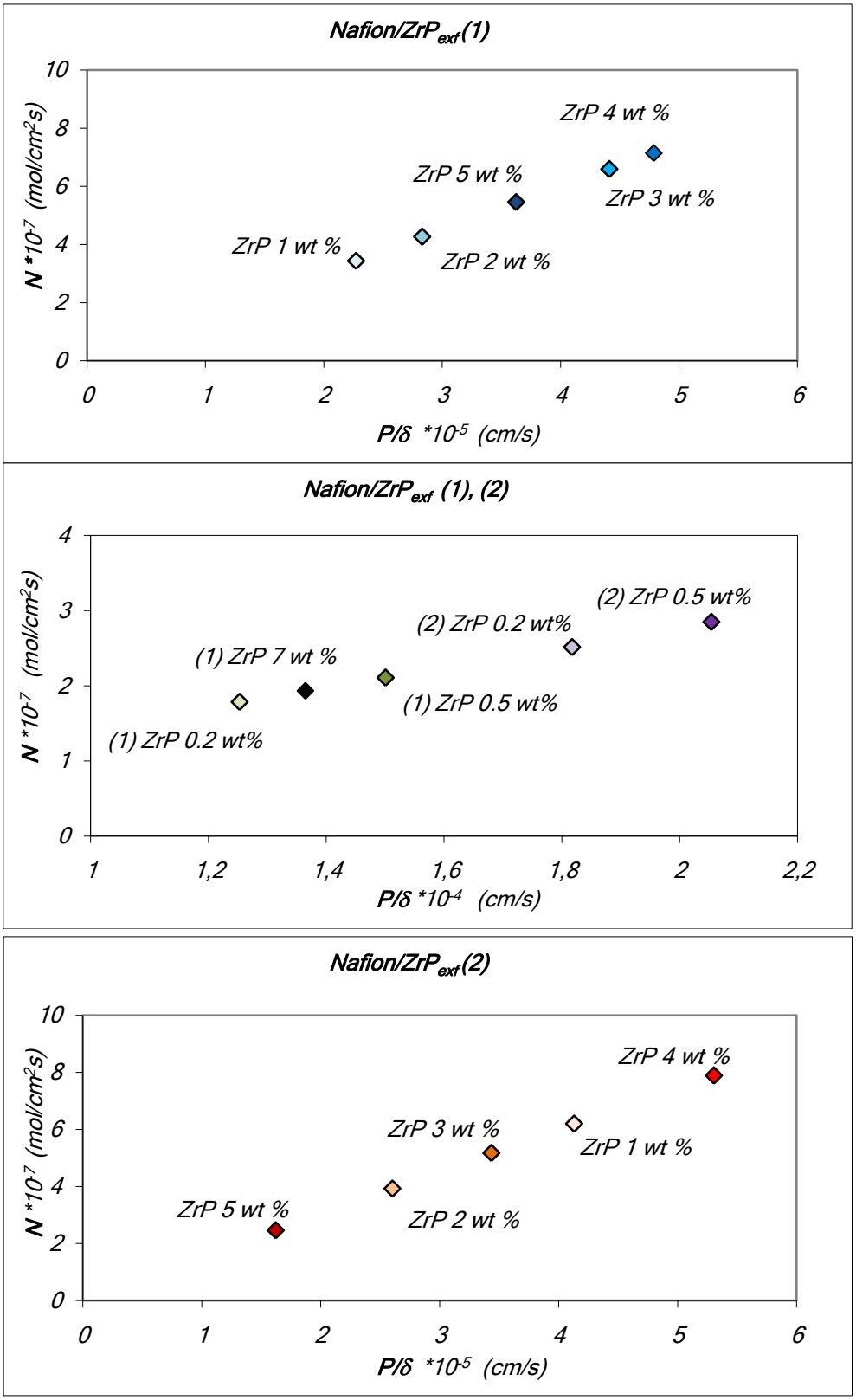

Fig. 5.2.7 Methanol flow as a function of P/δ coefficient for the studied membranes. Comparison of the performances of the Nafion/ZrP$_{exf}$ at different ZrP contents for preparation method (1) and (2), at T = 40 °C and 0 rpm.

- *T = 60 °C, static conditions*

In order to study the effect of the temperature on the Nafion/ZrP_{exf} membranes, the measurements have been done at 60°C

Membrane	*Permeability* (cm^2/s)	*P/δ* (cm/s)	*Flow* ($mol/cm^2 s$)	*Thickness* (μm)
Nafion/ZrP_{exf} 1 wt% (1)	*8.74E-07*	*8.74E-05*	*1.27E-07*	*100*
Nafion/ZrP_{exf} 2 wt% (1)	*9.70E-07*	*1.21E-04*	*1.72E-07*	*80*
Nafion/ZrP_{exf} 3 wt% (1)	*7.87E-07*	*1.05E-04*	*1.51E-07*	*75*
Nafion/ZrP_{exf} 4 wt% (1)	*1.04E-06*	*9.46E-05*	*1.37E-07*	*110*
Nafion/ZrP_{exf} 5 wt% (1)	*1.13E-06*	*9.83E-05*	*1.42E-07*	*115*
Nafion/ZrP_{exf} 1 wt% (2)	*1.15E-06*	*1.76E-04*	*2.44E-07*	*65*
Nafion/ZrP_{exf} 2 wt% (2)	*1.11E-06*	*9.27E-05*	*1.35E-07*	*120*
Nafion/ZrP_{exf} 3 wt% (2)	*7.05E-07*	*7.43E-05*	*1.09E-07*	*95*
Nafion/ZrP_{exf} 4 wt% (2)	*7.83E-07*	*9.79E-05*	*1.42E-07*	*80*
Nafion/ZrP_{exf} 5 wt% (2)	*9.82E-07*	*8.54E-05*	*1.25E-07*	*115*

(1), (2) mean two different preparation methods for the membranes

The lowest permeability value is obtained with 3 wt.% of filler content for both the two different preparation methods, even though the lowest methanol flow is obtained for Nafion/ZrP_{exf} 1 wt% (1) and Nafion/ZrP_{exf} 3 wt% (2). There is not a relationship between the permeability and the ZrP content increasing the temperature from 40 to 60 °C.

The thickness of the membranes do not increase proportionally with the filler content for Nafion/ZrP_{exf} membranes.

In figure 5.2.8 the flow values are reported as a function of P/δ coefficient for different ZrP content at 60°C. It is still evident that the values are an order of magnitude lower than the reference.

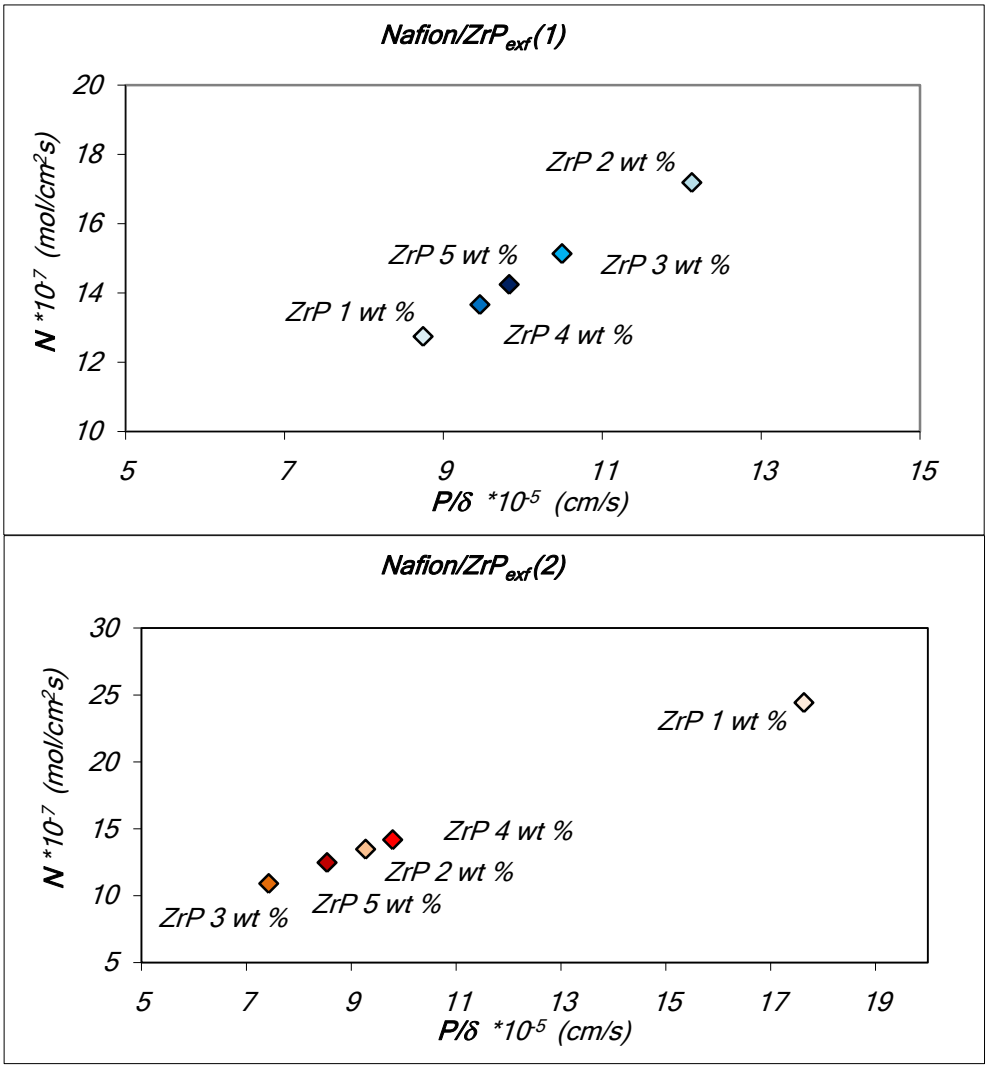

Fig. 5.2.8 Comparison the performances of the Nafion/ZrP$_{exf}$ at different ZrP wt % for preparation method (1) and (2), knowing the methanol flow (N) end the P/δ value at T = 60 °C and without stirring conditions.

In order to investigate the effect of the mixing rate on the methanol permeability and methanol flow, the measurement have been done at 450 rpm, the maximum rotating speed of the magnet, for different Nafion/ZrP$_{isg}$ and Nafion thermally treated, the same membrane previously studied at 0 rpm.

- *T = 40°C, 450 rpm*

Membrane	*Permeability* (cm^2/s)	*P/δ* (cm/s)	*Flow* ($mol/cm^2 s$)	*Thickness* (μm)
Nafion commercial	*3.38E-06*	*1.57E-04*	*2.23E-07*	*185*
Nafion by casting	*3.50E-06*	*4.12E-04*	*5.14E-07*	*75*
Nafion/ZrP_{isq} 4.7wt% from prec	*4.05E-06*	*2.45E-04*	*3.34E-07*	*105*
Nafion/ZrP_{isq} 10wt% from prec	*2.46E-06*	*9.46E-05*	*1.37E-07*	*215*
Nafion thermally treated (A)	*4.04E-06*	*1.72E-04*	*2.40E-07*	*200*
Nafion thermally treated (B)	*2.75E-06*	*1.25E-04*	*1.80E-07*	*210*
Nafion/ZrP_{isq} 5 wt%	*4.61E-06*	*3.18E-04*	*4.20E-07*	*101*
Nafion/ZrP_{isq} 10 wt%	*5.51E-06*	*3.24E-04*	*4.14E-07*	*108*
Nafion/ZrP_{isq} 15 wt%	*4.70E-06*	*2.54E-04*	*3.41E-07*	*111*
Nafion/ZrP_{isq} 20 wt%	*5.20E-06*	*2.47E-04*	*3.33E-07*	*114*

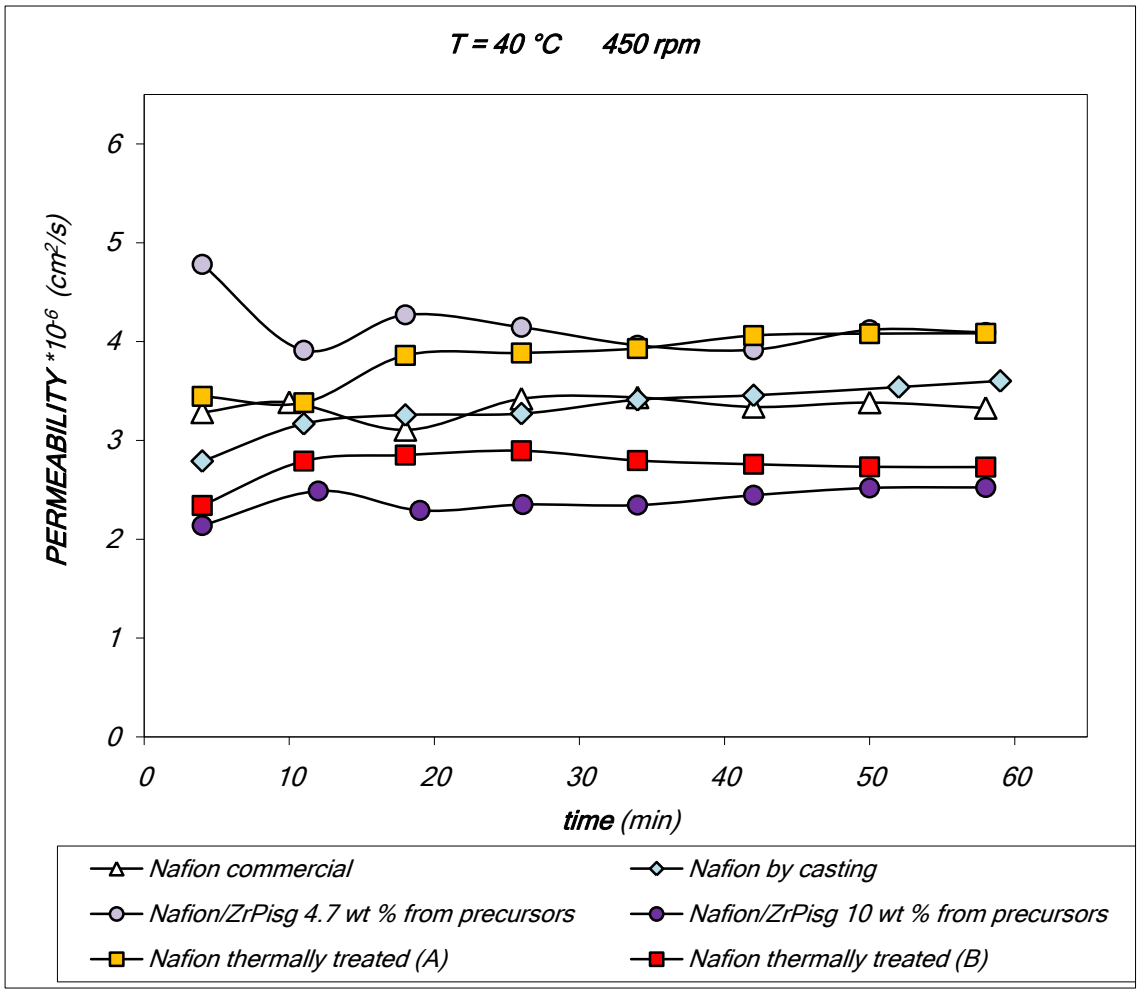

Fig.5.2.9 Permeability for different membranes

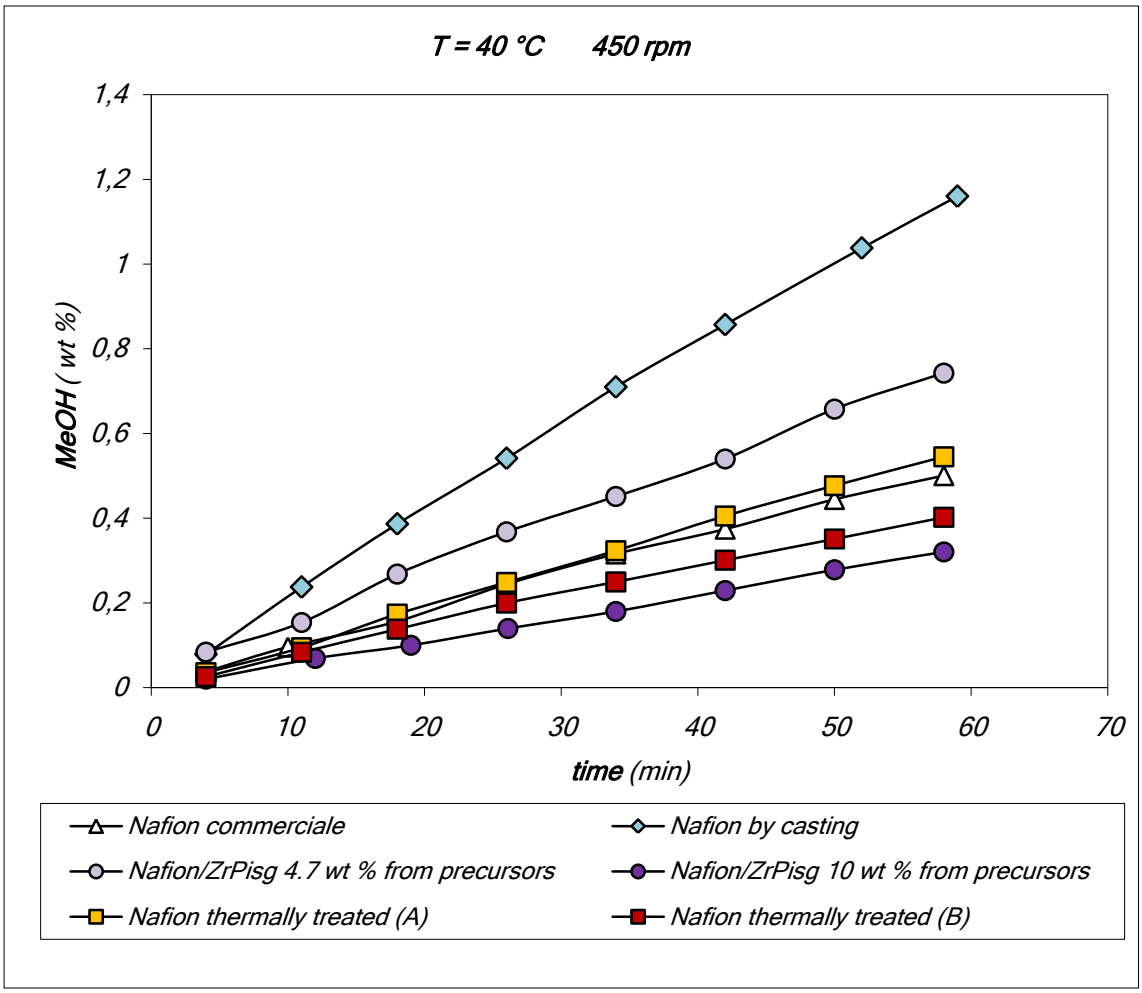

Fig. 5.2.10 Methanol concentration as function of time of different membranes

In figures 5.2.9-10 are reported the permeability and methanol concentration as a function of time for the same membranes studied at 40 °C and 0 rpm. The values are slightly higher at 450 rpm than those obtained at 0 rpm for each membrane, as expected.

The figures 5.2.11-12 show the permeability and the methanol concentration as a function of time for Nafion/ZrP_{isg} with different ZrP content.

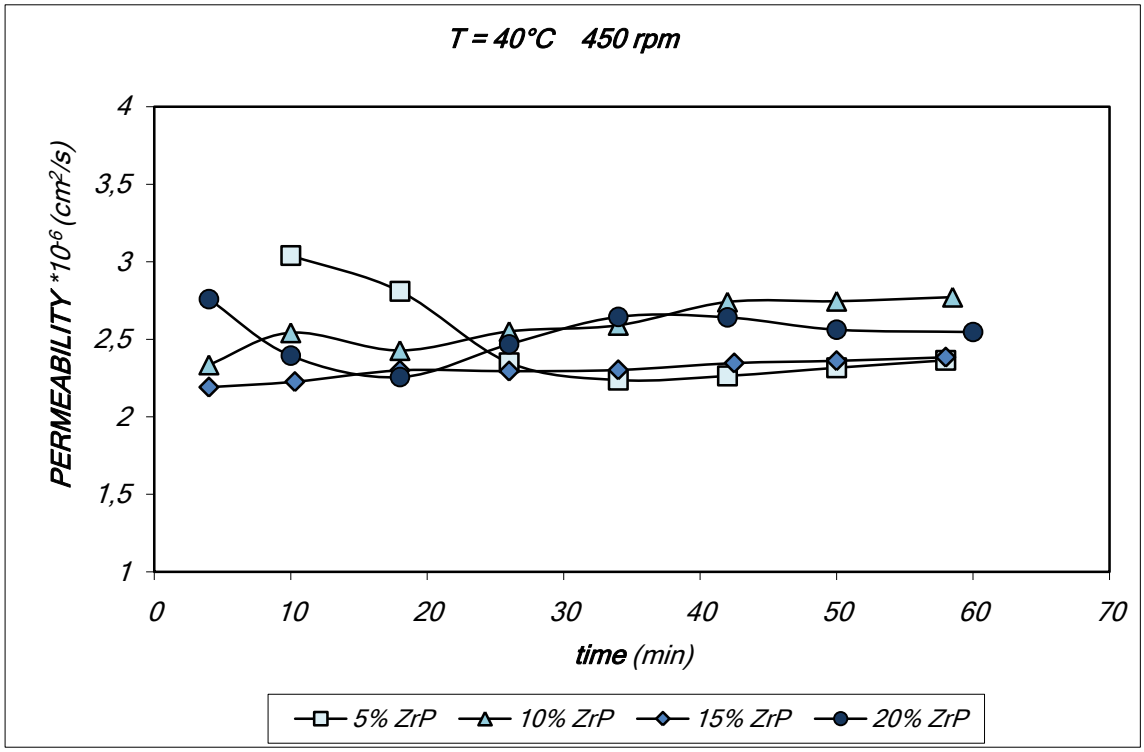

Fig. 5.2.11 Permeability for Nafion/ZrP_{isg} at different ZrP contents

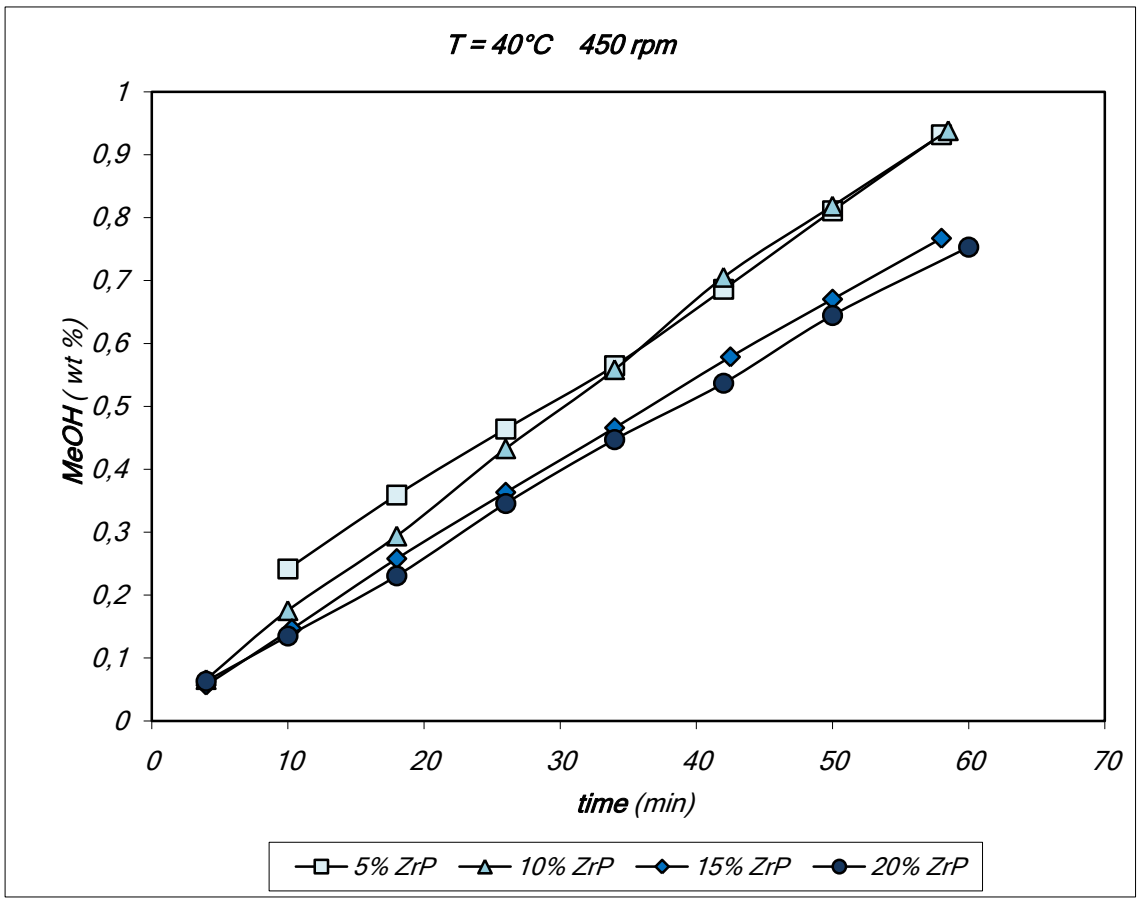

Fig. 5.2.12 Methanol concentration as function of time for Nafion/ZrP_{isg} at different ZrP contents

Summarizing some results we can investigate the effect of the temperature and the mixing rate on the methanol permeability.

The plots of the methanol permeability vs. temperature in a range from 22 to 60 °C are shown in Fig. 5.2.14. The regression curves for the data were generated using the following equation:

$$Y = A\exp\left(-\frac{B}{T}\right)$$

In the above equation, Y is the permeability of Nafion commercial, A is the pre-exponential factor, while B is the activation energy obtained by correlating diffusivity-temperature data with the Arrhenius approach. The data in table 5.2.1 are related to values of permeability calculated at different temperatures and 0 - 450 rpm for Nafion commercial.

*Table 5.2.1 Permeability *10^6 at different temperature and mixing rate for Nafion commercial*

Mixing rate (rpm)	Temperature (°C)		
	22	40	60
0	1.36	2.86	4.70
450	2.15	3.38	5.72

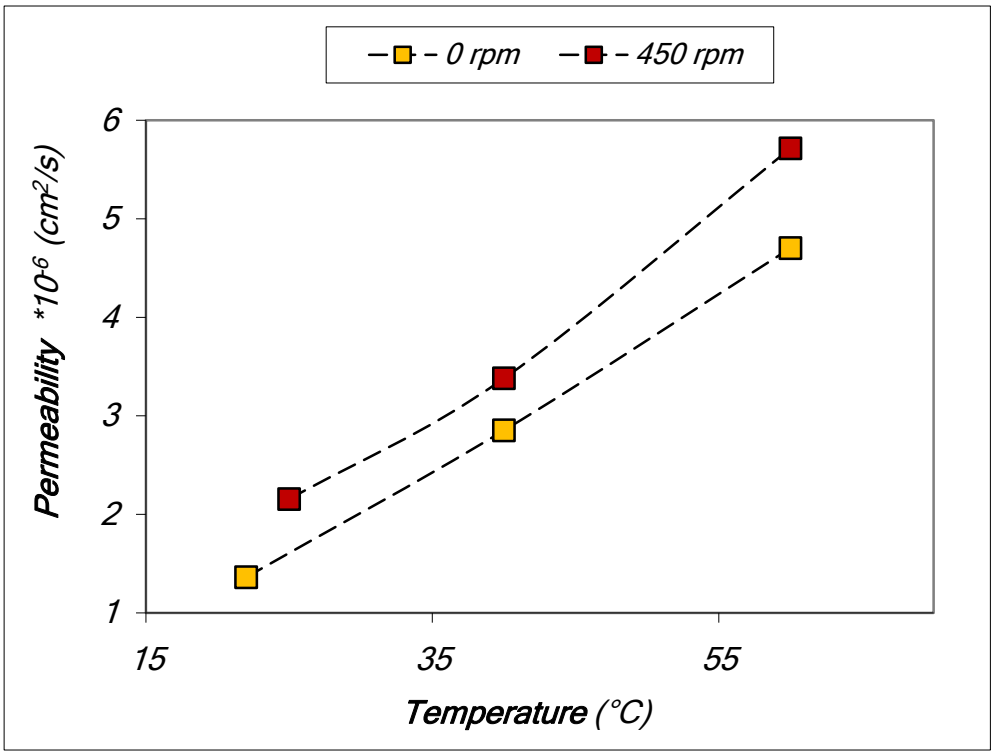

Fig. 5.4.14 Permeability of Nafion commercial as a function of temperature and mixing rate

0 rpm

Parameter	Value	StdErr	CV(%)	Dependencies
A	21.4	2.45	114	0.998553
B	3.79E*03	3.96	10.5	0.998553

450 rpm

Parameter	Value	StdErr	CV(%)	Dependencies
A	1.04	0.058	5.62	0.998492
B	2.76E*03	1.82	0.661	0.998492

Different values of activation energy are found for 0 and 450 rpm. This difference is thought to indicate that alternative diffusion mechanisms are involved in the transport through the polymeric membranes. [181]

5.3 Proton Conductivity

The through-plane (σ_{thp}) and in-plane (σ_{inp}) proton conductivity of the $NZrP_{exf}$ membranes were determined as a function of the filler loading at 40 °C and 100% RH. Table 5.3.1 shows that σ_{thp} decreases with increasing the filler loading going from 5.4×10^{-2} S cm^{-1} for neat Nafion to 8.2×10^{-3} S cm^{-1} for $NZrP_{exf}$ 7 wt.%. A similar behavior was already observed for sulfonated polyetherketone membranes filled with high aspect ratio ZrP particles [190].

In spite of the slightly lower filler content, the conductivity of $NZrP_{exf}$ 7 wt.% ($\sigma_{thp} = 1.7 \times 10^{-2}$ S cm^{-1}) is significantly lower than that of $NZrP_{isg}$ 10 wt.% ($\sigma_{thp} = 6.3 \times 10^{-2}$ S cm^{-1}). Taking into account the conductivity of neat Nafion ($\sigma_{thp} = 7.2 \times 10^{-2}$ S cm^{-1} at 100 °C, 90% RH [185]), the proportional decrease in conductivity determined by the presence of the filler is ≈13% for $NZrP_{isg}$ 10 wt.% and ≈76% for $NZrP_{exf}$ 7 wt.%. Therefore, as expected, the filler morphology has a strong influence also on the tortuosity of the conduction pathways.

The in-plane conductivity too decreases with increase in the ZrP_{exf} loading, but in this case the filler influence is less severe and the ratio $\sigma_{inp} / \sigma_{thp}$ increases from 3.3 (neat Nafion) to 6.1 ($NZrP_{exf}$ 5 wt.%). This seems to indicate that the preferred orientation of the ZrP sheets is parallel to the membrane surface.

Table 5.3.1 Methanol permeability (P) at 40 °C, in-plane (σ_{inp}) and through-plane (σ_{thp}) proton conductivity at 40 °C and 100% RH for Nafion/ZrP_{exf} membranes

ZrP wt.%	P (cm^2 s^{-1})	σ_{thp} (S cm^{-1})	σ_{inp} (S cm^{-1})	σ_{thp}/P (S cm^{-3} s)	$\sigma_{inp}/\sigma_{thp}$
0	$2.6 \cdot 10^{-6}$	0.054	0.18	$2.1 \cdot 10^{4}$	3.3
1	$2.5 \cdot 10^{-7}$	0.036	0.13	$1.4 \cdot 10^{5}$	3.6
3	$3.3 \cdot 10^{-7}$	0.023	0.14	$7.0 \cdot 10^{4}$	6.1
5	$2.9 \cdot 10^{-7}$	0.018	0.11	$6.9 \cdot 10^{4}$	6.1
7	$1.5 \cdot 10^{-6}$	0.008		$5.3 \cdot 10^{3}$	

5.4 The Swelling

Swelling, water and methanol uptake are closely related to the basic membrane properties and play an essential role in the membrane behavior, influencing above all the proton conductivity, the methanol crossover and the mechanical properties [192].

For each membrane, the calculation of the permeability P needs the knowledge of the thickness of the membrane which is assumed to be the same as that measured after membrane equilibration in a 5 wt% methanol/water solution.
Moreover, as it was previously said, methanol crossover decreases when the thickness of the membrane increases. However, this trend changes increasing the thickness because membrane resistance to transport phenomena became dominant [188]. For this reason, it is necessary knowing the real thicknesses of the wet membranes.

The swelling studies were carried out using samples having size L1xL2 and thickness δ.

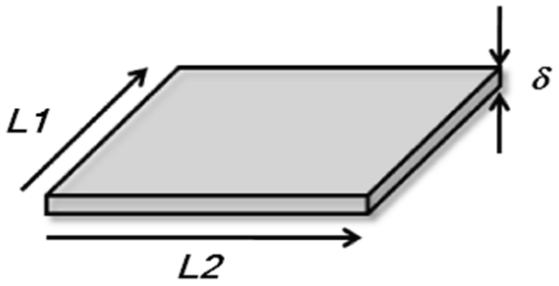

The samples were immersed in deionized water at least for 6/8 hours at room temperature and 100°C. Then, the thickness and size L1, L2 were measured using a micrometer (±0.002 mm) and a calibre after carefully removing the water from both surfaces.
The measurements were repeated three times and then a medium of the data was done.
Some results are showed in the table 5.4.1 and 5.4.2.

Table 5.4.1 Effect of water uptake on a sample of Nafion Commercial

	sample 1			*sample 2*		
	dry	*Wet*		*dry*	*5 wt.% MeOH*	
T (°C)	*20*	*20*	*100*	*20*	*20*	*100*
δ *micron*	*91*	*110*	*113*	*94*	*139*	*142*
$\%\Delta L/L_0$		*17,3*	*19,5*		*32,4*	*33,8*
L1 *mm*	*10*	*10,2*	*10,9*	*10,4*	*11,8*	*12,1*
$\%\Delta L/L_0$		*2,0*	*8,3*		*11,9*	*14,0*
L2 *mm*	*10,5*	*10,6*	*11,5*	*10,5*	*12*	*12,2*
$\%\Delta L/L_0$		*0,9*	*8,7*		*12,5*	*13,9*

Table 5.4.2 Effect of water uptake on a sample of Nafion/ZrP_{exf} 5 wt%

	sample 1			*sample 2*		
	dry	*Wet*		*dry*	*5 wt% MeOH*	
T (°C)	*20*	*20*	*100*	*20*	*20*	*100*
δ *micron*	*79*	*117*	*119*	*93*	*130*	*135*
$\%\Delta L/L_0$		*32,5*	*33,6*		*28,5*	*31,1*
L1 *mm*	*10,8*	*11*	*11,9*	*10,5*	*11,5*	*12*
$\%\Delta L/L_0$		*1,8*	*9,2*		*8,7*	*12,5*
L2 *mm*	*12*	*12,5*	*13*	*11*	*12*	*12,2*
$\%\Delta L/L_0$		*4,0*	*7,7*		*8,3*	*9,8*

Measurement uncertainty:
dry membrane at 20°C: < 0.5 %
wet membrane in 5 wt% methanol/water solution at 20°C:~ 1-3%
wet membrane in 5 wt% methanol/water solution at 100°C:~ 2-4%

As expected, the swelling of the membrane causes the increase in size and thickness of samples and it increases with temperature. Moreover, the uptake of water, or polar

solvents, depends on the filler content of the membrane, as evident in the following results, table 5.4.3 and figure 5.4.1

Table 5.4.3 Comparison of permeability, dry and wet thickness for NZrPisg at different filler contents at 40°C

Membrane	**Permeability** (cm^2/s)	**P/δ** (cm/s)	**Thickness** (μm) Dry	Wet
Nafion/ZrP_{isq} 5 wt%	4.61E-06	3.18E-04	101,3	101
Nafion/ZrP_{isq} 10 wt%	5.51E-06	3.24E-04	107,5	108
Nafion/ZrP_{isq} 15 wt%	4.70E-06	2.54E-04	111,3	111
Nafion/ZrP_{isq} 20 wt%	5.20E-06	2.47E-04	113,8	114

The linear regression of the data, allows to obtain a possible relationship between the thickness and the ZrP content for the wet and dry membrane (wet regression, dry regression), as shown in figure 5.4.1:

$$\text{Wet Regression:} \quad \delta = 125 + 4.21 * (\text{wt.\% ZrP})$$

$$\text{Dry Regression:} \quad \delta = 98 + 0.84 * (\text{wt.\% ZrP})$$

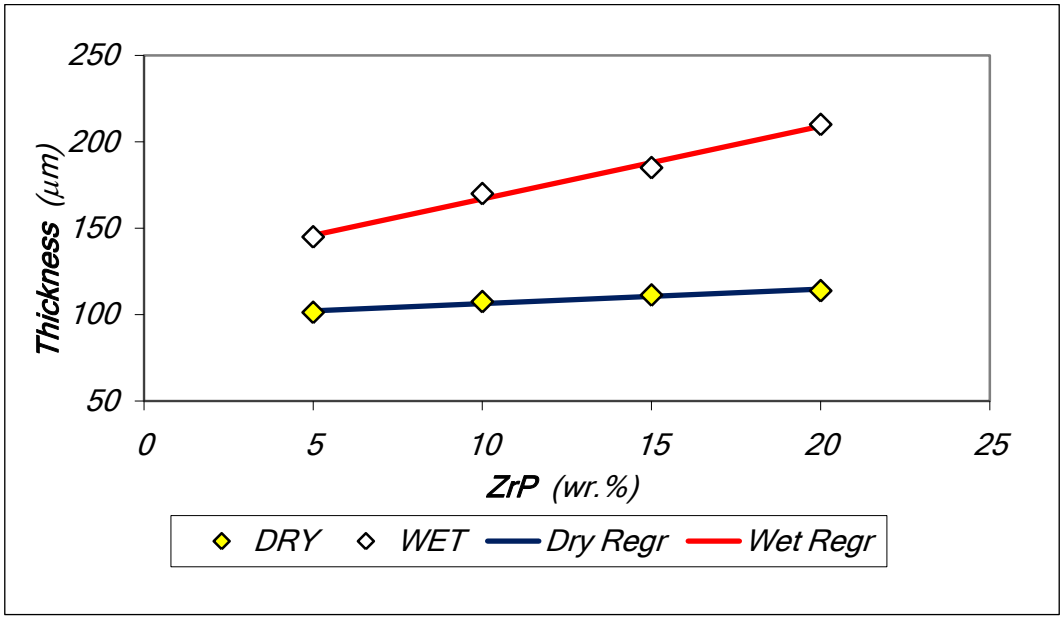

Fig. 5.4.1 Thickness as a function of filler content for dry and wet membrane

The slope of the "wet regression" line is higher than the "dry regression" line, justifying that the increasing of the content of ZrP increases to the absorption of water from the membrane.

On the other hand, methanol uptake contribute to the swelling of the membranes. Table 5.4.4 and figure 5.4.2 show the comparison of the effect of the water, methanol and a 5 wt.% methanol/water solution on the swelling.

Table 5.4.4 Effect of water and methanol on the swelling

membrane	***weight***	***thickness***	***weight***	***thickness***	***weight***	***thickness***
	g	*μm*	*g*	*μm*	*%ΔL/L$_0$*	*%ΔL/L$_0$*
	dry		*100 wt.% water*			
Nafion Standard	*0,064*	*80 +/-5*	*0,0830*	*100*	*22,89*	*10*
Nafion da Casting	*0,102*	*80 +/-5*	*0,1280*	*170*	*20,23*	*44,12*
	dry		*100 wt.% methanol*			
Nafion/ZrP$_{exf}$ 1 wt%	*0,041*	*90 +/-5*	*0,0624*		*34,46*	
Nafion/ZrP$_{exf}$ 5 wt%	*0,048*	*95 +/-3*	*0,0749*		*36,18*	
	dry		*5 wt.% methanol*			
Nafion/ZrP$_{exf}$ 1 wt%	*0,096*	*90 +/-5*	*0,1046*	*100*	*8,22*	*10*
Nafion/ZrP$_{exf}$ 5 wt%	*0,104*	*95 +/-3*	*0,1180*	*110*	*11,53*	*13,64*
	dry		*100 wt.% water*			
Nafion/ZrP$_{exf}$ 1 wt%	*0,033*	*90 +/-5*	*0,0347*		*4,32*	
Nafion/ZrP$_{exf}$ 5 wt%	*0,048*	*95 +/-3*	*0,0519*		*7,13*	

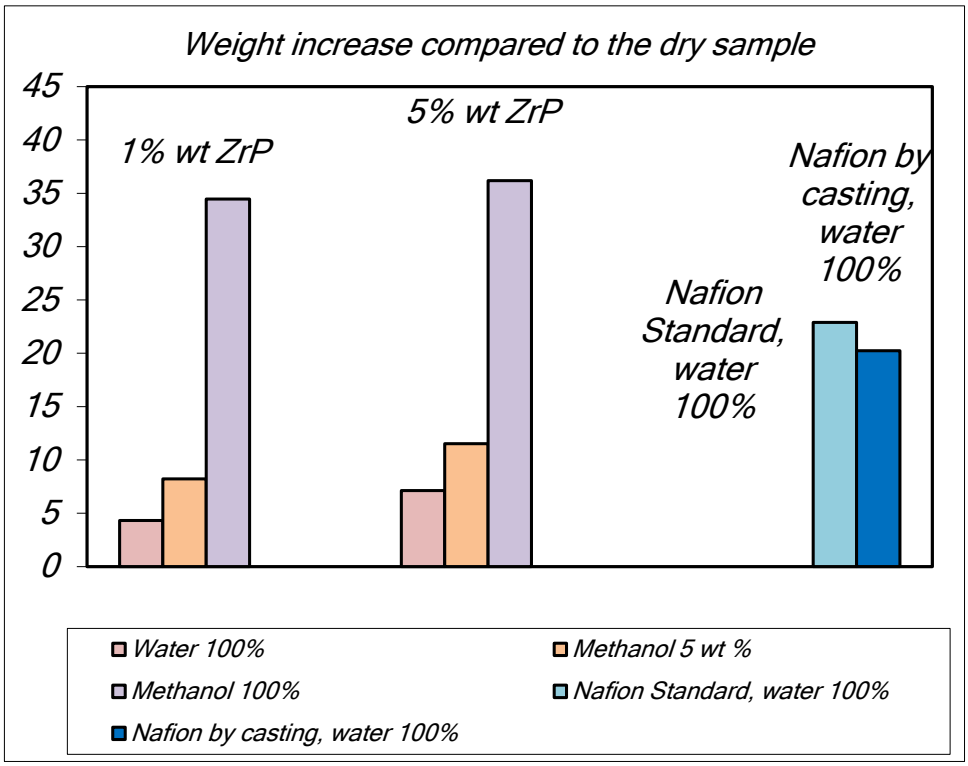

Fig. 5.4.2 Weight increase compared to the dry sample for the indicated membrane

In figure 5.4.2 is showed the weight increase compared to the dry sample for Nafion/ZrP_{exf} 1 and 5 wt%, Nafion by casting, Nafion commercial. Is clearly evident that the ZrP content contributes to the swelling as well as water, but slightly more than water.

Two well-defined trends are observed to be clearly related to the different filler morphologies. The swelling of the membranes filled with ZrP_{isg} increases with the filler loading being always greater than the swelling of the Nafion reference.This is probably due to the concomitant decrease in the degree of crystallinity of the ionomeric matrix. On the other hand, among $NZrP_{exf}$ membranes the proportional change in thickness is lower than that of the Nafion reference for loadings in the range 1-5 wt.%. Also, for this type of membranes the swelling increases with the filler loading, except for the sample $NZrP_{exf}$ 0.5 wt.% which shows an abnormal $\%\Delta L/L_0$ value.

From figure 5.4.3, it is evident that with the filler loading being the same, the membranes containing exfoliated ZrP swell to a lesser extent than those filled with in situ grown ZrP:

comparison between $NZrP_{exf}$ 5 wt.% and $NZrP_{isg}$ 5 wt.% shows that $\%\Delta L/L_0$ is ≈14 and ≈44%, respectively. This different swelling behaviour is consistent with the large difference in the elastic modulus of the two membrane types.

Preliminary experiments show that swelling in the thickness direction for composite membranes with filler loading ≤ 5 wt.-% approaches that of the Nafion reference membrane when temperature is increased from 40 to 80 °C. On the other hand, swelling in the surface direction is nearly independent of temperature in the range 40-60 °C, but increases at higher temperatures.

In Figure 8, the permeability values are reported as a function of ZrP content. It is clear that the presence of the inorganic filler strongly affects the permeability and that the filler influence depends to a large extent on its morphology: all membranes containing ZrP_{isg} exhibit higher permeability than the Nafion reference, whereas the opposite is observed for the membranes filled with ZrP_{exf} Comparison between figure 5.4.3 and 5.4.4 shows that both $\%\Delta L/L_0$ and P have similar dependence on filler loading. This suggested to plot P versus $\%\Delta L/L_0$ to highlight the relation between swelling and permeability.

From figure 5.4.5, it is seen that the permeability of the $NZrP_{isg}$ samples is nearly independent of swelling. This is likely due to the action of opposing factors as the increasing tortuosity of the diffusion pathways, arising from the increasing filler loading, lowers the methanol permeability, the increase in swelling, and therefore in the volume fraction of the liquid phase in the membrane, facilitates the methanol diffusion. The fact that the permeability of these membranes is always higher than that of Nafion leads to the conclusion that swelling prevails over tortuosity.

The Nafion-ZrP_{exf} membranes show a completely different behaviour: in this case, the presence of the filler gives rise to low swelling and tortuosity of the diffusion pathways, due to which the high aspect ratio of the ZrP_{exf} particles is expected to be greater than that originated by the same amount of ZrP_{isg} particles. Both these factors contribute to the lowering of the methanol permeability, and even a filler loading as low as 1 wt.% is enough to reduce by an order of magnitude the methanol permeability, which keeps around 2-3 $\times 10^{-7}$ cm^2 s^{-1} for loadings up to 5 wt. Finally, figure 5.4.5 allows to point out the beneficial effect of the filler morphology on the permeability reduction: on the basis of the solid line interpolating the permeability data of $NZrP_{exf}$, it can be estimated that the permeability of the Nafion reference would be much higher (by a factor of ≈5) than that of a $NZrP_{exf}$ membrane with the same swelling.

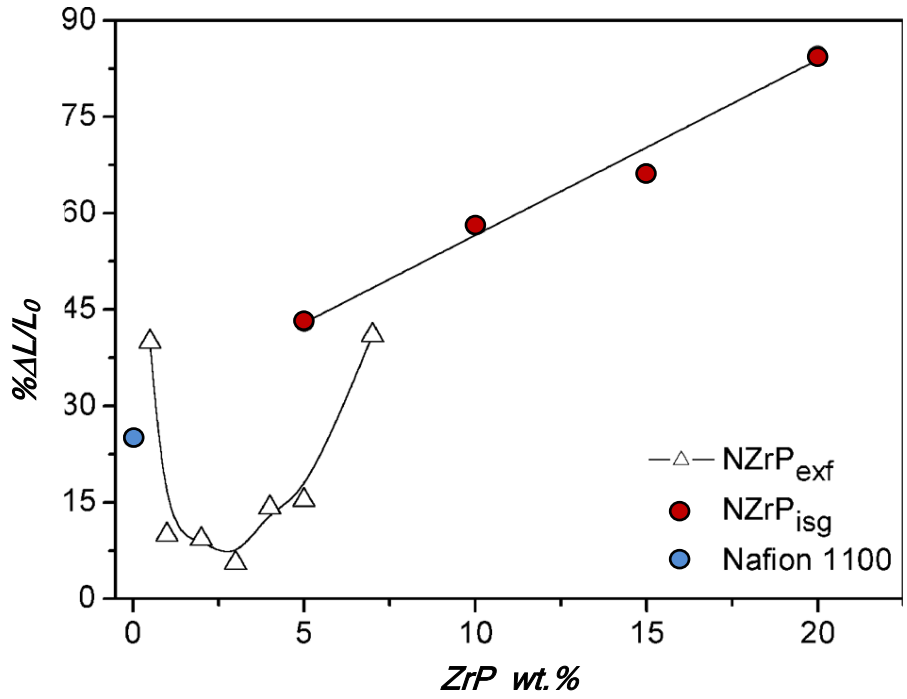

Fig. 5.4.3 Proportional change in thickness (%$\Delta L/L_0$) as a function of filler loading for initially dry $NZrP_{exf}$, $NZrP_{isg}$ and Nafion membranes after conditioning in a 5% methanol/water solution at 40 °C.

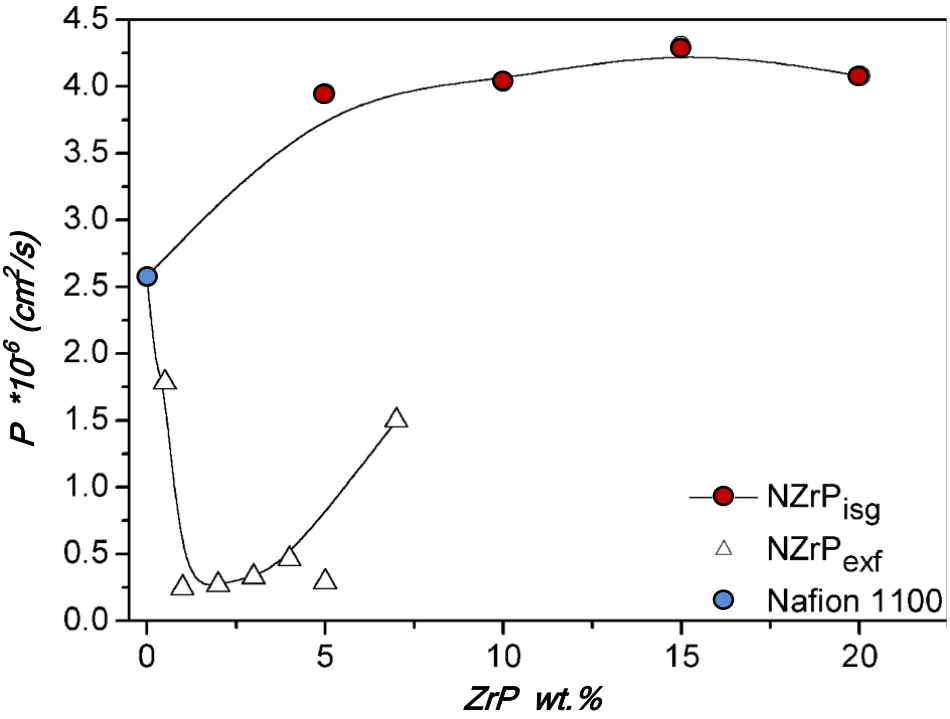

Fig. 5.4.4 Methanol permeability (P) at 40 °C as a function of filler loading for $NZrP_{exf}$, $NZrP_{isg}$ and Nafion membranes.

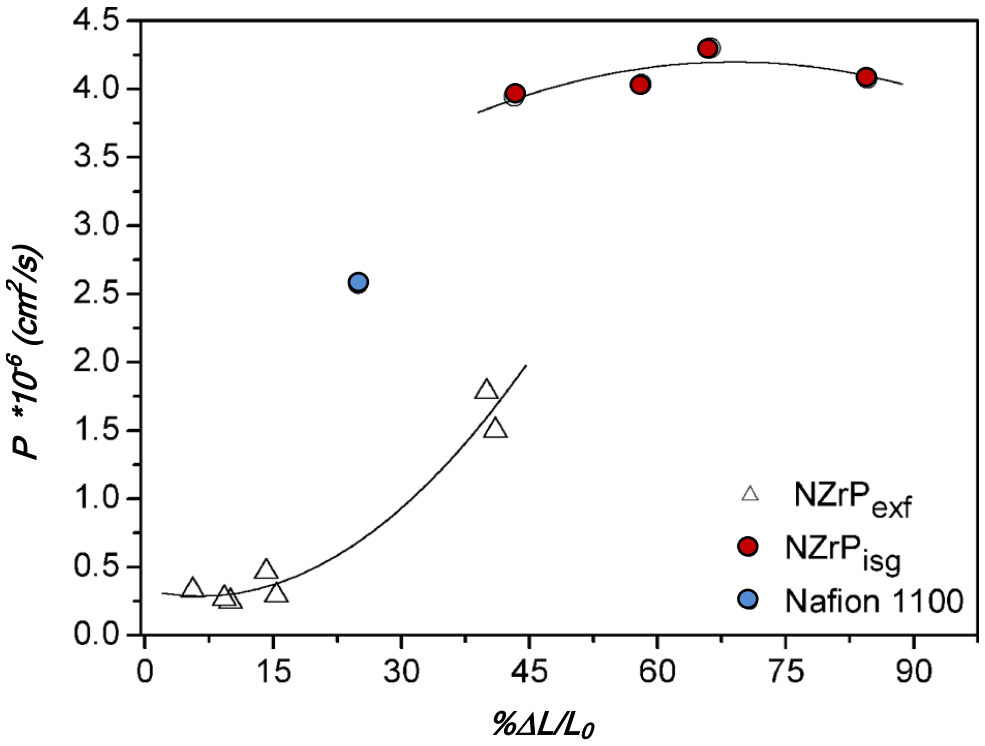

Fig. 5.4.5 Methanol permeability (P) at 40 °C as a function of swelling (%$\Delta L/L_0$) for $NZrP_{exf}$, $NZrP_{isg}$ and Nafion membranes

6. CONCLUSIONS

In this work, new nano-composite membranes containing inorganic fillers with low methanol permeability have been prepared .

Gel of exfoliated α-zirconium phosphate in dimethylformamide were used to prepare Nafion/ZrP composite membranes with filler loadings up to 7 wt.% by casting mixtures of Nafion solution in dimethylformamide and suitable amounts of 2 wt.% of ZrP gel.

The methanol permeability and the proton conductivity of Nafion composite membranes containing high aspect ratio particles of exfoliated α-zirconium phosphate (ZrP_{exf}) and Nafion composite membranes with loadings of in situ grown α-zirconium phosphate (ZrP_{isg}) have been studied. A new experimental apparatus has been used for the methanol permeability measurement. This appears more suitable to obtain permeability data if compared with other apparatus showed in literature, also changing some parameters such as the methanol concentration, temperature and mixing rate.

The results obtained show that the methanol permeability and the swelling behaviour of these membranes turned out to be strongly dependent on the inorganic filler content and the filler influence depends to a large extent on its morphology. The effect of ZrP content on the permeability is not the same in all the range of composition for both different preparation methods.

As a general trend, the Nafion/ZrP_{exf} membranes have a lower permeability and swelling then the Nafion/ZrP_{isg} with the same composition. The Nafion/ZrP_{isg} membranes have methanol permeability comparable with that of commercial Nafion. It is found that the filler content influences the proton conductivity.

The behaviour of the membranes was compared on the base of the selectivity (S) defined as the ratio σ_{thp} / P, where σ_{thp} is the through-plane conductivity and P is the methanol permeability.

The maximum selectivity was found for the membrane filled with 1 wt.% ZrP_{exf}; this value is seven times higher than that of the Nafion reference. Taking into account that both proton and methanol diffusion in ZrP_{exf} particles can only occur parallel to the layers (i.e. along the filler surface and through the interlayer region) it can be inferred that the filler gives rise for both proton and methanol to the same tortuosity increase of the diffusion pathways. This implies that, in comparison with neat Nafion, ZrP_{exf} makes proton diffusion easier than methanol diffusion. This is in agreement with the fact that ZrP is itself proton conductor. Finally, it can be observed that the progressively lower selectivity of the

membranes with increasing filler loading in the range 1-7 wt.% is the result of the concomitant decrease in proton conductivity and increase in methanol permeability.

In conclusion, layered materials suitable for exfoliation are promising candidates for the development of proton conducting hybrid membranes characterised by low permeability to methanol. Composite materials were obtained by filling Nafion membrane with proton conducting nano-composites made of α-zirconium phosphate. The new membranes obtained have significantly lower methanol permeability compared to Nafion, showing a possible commercial application interest.

APPENDIX

A. FUEL CELLS TYPES

Many types of fuel cells are currently being researched. The nine main types are the subject of this chapter and are differentiated from one another on the basis of the electrolytes and/or fuel used with that particular fuel cell type. The most common fuel cell types include the following:

- *Polymer electrolyte membrane fuel cells (PEMFCs)*
- *Alkaline fuel cells (AFCs)*
- *Phosphoric acid fuel cells (PAFCs)*
- *Solid oxide fuel cells (SOFCs)*
- *Molten carbonate fuel cells (MCFCs)*
- *Direct methanol fuel cells (DMFCs)*
- *Biological fuel cells (BFCs)*

A.1 PEM fuel cells

Thomas Grubb and Leonard Niedrach invented PEM fuel cell technology at General Electric in the early 1960s. GE developed a small fuel cell for the U.S. Navy's Bureau of Ships (Electronics Division) and the U.S. Army Signal Corps [194]. The fuel cell was fuelled by hydrogen generated by mixing water and lithium hydride. It was compact, but the platinum catalysts were expensive.

NASA initially researched PEM fuel cell technology for Project Gemini in the early U.S. space program. Batteries were used for the preceding Project Mercury missions, but Project Apollo required a power source that would last a longer amount of time. Unfortunately, the first PEM cells developed had repeated difficulties with the internal cell contamination and leakage of oxygen through the membrane. GE redesigned their fuel cell, and the new model performed adequately for the rest of the Gemini flights. The designers of Project Apollo and the Space Shuttle ultimately chose to use alkali fuel cells [4]. GE continued to work on PEM fuel cells in the 1970s, and designed PEM water electrolysis technology, which lead to the U.S. Navy Oxygen Generating Plant. The British Royal Navy used PEM fuel cells in the early 1980s for their submarine fleet, and during the

last decade, PEM fuel cells have been researched extensively by commercial companies for transportation, stationary, and portable power markets

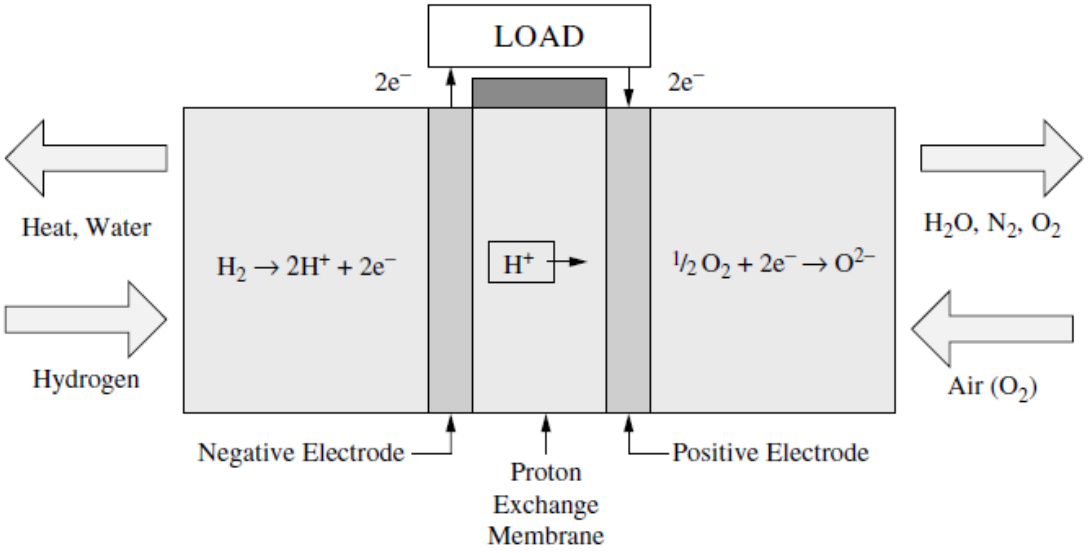

Figure A.1.1 The polymer electrolyte fuel cell (PEMFC).

Proton Exchange Membrane Fuel Cells (PEMFC) are believed to be the best type of fuel cell as the vehicular power source to eventually replace the gasoline and diesel internal combustion engines. PEMFCs are currently being developed and demonstrated for systems ranging from 1W to 2kW.

PEM fuel cells use a solid polymer membrane (a thin plastic film) as the electrolyte. The standard electrolyte material currently used in PEM fuel cells is a fully fluorinated Teflon-based material produced by DuPont for space applications in the 1960s. The DuPont electrolytes have the generic brand name Nafion, and the types used most frequently are 1135, 115, and 117. The Nafion membranes are fully fluorinated polymers that have very high chemical and thermal stability.This polymer is permeable to protons when it is saturated with water, but it does not conduct electrons.

The fuel for the PEMFC is hydrogen and the charge carrier is the hydrogen ion (proton). At the anode, the hydrogen molecule is split into hydrogen ions (protons) and electrons. The hydrogen ions permeate across the electrolyte to the cathode while the electrons flow through an external circuit and produce electric power. Oxygen, usually in the form of air, is supplied to the cathode and combines with the electrons and the hydrogen ions to produce water. The reactions at the electrodes are as follows:

Anode: $H_2 (g) \rightarrow 2H^+ (aq) + 2e^-$

Cathode: $½ O_2 (g) + 2H^+ (aq) + 2e^- \rightarrow H_2O (l)$

Overall: $H_2 (g) + ½ O_2 (g) \rightarrow H_2O (l)$

Compared to other types of fuel cells, PEMFCs generate more power for a given volume or weight of fuel cell. This high-power density characteristic makes them compact and lightweight. In addition, the operating temperature is less than 100ºC, which allows rapid start-up. These traits and the ability to rapidly change power output are some of the characteristics that make the PEMFC the top candidate for automotive power applications.
Other advantages result from the electrolyte being a solid material, compared to a liquid. The sealing of the anode and cathode gases is simpler with a solid electrolyte, and therefore, less expensive to manufacture. The solid electrolyte is also more immune to difficulties with orientation and has less problems with corrosion, compared to many of the other electrolytes, thus leading to a longer cell and stack life.
One of the disadvantages of the PEMFC for some applications is that the operating temperature is low. Temperatures near 100ºC are not high enough to perform useful cogeneration. Also, since the electrolyte is required to be saturated with water to operate optimally, careful control of the moisture of the anode and cathode streams is important. [199]

A.2 Solid oxide fuel cells

Emil Baur and H. Preis experimented with solid oxide electrolytes during the late 1930s. The initial designs were not as electrically conductive as they hoped, and many unwanted chemical reactions were reported. Solid oxide and molten carbonate fuel cells had a similar history up until the 1950s. O. K. Davtyan of Russia during the 1940s also performed experiments with electrolytes, but experienced unwanted chemical reactions and short life ratings [4]. Solid oxide research later began to accelerate at the Central Technical Institute in The Hague, Netherlands, the Consolidation Coal Company in Pennsylvania, and General Electric in Schenectady, New York [194].
Several issues with solid oxide arose, such as high internal electrical resistance, melting, and short-circuiting due to semiconductivity. Due to these problems, many researchers began to believe that molten carbonate fuel cells showed more short-term promise.

Recently, increasing energy prices and advances in materials has reinvigorated work on SOFC, and about 40 companies are currently researching this technology [194].

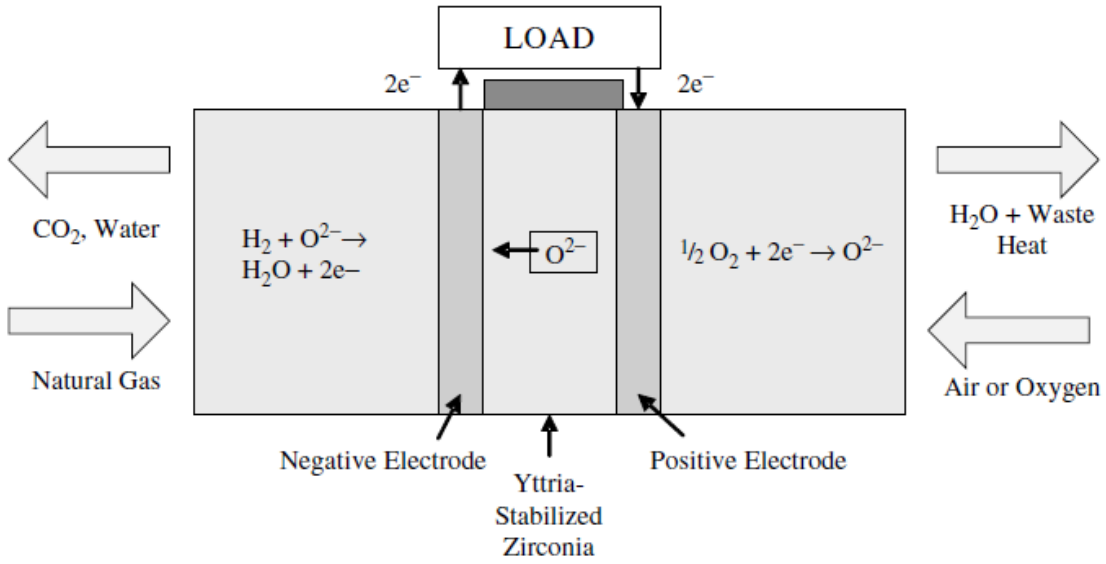

Figure A.2.1 A solid oxide fuel cell (SOFC).

Solid oxide fuel cells (SOFCs) seem promising for large, high-power applications such as industrial and large-scale central electricity generating stations. Some developers also see potential SOFC use in motor vehicles and are developing fuel cell auxiliary power units (APUs). The chemistry of the solid oxide fuel cells consists of an electrolyte that is a non-porous solid, such as Y_2O_3 stabilized ZrO_2 with conductivity based oxygen ions (O_2). The anode is usually made of a Co-ZrO_2 or Ni-ZrO_2 cement, while the cathode is made of Sr-doped $LaMnO_3$. Cells are being constructed in three main configurations: tubular, bipolar and a planar configuration adopted more recently by many other developers as shown in Figure A.2.1. The operating temperatures can reach 1000°C. Power-generating efficiencies could reach 60 to 85 percent with cogeneration and when cell output is up to 100 kW. The anode, cathode, and overall cell reactions are

Anode: $H_2\ (g) + O^{2-} \rightarrow H_2O\ (g) + 2e^-$
Cathode: $½\ O2\ (g) + 2e^- \rightarrow O^{2-}$
Overall: $H_2\ (g) + ½\ O_2\ (g) \rightarrow H_2O\ (g)$

SOFCs can be constructed in many ways. Tubular SOFC designs are closer to commercialization and are being produced by several companies around the world.

Tubular SOFC technology has produced as much as 220 kW. Japan has two 25-kW units online, and a 100 kW plant is being tested in Europe [200].

SOFCs that employ a ceramic, solid-state electrolyte (zirconium oxide stabilized with yttrium oxide) may be the only fuel cell technology with the potential to span market-competitive applications from residential loads as small as 2 kW to wholesale distributed generation units of 10 to 25 MW according to the Electric Power Research Institute (EPRI).

Even though SOFCs operate at higher temperatures than MCFCs, their simple efficiency is theoretically not as good as that of MCFCs. The waste heat that SOFCs produce (between 850 to 1000°C) is extremely beneficial when used for cogeneration or for driving an integrated gas turbine because it can boost overall system energy efficiency to very attractive levels. SOFCs are able to operate at a high enough temperature to incorporate an internal fuel reformer that uses heat from the fuel cell. The recycled steam and a catalyst can convert the natural gas directly into a hydrogen-rich fuel cell.

SOFCs coupled with small gas turbines are high-efficiency systems that have a combined rating in the range of 250 kW to 25 MW, and are expected to fit into grid support or industrial onsite generation markets.

These fuel cells could potentially compete head-on with wholesale power rates [201].

A.3 Molten carbonate fuel cells

Emil Baur and H. Preis in Switzerland experimented with high temperature solid oxide electrolytes in the 1930s. Many problems were encountered with the electrical conductivity and unwanted chemical reactions. O. K. Davtyan researched this further during the 1940s, but had little success. By the late 1950s, Dutch scientists G. H. J. Broers and J. A. A. Ketelaar built upon previous work, but were also unsuccessful. They then decided to focus on the electrolytes of fused (molten) carbonate salts instead, and successfully created a fuel cell that ran for six months. However, they found that the molten electrolyte was partially lost through reactions with gasket materials [27].

The U.S. Army's Mobility Equipment Research and Development Center (MERDC) at Ft. Belvoir tested many molten carbonate fuel cells made by Texas Instruments in the 1960s. These fuel cells ranged from 100–1000 Watts and were designed to run on hydrogen from a gasoline reformer.

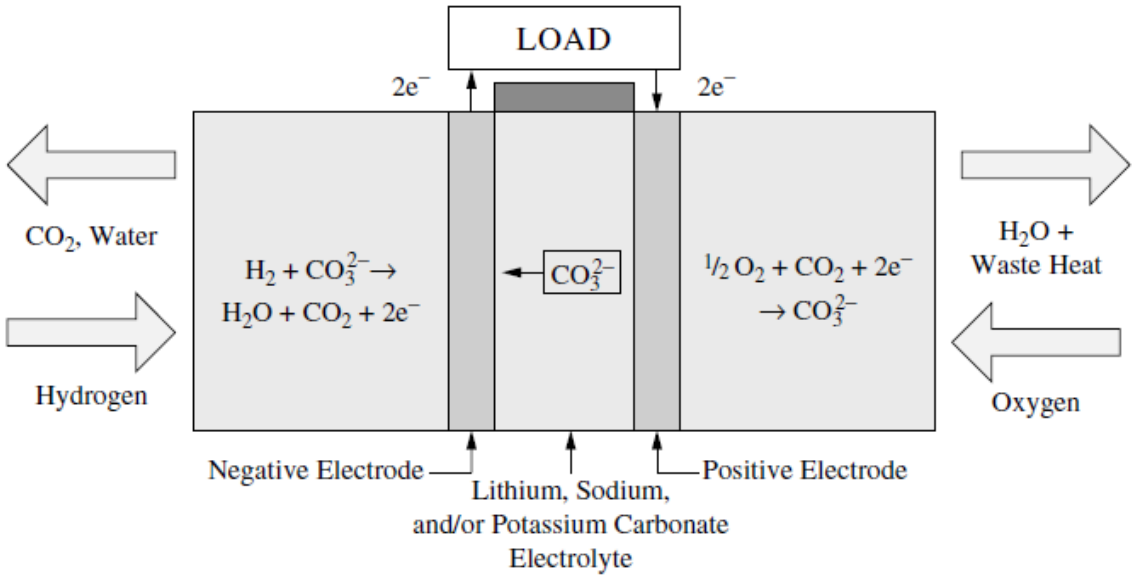

Figure A.3.1 A molten carbonate fuel cell (MCFC).

Two major corporations are pursuing the commercialization of molten carbonate fuel cells (MCFCs) in the United States: FuelCell Energy and M-C Power Corporation. The electrolyte in the molten-carbonate fuel cell uses a liquid solution of lithium, sodium, and/or potassium carbonates, soaked in a matrix. MCFCs have high fuel-to-electricity efficiencies ranging from 60 to 85 percent with cogeneration, and operate at about 620-660°C [201]. The high operating temperature is a big advantage because it enables a higher efficiency and the flexibility to use more types of fuels and inexpensive catalysts. This high operating temperature is needed to achieve sufficient conductivity of the electrolyte.

Molten carbonate fuel cells can use hydrogen, carbon monoxide, natural gas, propane, landfill gas, marine diesel, and coal gasification products as the fuel. MCFCs producing 10 kW to 2 MW MCFCs have been tested with a variety of fuels and are primarily targeted to electric utility applications. MCFCs for stationary applications have been successfully demonstrated in several locations throughout the world.

A diagram of a molten carbonate fuel cell is shown in figure A.3.

The reactions at the anode, cathode, and the overall reaction for the MCFC are [200]:

Anode: $H_2\ (g) + CO_3^{2-} \rightarrow H_2O\ (g) + CO_2\ (g) + 2e^-$

Cathode: $\frac{1}{2}\ O_2\ (g) + CO_2\ (g) + 2e^- \rightarrow CO_3^{2-}$

Overall: $H_2\ (g) + \frac{1}{2}\ O_2\ (g) + CO_2\ (g) \rightarrow H_2O\ (g) + CO_2\ (g)$

The high temperatures and the electrolyte chemistry also has disadvantages. The high temperature requires significant time to reach operating conditions and responds slowly to changing power demands. These characteristics make MCFCs more suitable for constant power applications. The carbonate electrolyte can also cause electrode corrosion problems. Furthermore, since CO_2 is consumed at the anode and transferred to the cathode, introduction of CO_2 and its control in air stream becomes an issue for achieving optimum performance that is not present in any other fuel cell.

A.4 Phosphoric acid fuel cells

Phosphoric acid fuel cells were slower to develop than other fuel cells. G. V. Elmore and H. A. Tanner conducted experiments with electrolytes that were 35 percent phosphoric acid, and 65 percent silica powder. They presented their experimental results in a paper "Intermediate Temperature Fuel Cells," in which they describe an acid cell that operated for six months with a current density of 90 mA/cm^2 and 0.25 volts without any deterioration[4].
During the 1960s and '70s, advances in electrode materials and issues with other fuel cell types created renewed interest in PAFCs. The U.S. Army explored PAFCS that ran with common fuels in the 1960s. Karl Kordesch and R. F. Scarr of Union Carbide created a thin electrode made of carbon paper as a substrate, and a Teflon-bonded carbon layer as a catalyst carrier. An industry partnership known as TARGET was primarily led by Pratt & Whitney and the American Gas Association, and produced significant improvements in fuel cell power plants, increasing the power from 15 kW in 1969 to 5 MW in 1983 [200].
The phosphoric acid fuel cell (PAFC) is one of the few commercially available fuel cells. Several hundred fuel cell systems have been tested, and these fuel cells have been installed all over the world. Most of the PAFC plants that have been built are in the 50 to 200 kW range, but large plants of 1 MW and 5 MW also have been built. The largest plant operated to date achieved 11 MW of grid-quality alternating current (AC) power [201].
A diagram of the phosphoric fuel cell is shown in Figure A.4.1.

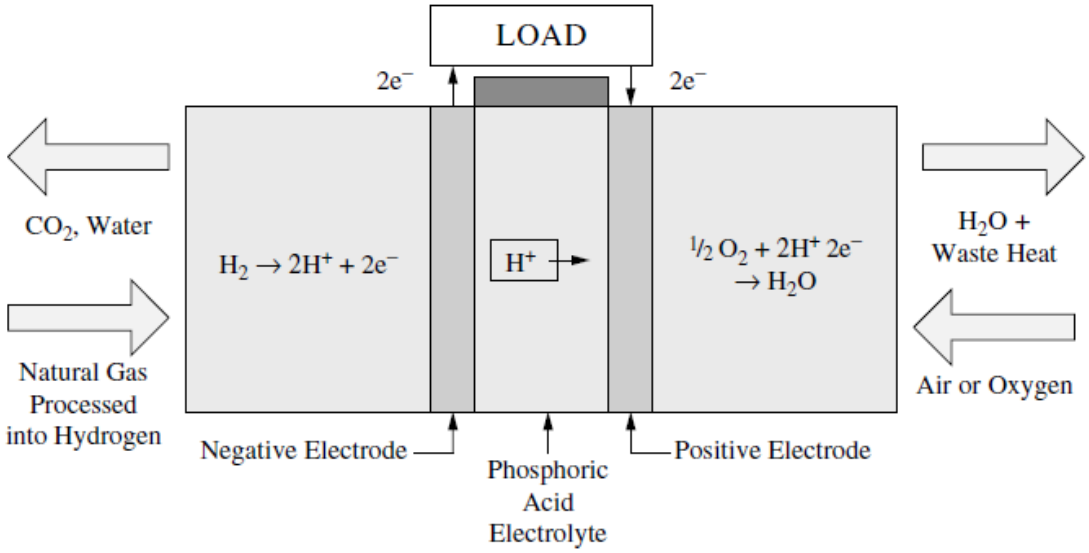

Figure A.4.1 A phosphoric acid fuel cell (PAFC).

PAFCs are very efficient fuel cells, generating electricity at more than 40 percent efficiency. About 85 percent of the steam produced by the PAFC is used for cogeneration. This efficiency may be compared to about 35 percent for the utility power grid in the United States. Operating temperatures are in the range of 150 to 220°C. At lower temperatures, PAFC is a poor ionic conductor, and carbon monoxide (CO) poisoning of the platinum catalyst in the anode can become severe [201].

Two main advantages of the phosphoric acid fuel cell include a cogeneration efficiency of nearly 85 percent, and its ability to use impure hydrogen as fuel. PAFCs can tolerate a carbon monoxide concentration of about 1.5 percent, which increases the number of fuel types that can be used. Disadvantages of PAFCs include their use of platinum as a catalyst (like most other fuel cells) and their large size and weight. PAFCs also generate low current and power comparable to other types of fuel cells [12].

Phosphoric acid fuel cells are the most mature fuel cell technology. The commercialization of these cells was brought about through the Department of Energy (DOE) and ONSI (which is now United Technologies Company (UTC) Fuel Cells) and organizational linkages with Gas Research Institute (GRI), electronic utilities, energy service companies, and user groups [200].

The chemical reactions for PAFCs are as follows:

Anode: $H_2\,(g) \rightarrow 2H^+\,(aq) + 2e^-$

Cathode: $\frac{1}{2}\,O_2\,(g) + 2H^+\,(aq) + 2e^- \rightarrow H_2O\,(l)$

Overall: $H_2\,(g) + \frac{1}{2}\,O_2\,(g) + CO_2 \rightarrow H_2O\,(l) + CO_2$

A.5 Alkali fuel cells

Francis Thomas Bacon (1904-1992) built an alkali electrolyte fuel cell that used nickel gauze electrodes in 1939 [4]. He employed potassium hydroxide for the electrolyte instead of the acid electrolytes, and porous "gas-diffusion electrodes" rather than the solid electrodes used since Grove. He also used pressurized gases to keep the electrolyte from "flooding" in the electrodes [200]. During World War II, he thought the alkali electrolyte fuel cells might provide a good source of power for the Royal Navy submarines in place of dangerous storage batteries in use at the time. In the following 20 years, he created large-scale demonstrations with his alkali cells using potassium hydroxide as the electrolyte, instead of the acid electrolytes used since Grove's time. One of the first demonstrations was a 1959 Allis-Chalmers farm tractor, which was powered by a stack of 1008 cells [4]. This tractor was able to pull a weight of 3000 pounds [4]. Allis-Chalmers continued fuel cell research for many years, and also demonstrated a fuel cell-powered golf cart, submersible, and fork lift. In the late 1950s and 1960s, Union Carbide also experimented with alkali cells. Karl Kordesch and his colleagues designed alkali cells with carbon gas-diffusion electrodes based upon the work of G. W. Heise and E. A. Schumacher in the 1930s. They demonstrated a fuel cell-powered mobile radar set for the U.S. Army, as well as a fuel cell-powered motorbike. Eduard Justi of Germany designed gas-diffusion electrodes around the same time [200]. Pratt & Whitney licensed the Bacon patents in the early 1960s, and won the National Aeronautics and Space Administration (NASA) contract to power the Apollo spacecraft with alkali cells [4].

Based upon the research, development, and advances made during the last century, technical barriers are being resolved by a world network of scientists. Fuel cells have been used for over 20 years in the space program, and the commercialization of fuel cell technology is rapidly approaching.

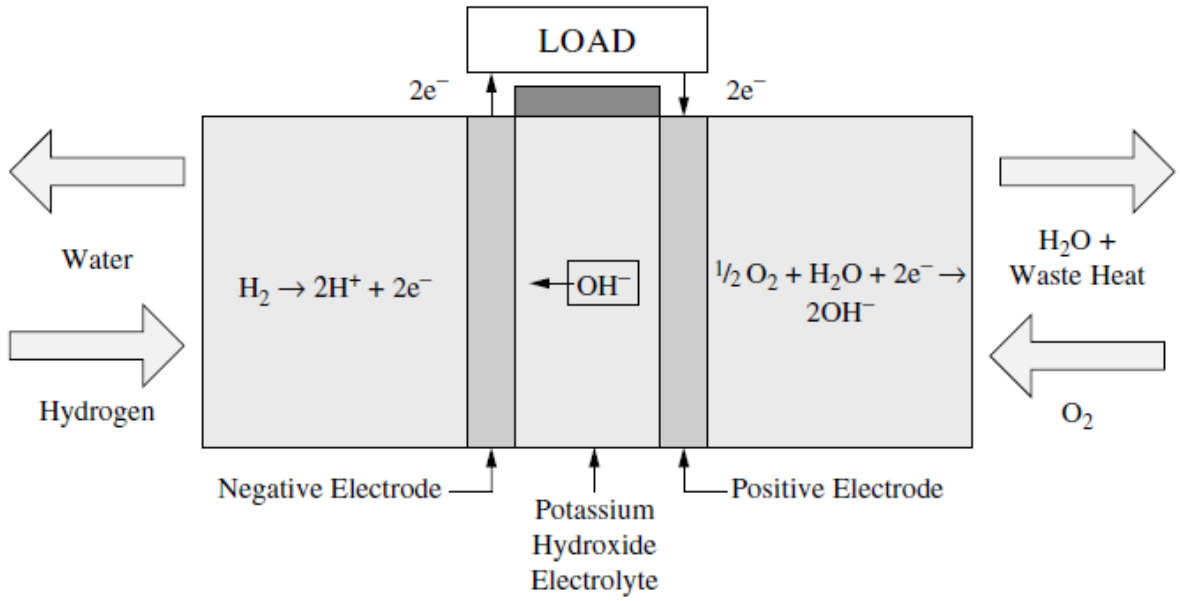

Figure A.5.1 An alkaline fuel cell (AFC).

Alkaline fuel cells (AFCs) have been used by NASA on space missions and can achieve power-generating efficiencies of up to 70 percent. The operating temperature of these cells range between room temperature to 250°C [201]. The electrolyte is aqueous solution of alkaline potassium hydroxide soaked in a matrix. (This is advantageous because the cathode reaction is faster in the alkaline electrolyte, which means higher performance). Several companies are examining ways to reduce costs and improve operating flexibility. AFCs typically have a cell output from 300 watts to 5 kW [200]. The chemical reactions that occur in this cell are as follows:

Anode: $2H_2\,(g) + 4(OH)^-\,(aq) \rightarrow 4H_2O\,(l) + 4e^-$
Cathode: $O_2\,(g) + 2H_2O\,(l) + 4e^- \rightarrow 4(OH)^-\,(aq)$
Overall: $2H_2\,(g) + O_2\,(g) \rightarrow 2H_2O\,(l)$

A diagram of the alkaline fuel cell is shown in figure A.5.1.
Another advantage of AFCs are the materials such as the electrolyte and catalyst used are low-cost. The catalyst layer can use either platinum or non precious metal catalysts such as nickel. A disadvantage of AFCs is that pure hydrogen and oxygen have to be fed into the fuel cell because it cannot tolerate the small amount of carbon dioxide from the atmosphere.

Over time, carbon dioxide degrades the KOH electrolyte which can lead to significant issues. Two commonly used solutions are refreshing the KOH electrolyte or carbon dioxide scrubbers. Due to these limitations, AFCs are not used for many power applications.

A.6 Biological Fuel Cells

A biological fuel cell is a device that directly converts biochemical energy into electricity. In biological fuel cells (BFCs), there is the redox reaction of a carbohydrate substrate such as glucose and methanol using a microorganism or enzyme as a catalyst. The biological fuel cell works like any other fuel cell, as illustrated in figure A.6.1. The main difference is that the catalyst in the biological fuel cell is a microorganism or enzyme. Therefore, noble metals are not needed for the catalyst and its operating conditions are typically neutral solutions and room temperature.

The fuel cell operates in liquid media, and advantages like low temperature and a near neutral environment can be obtained.

The possible potential applications of such fuel cells are:

1. *to develop new practical low power energy sources;*
2. *to manufacture a specific sensor based upon direct electrode interactions;*
3. *to electrochemically synthesize some chemicals.*

In the research and development of biological fuel cells, improvements have been made in several areas. The areas include the selection of the microorganisms, the use of different mediators to improve electron transfer, and the investigation of the kinetics in the process. In addition, various types of electrodes have been studied for efficient reactions [203].

A reaction diagram of a biological fuel cell is shown in figure A.6.1. In bacteria cells, mitochondria serve as the energy storage unit by accumulating or releasing chemical energy in the form of substances like nicotinamide adenine dinucleotide with high-energy hydrogen (NADH) or nicotinamide adenosine dinucleotide phosphate (NADPH). The NADH and NADPH act as electron transfer paths from the substrate to the metabolites. The NADH/NAD ratio increases as oxygen limitation becomes more severe [204].

Most of the substrate is turned into an electroactive substance through proper control of bacteria metabolism [203]. However, the biological reactions mentioned earlier only take place in diluted aqueous media, which is not suitable for different charge-transfer reactions. The electron transfer from these electroactive substances to the electrode is a

slow process. Therefore, a suitable redox mediator is needed to improve the electron transfer and the electrode reaction [10].

In a study done by the Helinski University of Toronto, a mediator, 2-hydroxy-1,4-naphtho-quinone (HNQ), was used to improve the electron transfer. When this mediator substance is present in the system, the color in the biofilm reactor changes [13]. The changes in the color occur because of the metabolic activity of the biofilm reactor and the electron transfer in the fuel cell anode. It offers a simple method of monitoring and controlling functions of the fuel cell [204].

Experimental tests of the bacterial fuel cells have resulted in several conclusions. First, the complex reactions make the conversion rate of electrical energy lower (15 to 25 percent) compared to that of chemical fuel cells. Secondly, the current density per anode volume increases when the size of the fuel cell decreases. Finally, the power output increases if the bacteria are immobilized. The next stage of research and development will be with an enzymatic fuel cell. Replacing the bacteria with an enzyme should make the process easier to control because enzymatic reactions are simpler. According to the estimation of the researchers at the Helinski University of Technology, the conversion rate of the Enzymatic Fuel Cell (EFC) is expected to be more than 50 percent [203]. Experiments have shown that the rate is in the range of 40 to 55 percent for the bacterial fuel cell when the substrate is glucose.

Similarly, the current density of the EFC is likely to improve significantly compared to that of the bacterial fuel cell.

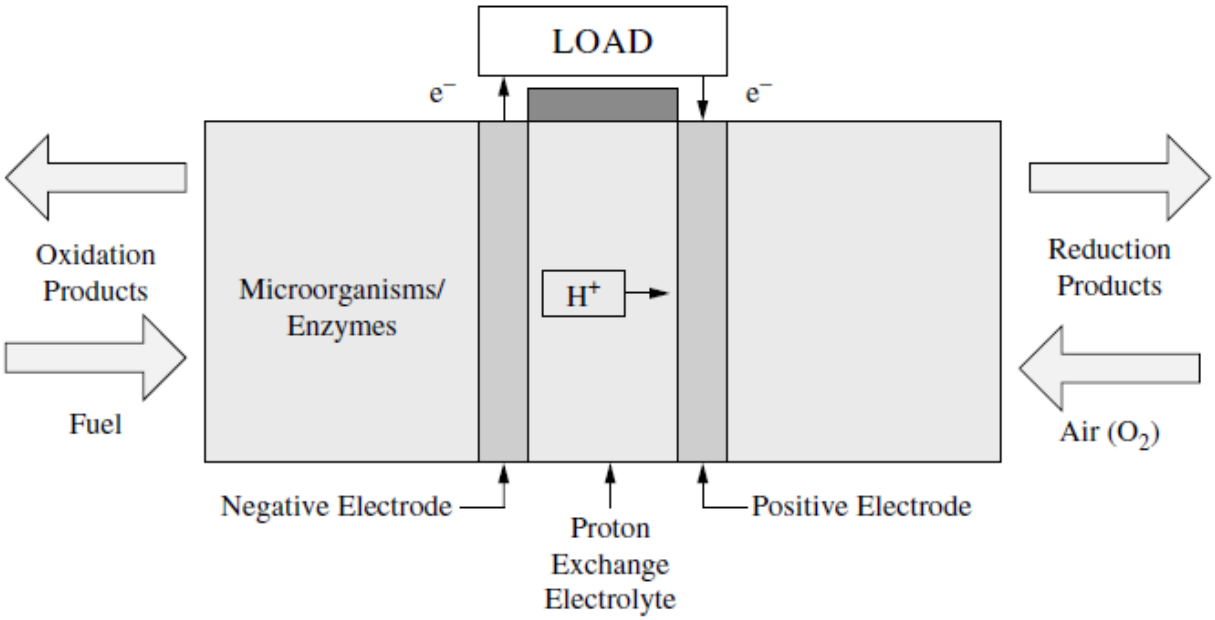

Figure A.6.1 A biological fuel cell (BFC).

References

1. *National Energy Technology Laboratory, U.S. Department of Energy, Fuel Cell Handbook, 2005, 1-35.*

2. *ENEA, Rapporto Energia e Ambiente, 2008, 7-16, 98-103.*

3. *Service, R. F. Science 2002, 296, 1222.*

4. *Lu, G. Q.; Wang, C. Y.; Yen, T. J.; Zang, X. Electrochem Acta 2004, 49, 821.*

5. *H.-C. Kuan, C.-S. Wu, C.-Y. Chen, Z.-Z. Yu, A. Dasari, Y.-W. Mai, Electrochem. Solid-State Lett. 9, 2006, A76*

6. *Li, Xianguo. Principles of Fuel Cells. 2006. New York: Taylor & Francis Group.*

7. *O'Hayre, Ryan, Suk-Won Cha, Whitney Colella, and Fritz B. Prinz. Fuel Cell Fundamentals. 2006. New York: John Wiley & Sons.*

8. *Barbir, Frano. PEM Fuel Cells: Theory and Practice. 2005. Burlington, MA: Elsevier Academic Press.*

9. *Collecting the History of Fuel Cells. http://americanhistory.si.edu/fuelcells/index.htm.Smithsonian Institution, 2006. Last accessed September 15, 2006. Last updated December 2005.*

10. *Stone, C. and A.E. Morrison. Solid State Ionics, 152-153, 2004, 1-13.*

11. *"Fuel Cells." Energy Research Center of the Netherlands (ECN). http://www.ecn.nl/en/h2sf/additional/fuel-cells-explained/. Last updated September 18, 2006.*

12. *Mikkola, Mikko. Helsinki University of Technology, Department of Engineering Physics and Mathematics, Masters Thesis, 2001.*

13. *Applyby, A., and Foulkes.F. Fuel Cell Handbook. 1989. New York: Van Nostrand Reinhold.*

14. *Aricò A.S., Srinivasan S., Antonucci V.,DMFCs: From Fundamental Aspects to Technology Development, Fuel Cells 1, 2001, 133-161*

15. *Adamson K.A., Pearson P., Journal of Sources , 2000, 548-555*

16. *Hamnett A., Kennedy B.J. Bimetallic, Electrochimica Acta, 33,1988, 1613-1618*

17. *Hamnett A., Catalysis Today, 38 ,1997, 445-457*

18. *Carrette L., Friedric K.A., Stimming U., Fuel Cells, 01, 2001, 5-39*

19. *Comyn, J. Polymer Permeability; Springer: New York, 1985.*

20. Newman, J.; Thomas, K. E. Electrochemical Systems, 3rd ed.; Wiley-Interscience: New York, 2004

21. Larminie J., Dicks A., Fuel cell systems explained, 2nd , 2003

22. Heinzel A., Barragan V. M., Journal of Power Sources 80, 1999, 70-74

23. Perry's Engineering Handbook 7th edition

24. Balmer R. Thermodynamics, West, St Paul, Minnesota, 1990

25. Parsons Inc. EG&G Services, Fuel Cells: A Handbook, 5th , 2000, 3-10, 5-19, 8-22

26. Bloom H., Cutman F., Electrochemistry, Plenum Press,1981, 121

27. Appley A.J., Foulkes F.R., A Fuel Cell Handbook, 2nd ,1993, 22

28. Libby B., Smyrl W. H, Cussler E.L., 49, 2003, 991-1001

29. Li X., Roberts E.P.L., Holmes S.M., Journal of Power Sources 154, 2006, 115-123

30. Service, R. F. Science 2002, 296, 1222.

31. Lu, G. Q.; Wang, C. Y.; Yen, T. J.; Zang, X. Electrochem Acta 2004, 49, 821.

32. Blum, A.; Duvdevani, T.; Philosoph, M.; Rudoy, N.; Peled, E. J Power Sources 2003, 117, 22.

33. Wiles, K. B. PhD Dissertation, Virginia Polytechnic Institute and State University, 2005.

34. Ezzell, B. R.; Carl, W. P.; Mod, W. A. US Patent 4,358,412, 1982.

35. Kelley, S. C.; Deluga, G. A.; Smyrl, W. H. Electrochem Solid State Lett 2000, 3, 407.

36. Paulson, L. D. Computer 2003, 36, 10.

37. Larminie, J.; Dicks, A. Fuel Cell Systems Explained, 2nd ed.,Wiley: New York, 2003.

38. Hamnett, A. Catalysis Today 1997, 38, 445.

39. Wasmus S.; Kuver A. J Electroanal Chem 1999, 461, 14.

40. Ravikumar, M. K.; Shukla, A. K. J Electrochem Soc 1996, 143, 2601.

41. Thomassin, J.-M.; Pagnoulle, C.; Bizzari, D.; Caldarella, G.; Germain, A.; Jerome, R. e-Polymers 2004, 18, 1.

42. Scott, K. Taama, W.; Cruickshank, J. J Appl Electrochem 1998, 28, 289.

43. Ge, J.; Liu, H. J Power Sources 2005, 142, 56.

44. Shao, Z.-G.; Wang, X.; Hsing, I. M. J Membr Sci 2002, 210, 147.

45. Wycisk, R.; Lee, J. K.; Pintauro, P. N. J Electrochem Soc 2005, 152, A892.

46. Thomassin, J.-M.; Pagnoulle, C.; Bizzari, D.; Caldarella, G.; Germain, A.; Jerome, R. e-Polymers 2004, 18, 1.

47. Scott, K.; Taama, W. M.; Argyropoulos, P. J Membr Sci 2000, 171, 119.

48. Hatanaka, T.; Hasegawa, N.; Kamiya, A.; Kawasumi, M.; Morimoto, Y.; Kawahara, K. Fuel 2002, 81, 2173.

49. Kerres, J.; Zhang, W.; Ullrich, A.; Tang, C.-M.; Hein, M.; Gogel, V.; Frey, T.; Jorissen, L. Desalination 2002, 147, 173.

50. Kim, D. S.; Park, H. B.; Rhim, JW.; Lee, Y.M. Solid State Ionics 2005, 176, 117.

51. Xu, W.; Lu, T.; Liu, C.; Xing, W. Electrochem Acta 2005, 50, 3280.

52. Cho, K.-Y.; Eom, J.-Y.; Jung, H.-Y.; Choi, N.-S.; Lee, Y. M.; Park, J.-K.; Choi, J.-H.; Park, K.-W.; Sung, Y.-E. Electrochem Acta 2004, 50, 583.

53. Sumner, M. J.; Harrison, W. L.; Weyers, R. M.; Kim, Y. S.; McGrath, J. E.; Riffle, J. S.; Brink, A.; Brink, M. H. JMembr Sci 2004, 239, 199.

54. Kim, Y. J.; Choi, W. C.; Woo, S. I.; Hong, W. H. JMembr Sci 2004, 238, 213.

55. Li, X.; Zhao, C.; Lu, H.; Wang, Z.; Na, H. Polymer 2005, 46, 5820.

56. Kim, B.; Kim, J.; Jung, B. J Membr Sci 2005, 250,175.

57. Shin, J.-P.; Chang, B.-J.; Kim, J.-H.; Lee, S.-B.; Suh, D. H. JMembr Sci 2005, 251, 247.

58. Okamato, K.; Yin, Y.; Yamada, O.; Islam, M. N.; Honda, T.; Mishima, T.; Suto, Y.; Tanaka, K.;Kita, H. J Membr Sci 2005, 258, 115.

59. Thangamuthu, R.; Lin, C. W. Solid State Ionics 2005, 176, 531.

60. Li, L.;Wang, Y. JMembr Sci 2005, 246, 167.

61. Lee, K.; Nam, J.-H.; Lee, J. H.; Lee, Y.; Cho, S. M.; Jung, C. H.; Choi, H. G.; Chang, Y.-Y.; Kwon, Y.-U.; Nam, J.-D. Electrochem Commun 2005, 7, 113.

62. Zhou, X.; Weston, J.; Chalkova, E.; Hofmann, M. A.; Ambler, C. M.; Allcock, H. R.; Lvov, S. N. Electrochem Acta 2003, 48, 2173.

63. Carretta, N.; Tricoli, V.; Picchioni, F. J Membr Sci 2000, 166, 189.

64. Yoon, S. R.; Hwang, G. H.; Cho, W. I.; Oh, I.-H.; Hong, S.-A.; Ha, H. Y. J Power Sources 2002, 106, 215.

65. Li, L.; Xu, L.;Wang, Y. Mater Lett 2003, 57, 1406.

66. Tricoli, V.; Carretta, N.; Bartolozzi, M. J Electrochem Soc 2000, 147, 1286.

67. Kim, D.; Aulice Scibioh, M.; Kwak, S.; Oh, I. H.; Ha, H. Y. Electrochem Commun 2004, 6, 1069.

68. Li, L.; Zhang, J.; Wang, Y. J Membr Sci 2003, 226, 159.

69. Kim, Y.-M.; Park, K.-W.; Choi, J. H.; Park, I. S.; Sung, Y. E. Electrochem Commun 2003, 5, 571.

70. Chang, H. Y.; Lin, C. W. J Membr Sci 2003, 218, 295.

71. Thomassin, J.-M.; Pagnoulle, C.; Caldarella, G.; Germain, A.; Jerome, R. Polymer 2005, 46, 11389.

72. Song, M.-K.; Park, S.-B.; Kim, Y.-T.; Rhee, H.-W. Mol Cryst Liq Cryst 2003, 407, 411.

73. Sauk, J; Byun, J; Kang, Y.; Kim, H. Korean J Chem Eng 2005, 22, 605.

74. Kim, D. S.; Shin, K. H.; Park, H. B.; Lee, Y. M. Macromol Res 2004, 12, 413.

75. Cho, K.-Y.; Jung, H.-Y.; Shin, S.-S.; Choi, N.-S.; Sung, S.-J.; Park, J.-K.; Choi, J.-H.; Park, K.-W.; Sung, Y.-E. ElectrochemActa 2004, 50, 589.

76. Einsla, R. A.; Kim, Y. S.; Hickner, M. A.; Hong, Y.- T.; Hill, M. L.; Pivovar, B. S.; McGrath, J. E. JMembr Sci 2005, 255, 141.

77. Kim, Y. S.; Sumner,M. J.; Harrison,W. L.; Riffle, J. S.; McGrath, J. E.; Pivovar, B. S. J Electrochem Soc 2004, 151, A2150.

78. Kim, J.; Kim, B.; Jung, B. J Memb Sci 2002, 207, 129.

79. Yin, Y.; Fang, J.; Cui, Y.; Tanaka, K.; Kita, H.; Okamoto, K. Polymer 2003, 44, 4509.

80. Gil, M.; Ji, X.; Li, X.; Na, H.; Hampsey, J. E.; Lu, Y. JMembr Sci 2004, 234, 75.

81. Qiao, J.; Hamaya, T.; Okada, T. Polymer 2005, 46, 10809.

82. Park, H.; Kim, Y.; Hong, W. H.; Choi, Y. S.; Lee, H. Macromolecules 2005, 38, 2289.

83. Jung, B.; Kim, B.; Yang, J. M. J Membr Sci 2004, 245, 61.

84. Shen, M.; Roy, S.; Kuhlmann, J. W.; Scott, K.; Lovell, K.; Hrsfall, J. A. J Membr Sci 2005, 251, 121.

85. Rhim, J. W.; Park, H. B.; Lee, C.-S.; Jun, J.-H.; Kim, D. S.; Lee, Y.M. J Membr Sci 2004, 238, 143.

86. Wu, H.; Wang, Y.; Wang, S. J Mater Electrochem Sys 2002, 5, 251.

87. Elabd, Y. A.; Napadensky, E.; Sloan, J. M.; Crawford, D M.; Walker, C. W. J Membr Sci 2003, 217, 227.

88. Kang, M.-S.; Kim, J. H.; Won, J.; Moon, S.-H.; Kang, Y. S. J Membr Sci 2005, 247, 127.

89. Guo, Q. H.; Pintauro, P. N.; Tang, H.; O' Connor, S. JMembr Sci 1999, 154, 175.

90. Zhang, X.; Liu, S.; Liu, L.; Yin, J. Polymer 2005, 46, 1719.

91. Miyatake, K.; Zhou, H.; Matsuo, T.; Uchida, H.; Watanabe, M.Macromolecules 2004, 37, 4961.

92. Einsla, B. R.; Hong, Y.-T.; Kim, Y. S.; Wang, F.; Gunduz, N.; McGrath, J. E. J Polym Sci Part A: PolymChem 2004, 42, 862.

93. Drioli, E.; Regina, A.; Casciola, M.; Oliveti, A.; Trotta, F.; Massari, T. JMembr Sci 2004, 228, 139.

94. Elabd, Y. A.; Napadensky, E.;Walker, C.W.;Winey, K. I. Macromolecules 2006, 39, 399.

95. Won, J.;Choi, S.W.;Kang, Y. S.;Ha, H. Y.;Oh, I. H.; Kim, H. S.; Kim, K. T.; Jo, W. J Membr Sci 2003, 214, 245.

96. Kim, J.; Kim, B.; Jung, B.; Kang, Y. S.; Ha, H. Y.; Oh, I.-W.; Ihn, K. J Macromol Rapid Commun 2002, 23, 753.

97. Serpico, J. M.; Ehrenberg, S. G.; Fontanella, J. J.; Jiao, X.; Perahia, D.; McGrady, K. A.; Sanders, E. H.; Kellogg, G. E.; Wnek, G. E. Macromolecules 2002, 35, 5916.

98. Nacher, A.; Escribano, P.; Del Rio, C.; Rodriguez, A.; Acosta, J. L. J Polym Sci Part A: Polym Chem 2003, 41, 2809.

99. Saarinen, V.; Kallio, T.; Paronen, M.; Tikkanen, P.; Rauhala, E.; Kontturi, K. Electrochem Acta 2005, 50, 3453.

100. Kang, M.-S.; Choi Y.-J.; Moon, S.-H. J Membr Sci 2002, 207, 157.

101. Qiao, J.; Hamaya, T.; Okada, T. Chem Mater 2005, 17, 2413.

102. Walker, C.W., Jr. J Power Sources 2002, 110, 144.

103. Hasiotis, C.; Deimede, V.; Kontoyannis, C. Electrochem Acta 2001, 46, 2401.

104. Manea, C.; Mulder,M. J Membr Sci 2002, 206, 443.

105. Pivovar, B. S.;Wang, Y.; Cussler, E. L. J Membr Sci 1999, 154, 155.

106. Walker, M.; Baumgartner, K.-M.; Kaier, M.; Kerres, J.; Ullrich, A.; Rauchle, E. J Appl Polym Sci 1999, 74, 67.

107. Pu, H.; Liu, Q.; Liu, G. JMembr Sci 2004, 241, 169.

108. Wang, J. T.; Wasmus, S.; Savinell, R. F. J Electrochem Soc 1996, 143, 1233.

109. Samms, S. R.;Wasmus, S.; Savinell, R. F. J Electrochem Soc 1996, 143, 1225.

110. Wang, J. T.; Wainright, J. S.; Savinell, R. F.; Litt, M. J Appl Electrochem 1996, 26, 751.

111. Kawahara, M.; Morita, J; Rikukawa, M; Sanui, K; Ogata, N. Electrochem Acta 2000, 45, 1395.

112. Xing, B. Z.; Savadogo, O. J New Mater Electrochem Syst 1999, 2, 95.

113. He, R.; Li, Q.; Xiao, G.; Bjerrum, N. J. J Membr Sci 2003, 226, 169.

114. Kim, H. J.; Lim, T. H. J Ind Eng Chem 2004, 10, 1081.

115. Smit,M.A.; Ocampo,A. L.;Espinosa-Medina, M. A.; Sebastian, P. J. J Power Sources 2003, 124, 59.

116. Sungpet, A. J Membr Sci 2003, 226, 131.

117. Bae, B.; Ha, H. Y.; Kim, D. J Electrochem Soc 2005, 152, A1366.

118. Liu, J.; Wang, H.; Cheng, S.; Chan, K.-Y. J Membr Sci 2005, 246, 95.

119. Hobson, L. J.; Nakano, Y.; Ozu, H.; Hayase, S. J Power Sources 2002, 104, 79.

120. Prakash, G. K. S.; Smart, M. C.; Wang, Q.-J.; Atti, A.; Pleynet, V.; Yang, B.; McGrath, K.; Olah, G. A.; Narayanan, S. R.; Chun, W.; Valez, T.; Surampudi, S. J Fluorine Chem 2004, 125, 1217.

121. Walker, C. W., Jr. J Electrochem Soc 2004, 151, A1797.

122. Yamaguchi, T.; Nakao, S. I.; Kimura, S. J Polym Sci Part B: Polym Phys 1997, 35, 469.

123. Yamaguchi, T.; Miyata, F.; Nakao, S. Adv Mater 2003, 15, 1198.

124. Yamaguchi, T.; Miyata, F.; Nakao, S. J Membr Sci 2003, 214, 283.

125. Yamaguchi, T.; Kuroki, H.; Miyata, F. Electrochem Commun 2005, 7, 730.

126. Xu, W.; Liu, C.; Xue, X.; Su, Y.; Lv, Y.; Xing, W.; Lu, T. Solid State Ionics 2004, 171, 121.

127. Ren, S.; Li, C.; Zhao, X.; Wu, Z.; Wang, S.; Sun, G.; Xin, Q.; Yang, X. JMembr Sci 2005, 247, 59.

128. Silva, V. S.; Ruffmann, B.; Silva, H.; Gallego, Y. A.; Mendes, A.; Madeira, L. M.; Nunes, S. P. J Power Sources 2005, 140, 34.

129. Zaidi, S. M. J.; Rahman, S. U. J Electrochem Soc 2005, 152, A1590.

130. Park, Y.-S.; Yamazaki, Y. Poly Bull 2005, 53, 181.

131. Munakata, H.; Yamamoto, D.; Kanamura, K. Chem Commun 2005, 31, 3986.

132. Ponce, M. L.; Prado, L. A. S. de, A.; Silva, V.; Nunes, S. P. Desalination 2004, 162, 383.

133. Silva, V.; Ruffmann, B.; Silva, H.; Mendes, A.; Madeira, M.; Nunes, S. Adv Matl Forum II, 2004, 455, 587.

134. Baglio, V.; Di Blasi, A.; Arico, A. S.; Antonucci, V.; Antonucci, P. L.; Serraino Fiory, F.; Licoccia, S.; Traversa, E. J New Mater Electrochem Sys 2004, 7, 275.

135. Bauer, F.; Willert-Porada, M. J Membr Sci 2004, 233, 141.

136. Jung, D. H.; Cho, S. Y.; Peck, D. H.; Shin, D. R.; Kim, J. S. J Power Sources 2003, 118, 205.

137. Ponce, M. L.; Prado, L.; Ruffmann, B.; Richau, K.; Mohr, R.; Nunes, S. P. JMembr Sci 2003, 217, 5.

138. Dimitrova, P.; Friedrich,K. A.;Vogt, B.; Stimming, U. J Electroanal Chem 2002, 532, 75.

139. Alberti, G.; Casciola, M.; Pica, M.; Di Cesare, G. Ann NYAcad Sci 2003, 984, 208.

140. Poltarzewski, Z.; Wieczorek, W.; Przyluski, J.; Antonucci, V. Solid State Ionics 1999, 119, 301.

141. Jung, D. H.; Myoung, Y.-B.; Cho, S.-Y.; Shin, D. R.; Peck, D. H. Int J Hydrogen Energy 2001, 26, 1263.

142. Hejze, T.; Gollas, B. R.; Sauerbrey, R. K.; Schmied, M.; Hofer, F.; Besenhard, J. O. J Power Sources 2005, 140, 21.

143. Chang, J.-H.; Park, J. H.; Park, G. G.; Kim, C.-S.; Park, O. O. J Power Sources 2003, 124, 18.

144. Peled, E.; Duvdevani, T.; Aharon, A.; Melman, A. Electrochem Solid State Lett 2000, 3, 525.

145. Hobson, L. J.; Ozu, H.; Yamaguchi, M.; Hayase, S. J Electrochem Soc 2001, 148, A1185.

146. Tang, H.; Pan, M.; Jiang, S.; Wan, Z.; Yuan, R. Colloids Surf A: Physicochem Eng Aspects 2005, 262, 65.

147. Sun, H.; Sun, G.; Wang, S.; Liu, J.; Zhao, X.; Wang, G.; Xu, H.; Hou, S.; Xin, Q. J Membr Sci 2005, 259, 27.

148. Kim, H. J.; Shul, Y. G.; Han, H. S. J Power Sources 2004, 135, 66.

149. Yang, B.; Manthiram, A. Electrochem Commun 2004, 6, 231.

150. Ma, Z. Q.; Cheng, P.; Zhao, T. S. J Membr Sci 2003, 215, 327.

151. Mex, L.; Sussiek, M.; Muller, J. Chem Eng Commun 2003, 190, 1085.

152. Kadirgan, F.; Savadogo, O. Russ J Electrochem 2004, 40, 1141.

153. Scott, D. S.; Hafele, W. Int J Hydrogen Energy 1990, 15, 727.

154. Makowski, H. S.; Lundberg, R. D.; Singhal, G. H. US Patent 3, 870, 841, 1975.

155. Hamley, I. W. The Physics of Block Copolymers; Oxford University Press: New York, 1998.

156. Weiss, R. A.; Sen, A.; Pottick, L. A.; Willis, C. L. Polymer 1991, 32, 2785.

157. Gouin, J. P.; Williams, C. E.; Eisenberg, A. Macromolecules 1989, 22, 4573.

158. Weiss, R. A.; Sen, A.; Willis, C. L.; Pottick, L. A. Polymer 1991, 32, 1867.

159. Lu, X.; Steckle, W. P.; Weiss, R. A. Macromolecules 1993, 26, 5876.

160. Venkateshwaran, L. N.; York, G. A.; DePorter, C. D.; McGrath, J. E.; Wilkes, G. L. Polymer 1992, 33, 2277.

161. Storey, R. F.; Chisholm, B. J.; Lee, Y. Polym Eng Sci 1997, 37, 73.

162. Mokrini, A.; Del Rio C.; Acosta, J. L. Solid State Ionics 2004, 166, 375.

163. Shin, C. K.; Maier, G.; Andreaus, B.; Scherer, G. G. JMembr Sci 2004, 245, 147.

164. Yang, Y. S.; Shi, Z. Q.; Holdcroft, S. Macromolecules 2004, 37, 1678.

165. Yang, J. E.; Lee, J. S. Electrochim Acta 2004, 50, 617.

166. Silva, V. S.; Weisshaar, S.; Reissner, R.; Ruffmann, B.; Vetter, S.; Mendes, A.; Madeira, L. J.; Nunes, S. J Power Sources 2005, 145, 485.

167. Yamazaki, Y.; Jang, M. Y.; Taniyama, T. Sci Tech AdvMater 2004, 5, 455.

168. Jang, M. Y.; Yamazaki, Y. Solid State Ionics 2004, 167, 107.

169. Jorissen, L.; Gogel, V.; Kerres, J.; Garche, J. J Power Sources 2002, 105, 267.

170. Manea, C.;Mulder,M. Desalination 2002, 147, 179.

171. Wiley, R. H.; Venkatachalam, T. K. J Polym Sci Part A: PolymChem 1966, 4, 1892.

172. Pu, H. T.; Liu, Q. Z.; Qiao, L.; Yang, Z. L. Polym Eng Sci 2005, 45, 1395.

173. Pu, H. T.; Liu, Q. Z. PolymInt 2004, 53, 1512.

174. Rozier J., Jopnes D., Recent progress in membranes for medium temperature fuel cells, 2001, 229-308

175. Casciola M., Bagnasco G, Donnadio A., Micoli L., Pica M., Sganappa M., Turco M., Fuel Cells, 9, 2009, 235-149

176. Alberti G., Casciola M., Capitani D., Donnadio A., Narducci R., Pica M., Sganappa M., Electrochimica Acta 52, 2007, 8125-8132

177. Alberti G., Casciola M.,Pica M., Tarpanelli T., Sganappa M., Fuel Cells 3, 2005, 366-375

178. Alberti G., Casciola M., Donnadio A., Narducci R., Pica M., Sganappa M., Desalination 199, 2006, 280-282

179. Carretta N., Tricoli V., Picchioni F., J. Membrane Sci. 166, 2000, 189

180. Nunes S.P., Ruffmann B., Rikowski E., Vetter S., Richau K., J. Membrane Sci. 203, 2002, 215

181. Xiangyang Zhou a, Jamie Weston a,b, Elena Chalkova a, Michael A. Hofmann c, Catherine M. Ambler c, Harry R. Allcock c, Serguei N. Lvov Electrochimica Acta 48, 2003, 2173/2180

182. M.Casciola, G. Alberti, A.Donnadio, M. Pica, F. Marmottini, A. Bottino, P. Piaggio, J. Mater. Chem. 2005, 15, 4262.

183. G. Alberti, S. Allulli, U. Costantino and M.A. Massucci, J. Inorg. Nucl. Chem. 1975, 37, 1779.

184. G. Alberti, M. Casciola and U. Costantino, J. Colloid Interface Sci. 1985, 107, 256.

185. G. Alberti, M. Casciola, D. Capitani, A. Donnadio, R. Narducci, M. Pica, M. Sganappa, Electrochim. Acta. 2007, 52, 8125.

186. G. Alberti, M. Pica, T. Tarpanelli, PCT Patent WO2005105667A1.

187. Bockris J.O'M Conway B.E., Yeager E., White R.E., Plenum Press 1, 3, 1981, 220

188. Jung D.H. et al Power Source 71, 1998, 169 / Narayanan S.R. et al. Annu. Battery Conf. Appl. Adv. 11 (1996) 113

189. A. Clearfield, G.D. Smith, Inorg. Chem. 1969, 8, 431.

190. G. Alberti, M. Casciola, Annu. Rev. Mater. Res. 2003, 33, 129.

191. Kim J., Lee S-M., Srinivasan S., Chamberlin C.E., Journal of the Electrochemical Society 142,1995, 2670-2674

192. Zawadzinski T., Springer T. , Uribe F. Solid State Ionics 60, 1993, 199

193. O' Hayre, Ryan, Suk-Won Cha, Whitney Colella, and Fritz B. Prinz. Fuel Cell Fundamentals. 2006. New York: John Wiley & Sons.

194. Barbir, Frano. PEM Fuel Cells: Theory and Practice. 2005. Burlington, MA: Elsevier Academic Press

195. Shukla, A. K., P. Suresh, S. Berchmans, and A. Rajendran. Current Science, 87, No. 4. August 25, 2004.

196. Coors, W.G., Journal of Power Sources, Vol. 118, Issue 1 – 2, 2003, pp. 150 – 156.

197. Coors, W.G., Journal of the Electrochemical Society, Vol. 151, Issue 7, 2004, pp. A994 – A997.

198. Smedley, S., Fifteenth Annual Battery Conference on Applications and Advances (Cat.No.00TH8490), 1999, pp. 65 – 70.

199. Lin, Bruce., Princeton University, Masters Thesis, 1999.

200. "Fuel Cell Basics." Fuel Cells 2000. Last accessed September 13, 2006. http://www.fuelcells.org/basics/how.html.

201. Rossi, C et al., Proc. MicroNanotechnology for Space Applications. Vol.1. April 1999.

202. Hirschenhofer, J.H. et al. The Fuel Cell Handbook, 4th ed. 1998. Reading, PA: Parsons Corporation.

203. Halme, Aarne, Xia-Chang Zhang, and Niko Rintala. Automation Technology Laboratory, Helinski University of Technology, 1998. http://www.automation.hut.fi/research/bio/sfc00pos.htm. Last accessed September 19, 2006.

204. Heller, Adam. "Biological Fuel Cell and Method." TheraSense, Inc. U.S. Patent # 6,294,281. September 25, 2001